POLITECNICO DI TORINO

Master's degree programme in Civil Engineering

Master Thesis

Structural health monitoring of a modular tensegrity bridge

Supervisors

Prof. Rosario Ceravolo (Politecnico di Torino)

Prof. Christian Bucher (TU Wien)

Candidate

Linda Scussolini

A.Y. 2020/2021

To my father

Abstract

Tensegrity structures still represent a relatively new field of research in civil engineering; in particular, if on one hand the design of these structures, including static and dynamic analysis, has been explored by researchers, structural health monitoring is still an almost completely new topic to research about. The main purpose of this dissertation is to evaluate the feasibility of structure health monitoring or damage detection in tensegrity structures using output-only vibration measurements. The changes in the natural frequencies of the structure, which is represented by a modular pedestrian tensegrity bridge designed on purpose for this study, have been evaluated through changes in damage scenarios. The damage detection consequently leads to an optimal sensor positioning within the structure, obtaining as main result the number of sensors and, also, an approximate location of the sensors' position. The minimum number of uniaxially sensors needed to detect the damage within the structure is 32: considering that the analysed cases of sensors' number vary between 8 and 128, the result, which can be considered low, could be related to the size of the structure, which is relatively small. The location of sensors' position has been detected as uniformly distributed in the tension cables, that represent the part of the structure most affected by every type of considered damage. Therefore, some proposals for a more specific study of the sensors' location have been pointed out as possible future developments of this dissertation. It is important to highlight that the obtained results are mainly related to the analysed structure: the found number of sensors and their location is therefore valid only for the specific case of a modular tensegrity bridge. Nevertheless, this dissertation can represent a basis for this type of study, adapting the developed method to a different type of tensegrity structure.

Contents

List of figures

List of tables

1 Introduction

Civil engineering has always been a field subjected to a continuous evolution and change, aimed at the search for new technologies and systems. The need for new typologies of structural systems has led to a constant experimentation.

One of the fields that are still open nowadays, is represented by tensegrity systems. The term tensegrity itself contains already a simple and brief description of these type of structures: indeed, the word '*tensegrity*' is nothing else than the contraction of tensile integrity. This aspect already explains how tensegrity structure work: they are equilibrated structures made of elements only in tension and in compression.

This type of structures represents a particularly interesting and challenging field not only in terms of aesthetics, but also of functionality. One of the advantages of tensegrity structures is indeed their applicability to different field, like art, architecture, design, civil engineering, and biomedical engineering. The transversality of these systems made the existence of a diversified and rich research field possible.

However, if on one hand these structures have been widely used for art works, on the other hand, their application in civil engineering field is mostly unexplored and only a few examples of existing tensegrity structures can be found.

Moreover, the greatest part of the research is mainly focused on the form-finding and on the design of these structure, while only a minimum part of research is focused on their structural health monitoring.

The assessment of damage levels and the prediction of the course of the structural health is necessary in most structures. Considering that the application of tensegrity structures in civil engineering, as mentioned before, is still a developing field, the need for their health monitoring can be considered even emphasized.

Nowadays, structural health monitoring is not only used for more critical applications (i.e., all the applications related to the safety of humans), but also to predict lifetimes, program a scheduled maintenance or evaluate the structural performance. With the improvements made in technologies, sensors and sensing systems are mainly used to predict the health of a structure.

Therefore, the aim of this thesis is to identify a monitoring system constituted by sensor, which could work properly for a tensegrity structure. Exploiting the fact that tensegrity systems could be modular, a modular tensegrity bridge is first designed, then its dynamic behaviour is analysed and used to identify different damage mechanisms (such as relaxation or cutting of a tendon), and, in the end, a system of sensors is designed for that specific structure. All the steps are carried out by means of the finite element software SlangTNG.

The thesis will be divided in 4 different chapters. The first chapter will give an introduction on tensegrity structures, in order to understand better how tensegrity has been defined throughout the years, since its invention in the middle of the XX century until the present day. Moreover, few examples of tensegrity structures and of tensegrity-inspired structures will be presented and, also, the advantages and disadvantages of this type of structural system.

In the second chapter, the structure and its design will be presented. All the main points of the design of a tensegrity structure will be considered: in particular, the form-finding step will be analysed. In the same chapter, the static analysis, with and without applied loads, will be carried out and presented, to have a structure that is completely verified from a static point of view.

In the third chapter, the dynamic analysis of the structure will be carried out: first, the principles of the modal analysis will be introduced from a theorical point of view, then it will be applied to the previously designed structure. Subsequently, the response of the structure in case of free vibrations will be analysed using an iterative solution given by Newmark's method. A study of fundamentals of signal theory, in particular for what concerns the concept of Fourier transform, will be deepened in this chapter too, in order to introduce the frequency response function. This will be then exploited to analyse the previously studied response of the structure.

In the fourth chapter, finally the structural health monitoring will be presented, from a theorical point of view first, and then applied to the case. This will be vibration-based and completely carried out on the finite element model of the structure. Therefore, different possible causes of damage will be analysed and compared in terms of fundamental frequencies of the system, response of the structure and frequency response function with respect to the healthy situation. In this same chapter, the sensors system will be designed, to prevent the structure from damage, exploiting the direct relation between the number of sensors and the number of degrees of freedom of the structure. The natural frequency will be considered as main damage indicator and the design of the sensors' system will be mainly based on the shift between the natural frequencies for a different number of sensors.

Finally, the conclusions will summarize the work done in this dissertation, by identifying the best sensors' system design for the type of tensegrity structure analysed. As previously mentioned, structural health monitoring for tensegrity structures is still a developing field and, consequently, it's also interesting to address possible future developments in this last chapter.

2 Tensegrity structures in civil engineering

2.1 Definitions

As briefly mentioned in the introduction, the term tensegrity comes from the contraction of the two words ‘tensile’ and ‘integrity’. More in general, it is possible to say that the term tensegrity contains all “*the structural rules, involving the creation of complex systems elements which are only compression or tension*”. Basically, the term tensegrity reflects the structural rules governing this type of structures.

A lot of different definitions about tensegrity were given among the years and, according to Motro, we can speak of an “ambiguity” of definitions. In particular, two big families can be distinguished: the definition according to the patents and an extended definition.

Despite tensegrity structures were studied since twenties of the XX century, their first definition, contained in his own patent, registered in 1959 and granted in 1962, was given by Robert Buckminster Fuller, who described the tensegrity principle as “*an island of compression inside an ocean of tension*”. According to this statement, the only requirement for having a tensegrity system is to have some compression matter inside a tension matter. The generality of this definition allows its application not only to the field of civil engineering, but also to other type of works (such as art works).

In 1963, David Georges Emmerich proposed its own patent (granted one year later), studying more complex structures, calling them “*structures tendues et autotendants*”. Emmerich stated that he invented the first set of “autotendants” (i.e., self-tensioning) structural units in 1958, as opposition to the structural principle of self-supporting elements (“autoportants” in French). Emmerich patented a similar system in 1959, called “Pearl Frameworks”, where he gave the following definition of the basic static principle “Séparation des travaux de compression et de traction. Structure compensée.": this means that the structure was made stable by applying tension obtained by the load itself or by pre-stressing.

A third patent called “Continuous tension, discontinuous compression structures” was registered by Snelson in 1960; the patent was then granted in 1965. Being Snelson an artist, more precisely a sculptor, he based the definition of tensegrity mainly on his art works and the principle they are built with, saying that “*Tensegrity describes a closed structural system composed of a set of three or more elongate compression struts within a network of tension tendons, the combined parts mutually supportive in such a way that the struts do not touch one another, but press outwardly against nodal points in the tension network to form a firm, triangulated, prestressed, tension and compression unit*”.

When discussing about the definitions proposed in the above-mentioned patents, the fact they were all registered and granted in the same range of time certainly stands out. From a chronological point of view, the patents are not so well distinguishable. The main consequence is that it is not possible to affirm for sure who is the inventor of tensegrity systems, still representing a controversial matter of study.

On the other side, all the definitions contain the same basic concept. So, combining the three different definitions, Motro proposed its own patent-based definition: "*Tensegrity systems are spatial reticulate systems in a state of self-stress. All their elements have a straight middle fibre and are of equivalent size. Tensioned elements have no rigidity in compression and constitute a continuous set. Compressed elements constitute a discontinuous set. Each node receives one and only one compressed element*".

This definition represents a good description of the basic principles governing tensegrity structures: first of all, the spatiality and the structural layout that give pure compression or pure tension in elements are referred to as "*spatial reticulate systems*". Then, it's clear that the stiffness in these structures is given by the application of self-stress, without any other load applied.

The continuity and discontinuity of respectively tension elements and compression elements are pointed out, as well as the fact that tension elements have no rigidity in compression. There is no need to make the same statement for compression elements having no rigidity in tension, because from a practical point of view an element in compression and in tension is usually used, even if at the end it is not subjected to tension.

Some fundamental points can therefore be derived from this patent-based definition: tensegrity systems are composed by elements in compression and elements in tension, i.e., struts and cables; compression struts represent a discontinuous set inside a continuous set of tension cables, obtaining a totally equilibrated structural system. The need for an extended definition comes from the restricted field of application of the previous definitions.

A first extended definition was proposed by Anthony Pugh in its own book "An introduction to tensegrity" (1976) and it describes a tensegrity system as established when "*a set of discontinuous compression components interacts with a set of continuous tensile components to define a stable volume in space*".

According to Motro, this last definition needs to be slightly changed to include two different aspects regarding tensegrity: the compression elements are included inside the tension elements (the expression 'interacts with' doesn't underline this characteristic) and the stability of the volume in space is the self-equilibrium stability.

So, Motro suggested the following extended definition: "*A tensegrity system is a system in a stable self-equilibrated state comprising a discontinuous set of compressed components inside a continuum of tensioned components*".

As briefly mentioned in the introduction of this dissertation, tensegrity systems still represent nowadays an open research field; this led to the presentation of new studies and, therefore, of new definitions. Consequently, throughout the years, other definitions were suggested by different authors who studied the structural behaviour and the form of tensegrity structures. Here are some of these definitions as example.

Miura and Pellegrino in 1999 gave a more encompassing interpretation of a tensegrity system as "*any structure realized from cables and struts, to which a state of prestress is imposed that imparts tension to all cables*".

Oliveira and Skelton proposed in 2009, in the first chapter of their book "Tensegrity Structures", the following definition of tensegrity system: "*A tensegrity system is composed of any given set of strings connected to a tensegrity configuration of rigid bodies*". According to the authors, a configuration is said to be tensegrity if there exists a connectivity between the tensile parts of structures that stabilizes the whole configuration without any external force applied. The tensile parts are referred by the authors to as strings.

Hanaor gave a more general definition, describing tensegrity structures as "*internally prestressed, free-standing pin-joined networks, in which the cables or tendons are tensioned against a system of bars or struts*". As underlined from the author in his definition, the main difference between tensegrity structures and conventional prestressed cable networks is the internal pre-stress, which makes the whole structure free-standing, without any need for massive anchorage systems.

The above-mentioned definitions are different between each other, but they all have some common points, which are the characteristic making a structure to be called tensegrity. In summary, it can be said that tensegrity structures represent a class of structures made of discontinuous compression elements inside a network of continuous tension element, to which pre-stress is applied in order to reach a state of self-equilibrium without any external load applied.

2.2 Motivations

Having largely defined this type of structures, is now possible to point out the reasons why they should be used.

One of the main advantages of tensegrity structures is given by the nature itself of tensegrity: the presence of pure tension and pure compression elements make the stabilization of the structure possible. Indeed, the tension stabilizes the structure: if compression elements loose stiffness when they are loaded, the tension elements gain stiffness when a load is applied. In the case of axially loaded members, the forces given by loading act through the mass centre: in the case of compression, the cross-section of the element will increase, while, in the case of tension, it will decrease. So, a large stiffness-mass ratio can be achieved using more tensile elements than compression ones.

The fact that the elements of a tensegrity structure are only axially loaded implies a higher reliability when modelling it: in particular, if an element is axially loaded only, it will not experience any type of bending. Member that experiences deformation in only one dimension are in general more reliable than elements that experience deformation in two or three dimensions.

Tensegrity structures are also mostly modular and lightweight structures; therefore, they can be adapted to different locations and purposes. As it will be pointed out in the next section, only in the civil engineering field there are many examples of applications: tensegrity modules can be used for example in the case of bridges, as well as in the case of roof skeletons, arches, or towers. Moreover, the modules allow to obtain different types of structures just rotating of some degrees the module or just changing the basic module, for example using a simplex rather than a tripod.

Their lightweight is fundamental not only from a structural point of view, but also aesthetically: the aesthetic appearance of this type of systems is indeed very pleasant, due to the feeling of lightness they give within the space in which they are designed. Lightweight constructions have a lot of different benefits: for example, they are more affordable than heavyweight constructions, and more sustainable, with important savings from an environmental point of view.

Tensegrity systems are very efficient: as said before, tensegrities are lightweight structures, with a very small mass, being formed only by steel or aluminium elements. This means that the material is needed only for compression and tension elements, which also represent the essential load paths. All the longitudinal members are so arranged in a way (sometimes unusual and non-orthogonal) that a very high strength is achieved with a very small mass. Moreover, sometimes very high levels of strength can be achieved with a relatively low stiffness.

A lot of studies have shown that tensegrity structures can be self-deployable structures: they can therefore experience a large change of shape from a compact configuration to an extended serviceable and functioning configuration due to their capability to carry considerable displacements. In a world like the one we are living in, where adaptability and portability of structures are becoming more and more important, this is a unique advantage. For example, the portability of a structure allows to manufacture it in a factory and only on a second time to install it in the construction site. This not only would reduce the costs, but also the labour requirements.

The easy tunability of these structures allow to make small adjustments of a damaged structure; nowadays, the health monitoring of structures has become a fundamental aspect of structural design, and therefore there is increasingly the need for structures designed to allow tuning.

Another aspect is the possibility to exploit the members composing tensegrity structure not only as a load-carrying member of the structure, but also for example as a sensor, as an actuator, as a thermal insulator or as an electrical conductor. Therefore, with a proper choice of materials and geometry, the electrical, thermal, and mechanical energy inside the structure can be controlled.

The last aspect is given by the transversality of tensegrity: this is a principle which has a very extended field of applications. For example, tensegrity can be naturally found in biology: it is the case of the nanostructure of spider fibers, where amino acids form hard sheets, organized in a discontinuous way, that can take compression, and thin strands, in a continuous network, that can take tension. Also, cells have been described using a tensegrity model, but examples of tensegrity models can be found also in the inorganic chemistry field, for example in the case of amorphous silicon, and in anatomy field, for example the human spine.

As said so far, tensegrity systems have a lot of advantages and they certainly represent an interesting field of research, but they also represent a challenging design problem. Especially in the field of civil engineering, designing a tensegrity structure requires an initial "guess" of the structure's topology, which should be optimized to have a self-equilibrated structure.

Moreover, tensegrity has a limited load bearing: when major external loads are applied, these structures tend to deflect. That is the reason why, for examples, when designing tensegrity bridges only pedestrian bridges are considered. Also, in the case of existing structures, as we will see in the next chapter, the structures will always be minimum load bearing structures, such as towers, domes, or pedestrian bridges.

If the lightweight characteristic represents one of the main advantages, it can also be considered as a disadvantage: the size of the elements is indeed limited by the bulk density, because when this last one decreases, the structure size increases.

The level of pre-stress to be applied in the design stage also represents a challenging problem: the pre-stress should be high enough to support critical loads and to make the cables stay in tension, but they shouldn't be so much large to overcome the strength in tension.

The arrangement of the bars can also represent a disadvantage for two main reasons: the first one is that the compression bars should have a cross-sectional area large enough to bear both the strength in compression and the buckling of the single bars, but not too large, otherwise one could have the “bar congestion” problem. The bar congestion is basically the creation of a system of overlapping compression bars, which, obviously, cannot be realized from a practical point of view.

A second reason is related not only to the arrangement of the compression bars, but also to the arrangement of the tension cables: the way all the elements are arranged can determine the complexity of the structure. If the structure is too complex, it will be very difficult to be built, and it will require a lot of labour requirements, contrasting with the small amount of building material used. Therefore, if, on one hand, it is possible to reduce the expenses due to what is saved from material, the costs for the labour requirements and for the design will be relevant.

This very high design complexity is enhanced by the unavailability of codes regulating the design of tensegrity: when a tensegrity structure is designed, there are no guidelines or templates to refer to, also because only a few structures have been built.

As widely explained in the definitions related chapter, tensegrity was discovered in the first decades of the XX century, but it was studied only starting from the half of the last century. This means that it represents a relatively new concept: if on one hand it represents an interesting field of research, on the other hand dealing with a technology that so much has still to be discovered about adds some level of difficulty to any possible case study considered.

2.3 Examples of application in civil engineering

Due to their transversality, tensegrity structures have been used in different fields. However, in civil engineering field, only few examples exist, even if in different shapes, and most of the structures cannot be properly defined as tensegrity, but more as tensegrity-inspired structures. On the other hand, due to their innovativeness, tensegrity structures have been largely used for art works.

The most known examples are the art works of Snelson, in particular his towers, not only as decorative miniature objects, but also made on a human-scale. One of his most famous works is indeed the Needle Tower, composed of interconnected tensegrity modules with elements made of aluminium and stainless steel. Snelson designed two different Needle Towers: one has been built in 1968 as a part of the Hirnshon Museum & Sculpture Garden in Washingon D.C., the other one has been built in 1969 in the Kröller Müller Museum in Otterlo (Holland).

Figure 1 - Needle Tower I (Courtesy of: http://www.civicartsproject.com)

Figure 2 - Needle Tower II (Courtesy of: https://www.flickr.com)

Another example of tower, whose structural design was done by Mike Schlaich, is given by the Warnow Tower: the basic idea is the same than the Needle Tower one, but it represents the tallest tensegrity tower ever built. The tower was built in 2003 as part of the Gardening Fair in Rostock (Germany). The structure is constituted by six Simplex modules made of aluminium and stainless steel: each module is then rotated by 30° in turn. The needle on the top was added to give a greater height to the tower, which in total is 49.2 meters tall.

Figure 3 - Warnow Tower (Courtesy of: https://tensegritywiki.com/)

Even if there are not many existing tensegrity structures, it is possible to say with certainty that there are other concepts like tensegrity, more used in the case of civil engineering application. One of these concepts is represented by the tensile structures and some of the most famous examples of application of tensile structures in civil engineering field is given by the architect and engineer Frei Otto. His most well-known work is represented by the Munich Olympic Stadium, but are worth it to be mentioned also the Music Pavilion of the Bundesgartenschau in Kassel (Germany), built in 1955, and the German Pavilion at the World's Fair in Montreal (Canada), built in 1967. Frei Otto studied how to exploit the tensile properties of the materials from a structural point of view. Tensegrity structures and tensile structures are different, and they shouldn't be confused, but the basic idea beyond their structural principle is undeniably very similar: both the structures want to exploit the properties of the materials to reach a state of self-equilibrium.

Figure 4 - Munich Olympic Stadium (Courtesy of: https://www.alamy.it/)

Figure 5 - Munich Olympic Stadium (Courtesy of: https://www.alamy.it/)

The tensegrity principle is mostly employed to design skeletons in the case of roofs. The architect Roberto Ferreira designed, exploiting the tensegrity principle, the roof of the Stadium of the city of La Plata (Argentina). The roof is composed by some masts suspended by triangular pre-compressed elements (i.e., cables). The masts are made of metal, while the cables are made of steel. This skeleton is then covered by a membrane made of a mesh with a Teflon cover. The weight of the roof is supported by a perimetral compression ring made of steel tubes.

Figure 6 - La Plata Stadium (Courtesy of: https://90lineas.com/)

Figure 7 - La Plata Stadium (Courtesy of: https://www.stadiumguide.com/)

An additional interesting example of application of a tensegrity structure as a roof skeleton is given by the White Rhino, built in Chiba (Japan) in 2001. This structure has been built in the University of Tokyo's experimental centre as location of different university's laboratories. The basic tensegrity skeleton is the so-called Simplex, which is one of the simplest tensegrity frames. In the case of the White Rhino, in addition to the twisted triangular prism constituted by nine tendons and three compression struts, three more tendons were placed between six unconnected point of the Simplex skeleton, to improve the overall rigidity of the frame. Therefore, it's possible to say that its shape is rather trapezoidal than prismatic.

Figure 8 - White Rhino (Courtesy of: https://www.researchgate.net/)

For what concerns infrastructures, such as bridges, the most important example is the well-known Kurilpa Bridge, built in 2009 in Sidney (Australia). The pedestrian bridge was designed by the architecture-engineering firm Ove Arup & Partners. However, it is necessary to underline that it is not possible to define that bridge as a tensegrity structure, but it's more suitable referring to as a "tensegrity-inspired" structure, as reported by the designers themselves. The bridge is constituted by compression masts and tension cables and wants to recall the modularity of tensegrity structures.

Figure 9 - Kurilpa Bridge (Courtesy of: https://aehistory.wordpress.com/)

A further example of pedestrian tensegrity bridge is represented by the Pylons Bridge, built in Purmerend (Netherlands) in 2000 and designed by the architect Jord den Hollander. The structure has a modular nature, like in the case of the Kurilpa Bridge, made of both pre-stressed and compressed elements. The pre-stressed elements connect the compressed ones, which, therefore, never touch each other. The deck is indirectly suspended between 36 columns, connected to the deck itself and to the foundations through tensile cables. This configuration allows to have the visual effect as the deck is completely floating.

Figure 10 - Pylons Bridge (Courtesy of: https://www.octatube.nl/)

3 Design of a tensegrity structure

3.1 An overview on the design of tensegrity structures

In the previous chapter, tensegrity structures have been defined as an assembly of continuous tension elements containing a discontinuous set of compressive elements. Therefore, the tensegrity structure configuration itself depends on how all the elements composing it are assembled.

The elements, however, cannot be randomly assembled, but they should be built in a specific way. In particular, the structure configuration should be done in such a way to reach a state of self-equilibrium, when it is subjected only to pre-stress of the tension elements.

Indeed, a tensegrity structure is, by definition, a self-equilibrated structure when no external loads are applied. In general, it can be said that, if a tensegrity structure results to be stable, its topology is acceptable. Therefore, the topology should be defined firstly: by topology is meant the relational structure between the elements, so the number of nodes, compression bars and tension cables, and how all these elements relate to one another. Then, the analysis of the structure can be done.

A complete analysis of a tensegrity structure is made of three steps:

1. The first step is represented by form-finding, without any external load applied, which consists in finding a stable self-stress state.
2. Implementation of self-stress, which is done applying the pre-stress to the structure; from an undeformed configuration, which is the one resulting from form-finding, we pass to a deformed configuration, where the compressed bars are shortened of a defined length.
3. Application of external loading and study of the structure behaviour with loads applied.

The tensegrity systems should also be characterized: this can be done computing the number of self-stress states and the number of infinitesimal mechanisms, which allow to determine if a system is statically and/or cinematically indeterminate. Defining the number of members with bilateral rigidity (i.e., the number of compression bars plus the number of tension cables) b and the number of nodes N, the number of self-stress states s can be defined as:

$$s = b - r_A \tag{2.1}$$

Correspondingly, the number of mechanisms m can be defined as:

$$m = N - r_A \tag{2.2}$$

The term r_A represents the rank of the equilibrium matrix $[A]$, defined in a such way that:

$$[A]\{T\} = \{f\} \tag{2.3}$$

with $\{T\}$ as the vector of internal forces and $\{f\}$ the vector of external actions on nodes.

Designing a tensegrity system cannot be defined as a simple and linear process: as pointed out in the previous chapter, tensegrity systems have no codes or regulations available to refer to. Moreover, their behaviour when subjected to external loads is a non-linear behaviour and their flexibility can lead to very large displacements even for small deformations in the case of critical elements.

This complex behaviour coupled with the design parameters which should be considered makes the design of tensegrity structures a challenging task. This implies continuous modifications, for example in material properties or in the pre-stress applied to the tension cables.

3.2 Theoretical background

3.2.1 Form-finding process

Form-finding is defined as "*finding an optimal shape of a form-active structure that is in (or approximates) a state of static equilibrium*" (Veenendal, Block, 2012). Form-finding is relevant in structures with form-active shapes, which cannot be known in advance: when no bending occurs and loads are transmitted only through axial forces, the shape is determined by forces and vice versa. This principle can be referred to as "principle of form follows force".

The form-finding process can be done using different methods, which, basically, can be divided in three different classes: stiffness matrix methods, geometric stiffness methods and dynamic equilibrium methods.

Stiffness matrix methods exploit the properties of the elastic and geometric stiffness matrices and, in particular, the stiffness matrix is used to make the calculations converge to a self-equilibrated and stable configuration. This method requires an iterative algorithm: for a given topology system, the stiffness matrix, which should be positive definite, should be used to calculate the nodal displacements and the nodal coordinates, until the out-of-balance forces are lower than a value imposed as initial condition.

Geometric stiffness methods, as can be understood by the name, exploit the geometric stiffness matrix only, being therefore material independent. One well-known and of the most used method included in this category is the force density method: it uses the ratio between the normal stress acting on the element and the length of the element, called force-density coefficient, to express the equilibrium equations of forces at each node of the structure. Force density method was first proposed by Linkwitz and Sheck, but it has been revisited throughout the years by other authors.

Dynamic equilibrium methods have as their main point to solve the problem as a dynamic problem in order to obtain a steady-state solution, which is also corresponding to the static solution of the static equilibrium. One of the most famous methods belonging to this group is the dynamic relaxation method, first proposed by Barnes. Dynamic relaxation transforms a time-independent equilibrium problem, which would be the static problem, to a time-dependent equilibrium problem, which would be the dynamic problem, in order to find the equilibrium configuration corresponding to that tensile stress distribution.

In the case of this dissertation, the form-finding process is based on the above-mentioned force-density method: the nodal coordinate differences between the linked nodes are associated to the force-densities coefficients, which are in equilibrium with the external loading forces. Since the nodes' coordinates are part of the equilibrium equation, force-density method is a suitable method for form-finding. In particular, it can be applied to a tensegrity structure because both cables and bars are respectively subjected to pure tension and pure compression, being only axially loaded.

Consequently, a new coefficient, called forced-density coefficient and defined as the ratio between the normal stress acting on the element and the reference length of the element, is introduced.

Referring to the element as e, one has:

$$q_e = \frac{T_e}{l_e^0} \tag{2.4}$$

Writing the equilibrium equation for the element e connected by the nodes i and j and substituting the previous equation, it follows:

$$\sum_e \frac{(x_i - x_j)}{l_e^0} T_e = f_{ix} \tag{2.5}$$

$$\sum_e (x_i - x_j) q_e = f_{ix} \tag{2.6}$$

This equation can be rewritten in a matrix form (i.e., the form used in the calculations), introducing the connectivity matrix $[C]$, as:

$$[C]^T [Q][C]\{x\} = \{f_x\} \tag{2.7}$$

$[Q]$ is a diagonal square matrix, that contains the force-density coefficients vectors:

$$[Q] = diag(q) \tag{2.8}$$

Considering the index i referred to the elements of the structure and the index j referred to the nodes of the structure, the elements $C(i,j)$ of the connectivity matrix $[C]$ are defined as:

$$C(i,j) = \begin{cases} +1 & for\ node\ i \\ -1 & for\ node\ j \\ 0 & otherwise \end{cases} \tag{2.9}$$

When a system is in equilibrium, the force-density vector $\{q\}$ and the vector of the external forces applied to the nodes $\{f\}$ are related by the so-called equilibrium matrix $[A]$ as follows:

$$[A]\{q\} = \{f\} \tag{2.10}$$

The equilibrium matrix $[A]$ is completely defined by the connectivity matrix $[C]$ and by the nodal coordinates' vectors $\{x\}$, $\{y\}$ and $\{z\}$ as:

$$[A] = \begin{bmatrix} [C]^T diag([C]\{x\}) \\ [C]^T diag([C]\{y\}) \\ [C]^T diag([C]\{z\}) \end{bmatrix} \tag{2.11}$$

The first condition that should be satisfied involves the existence of at least one state of self-stress; this first rank condition can be written as follows:

$$rank(A) < \ n_e \tag{2.12}$$

where n_e is the total number of elements.

The second condition of form-finding using the force-density method involves the infinitesimal and inextensional matrix $[\Lambda]$:

$$[\Lambda] = [U_k]^T([I_{dim}] \otimes [D])[U_k] \tag{2.13}$$

The above-mentioned Kronecker tensor product results in:

$$[I_{dim}] \otimes [D] = \begin{bmatrix} [D] & \cdots & 0 \\ \vdots & \ddots & \vdots \\ 0 & \cdots & [D] \end{bmatrix}_{dim\ x\ dim} \tag{2.14}$$

where the subscript *dim* refers to the dimension of the problem (i.e., in our case, three dimensional).

$[D]$ is the force-density matrix given by the equation *(2.15)*, defined as:

$$[D] = [C]^T[Q][C] \tag{2.15}$$

$[U_k]$ is called the matrix of mechanisms and it is the right null-space matrix composed by the left singular vectors $\{u_k\}$ resulted from the Singular Value Decomposition (SVD) of the equilibrium matrix $[A]$. This means that, for the equilibrium matrix $[A]$ of dimensions m x n, there exist:

- An orthogonal matrix $[U] = [\{u_1\}, \dots, \{u_m\}]$
- An orthogonal matrix $[W] = [\{w_1\}, \dots, \{w_n\}]$
- A matrix $[V]$ with m positive elements v_{ii} $(i = 1, \dots, m)$

so that:

$$[A] = [U][V][W]^T \tag{2.16}$$

The coefficients v_{ii} are defined as the singular values of the matrix $[A]$, the vector $\{u_i\}$ is the i-th left singular vector and $\{w_i\}$ is the i-th right singular vector.

The left-singular vector $\{u_i\}$ doesn't represent a pure mathematical element, but it has a physical interpretation: defining r as the rank of the equilibrium matrix $[A]$, "*the first r equations show that the first r left-singular vectors are the external loadings in equilibrium with the internal stresses in the corresponding right-singular vectors, multiplied by the corresponding singular values. Therefore, we have r orthogonal sets of loadings and their* *corresponding orthogonal stresses in the members. The remaining s equations show that the last s right-singular vectors are self-equilibrated internal stresses of the members*" (Gan, 2020).

A similar interpretation can be derived for the right-singular vector $\{w_i\}$: defining k as the difference between the total number of infinitesimal mechanisms and the rank r of the equilibrium matrix $[A]$, "*the first r equations show that the first r left-singular members corresponding with the right-singular vectors, divided by the corresponding singular values. Hence, we have r orthogonal sets of nodal displacements and their corresponding orthogonal strains in the members. The remaining k equations show that the last k left-singular vectors are zero energy of displacement modes, i.e., no strains in the members*" (Gan, 2020).

Calculating the eigenvalues of the matrix $[\Lambda]$ it is possible to obtain the rigid body displacements and the positive stiffnesses. The positive stiffnesses correspond to the self-stress states.

$$eig(\Lambda) = \{\lambda_k > \cdots > \lambda_1 > 0 \qquad \lambda_r = \cdots = \lambda_1 = 0\} \tag{2.17}$$

So, it is necessary now to check if there are one or more positive values between the eigenvalues; if this situation is verified, it possible to proceed with the second rank condition, defined as:

$$rank(D) < n_n - dim \tag{2.18}$$

where n_n is the total number of nodes.

3.2.2 Implementation of self-stress through an iterative procedure

The behaviour of a structures is defined non-linear when the structure itself experiences large deformations and displacements under external loading. When the structural behaviour is non-linear, the structural stiffness does not remain constant like in the case of a linear analysis, but it becomes strictly related to its deformation. Tensegrity systems are non-linear systems, therefore an iterative procedure when analysing their behaviour is required.

Non-linearity can have different origins: it can origin from the material (like in the case of plasticity), or it can have a geometrical origin. In the case of tensegrity structures, the non-linearity has a geometrical origin, whereas the material non-linearities are not considered.

The iteration is repeated until the convergence to an equilibrium state is achieved; in this stage, no external actions are considered.

The system to be solved is:

$$([K_L] + [K_G])\{u\} = [R] - [F] \tag{2.19}$$

$\{u\}$ is the displacement vector of the system, $[R]$ represents the external actions and $[F]$ represents the internal efforts.

$[K_L]$ and $[K_G]$ are the linearised stiffness matrix, which considers the small-deformation truss analyses, and the geometrical stiffness matrix, which considers the self-stresses (or pre-stresses).

The sum of the linearised and the geometrical stiffness matrix results in the tangent stiffness matrix, which relates the displacement vector to the external forces vector.

$$[K_T] = [K_L] + [K_G] \tag{2.20}$$

The linearised stiffness matrix $[K_L]$ is defined as:

$$[K_L] = \frac{EA}{L_0} \tag{2.21}$$

where E is the elastic modulus, A is the cross-sectional area and L_0 is the free length of the bar when no loads are applied.

The geometrical stiffness matrix $[K_G]$ is defined as:

$$[K_G] = \frac{SA}{L_0} \tag{2.22}$$

Where S is the Piola-Kirchhoff stress matrix, A is the cross-sectional area and L_0 is the free length of the bar when no loads are applied.

The implementation of self-stress or pre-stress is done exploiting an iterative process and, in the case of tensegrity structures, the Newton-Raphson procedure has been used, which exploits the tangent-line approximation.

Considering $f(x)$ as a generic well-behaved function, r as the root of the equation $f(x) = 0$ and x_0 as the estimate of r, it is possible to write:

$$r = h + \ x_0 \tag{2.23}$$

The equation $f(x) = 0$ can be rewritten considering $x = r$ as:

$$f(r) = 0 = f(h + x_0) \approx f(x_0) + hf'(x_0) \tag{2.24}$$

If the derivative $f'(x_0)$ is not close to 0, one has:

$$h \approx -\frac{f(x_0)}{f'(x_0)} \tag{2.25}$$

Substituting the equation *(2.25)* into the equation *(2.23)*:

$$r = x_0 + h \approx x_0 - \frac{f(x_0)}{f'(x_0)} \tag{2.26}$$

This equation *(2.26)* can be then rewritten as:

$$x_1 = x_0 - \frac{f(x_0)}{f'(x_0)} \tag{2.27}$$

Extending the equation *(2.27)* to a more general case:

$$x_{n+1} = x_n - \frac{f(x_n)}{f'(x_n)} \tag{2.28}$$

The geometric interpretation of this equation is given by the tangent of the function and the non-linear problem is so replaced by a set of linear problems.

In the case of a tensegrity structure, the procedure will be the following:

1. Initialization conditions of the problem.
2. The matrix $[R]$ is defined as the difference between the global resisting force and the internal efforts of the system due to the loading condition.
3. The displacements are found as function of the tangent stiffness of the structure and of the matrix $[R]$.
4. The displacement vector is updated.
5. The procedure is repeated as many times as a convergence is ensured.

3.2.3 Structure's behaviour under external loads

When designing a tensegrity structure under the action of external loads, the cross-section area of steel elements should be studied differently in the case of tension cables and compression bars. Indeed, if in the case of tension cables, it is necessary only to verify the acting tension force, in the case of compression bars, not only the acting compression force needs to be verified, but the effects of buckling should be considered too.

According to the EN 1993-1-1 (Design of steel structures: general rules and rules for buildings), the design value of the tension force should satisfy:

$$\frac{N_{Ed}}{N_{t,Rd}} \leq 1 \tag{2.29}$$

The resisting tension force should be computed as:

$$N_{t,Rd} = min \begin{cases} N_{pl,Rd} = \dfrac{Af_y}{\gamma_{M0}} \\ N_{u,Rd} = \dfrac{0{,}9A_{net}f_u}{\gamma_{M2}} \end{cases} \tag{2.30}$$

where $N_{pl,Rd}$ is the design plastic resistance of the gross cross-section and $N_{u,Rd}$ is the design ultimate resistance of the net cross-section.

The characteristic yielding strength f_y and the characteristic ultimate strength f_u are steel properties, defined with respect to the type of steel chosen.

In the case of tubular solid cross-section, the gross cross-section area and the net cross-section area are the same, so:

$$A = A_{net} \tag{2.31}$$

On the other hand, the design value of the compression force should satisfy:

$$\frac{N_{Ed}}{N_{c,Rd}} \leq 1 \tag{2.32}$$

The resisting compression force should be computed as:

$$N_{c,Rd} = \frac{Af_y}{\gamma_{M0}} \tag{2.33}$$

For what concerns buckling, according to the paragraph 6.3 of EN 1993-1-1, a compression member should be verified as follows:

$$\frac{N_{Ed}}{N_{b,Rd}} \leq 1 \tag{2.34}$$

The acting compression force should be then lower or at least equal to the design buckling resistance of the compression member, defined as:

$$N_{b,Rd} = \frac{\chi Af_y}{\gamma_{M1}} \tag{2.35}$$

χ is the reduction factor for the relevant buckling mode:

$$\chi = \frac{1}{\phi + \sqrt{\phi^2 - \bar{\lambda}^2}} \tag{2.36}$$

It depends both on the non-dimensional slenderness $\bar{\lambda}$ and on the factor ϕ, defined as:

$$\phi = 0{,}5[1 + \alpha(\bar{\lambda} + 0{,}2) + \bar{\lambda}^2] \tag{2.37}$$

$$\bar{\lambda} = \sqrt{\frac{Af_y}{N_{cr}}} \tag{2.38}$$

N_{cr} is the critical buckling load, defined as "*the load at which the current equilibrium state of a structural element or structure suddenly changes from stable to unstable, and is, simultaneously, the load at which the equilibrium state suddenly changes from that previously stable configuration to another stable configuration with or without an accompanying large response (deformation or deflection). Thus, the buckling load is the largest load for which stability of equilibrium of a structural element or structure exists in its original (or previous) equilibrium configuration*". (Jones, 2006)

A system can be defined as stable if "*every small disturbance of the system results only in a small response after which the structure always returns to its original equilibrium state*" (Jones, 2006); on the other hand, if the same small disturbance results "*in a sudden change in deformation mode or displacement value after which the system does not return to its original equilibrium state*" (Jones, 2006).

From a practical point of view, N_{cr} can be calculated through the Euler's formula:

$$N_{cr} = \frac{EJ\pi^2}{l_0^2} \tag{2.39}$$

where E is the elastic modulus of the material and J is the inertia moment of the cross-section. In the case of a circular cross section, considering d as the diameter of the cross-section, J can be calculated as:

$$J = \frac{\pi}{64} d^4 \tag{2.40}$$

The critical load depends also on l_0, which is the effective length of the considered member. In general, the effective length l_0 depends on the boundary conditions, but in the case of tensegrity structures, the effective length of the compression members can be safely assumed as exactly equal to the distance between the nodes defining the members.

3.3 Case study: a pedestrian modular bridge

3.3.1 General description of the structure

In the first chapter of this dissertation, the wide range of applications of tensegrity structures has been largely pointed out. In particular, from the examples which have been reported, it can be understood that not a lot of bridges based on the tensegrity principle have already been built, except for the tensegrity inspired Kurilpa bridge and the pedestrian bridge in the Netherlands.

Some research studies on the design tensegrity bridges have been already made. Since there are not existing regulations regarding tensegrity structures, this previous research allows to have a guideline on the design of this case study. Consequently, a more precise design can be carried out.

With these premises, the choice of focusing the study on a pedestrian modular bridge was made. The modularity of the pedestrian bridge implies a very high adaptability of the structure, making it suitable for different locations. However, as previously stated in this dissertation, tensegrity structures are not high load bearing structures. Therefore, the bridge is pedestrian.

The case study of this dissertation is therefore represented by a modular tensegrity bridge, which has to be built in Vienna, Austria. The bridge is composed by 4 modules, that are equal to each other, in order to make the structure suitable not only in this specific case, but also considering a different number of modules, a different total length or a different location.

Each module is based on a simple geometric figure: it is built as a hexagon, which is 2.5 meters long for a total length of the bridge of 10 meters. Moreover, each module is 3.46 meters tall and 2 meters wide. On each module will be then installed a deck, for a net width of still 2 meters, but a net height of 1,96 meters.

The geometrical characteristics are reported in the table below.

Table 1 – Hexagon module's geometrical characteristics

L [m]	2,50
W [m]	2,00
W_N [m]	2,00
H [m]	3,46
H_N [m]	1,96

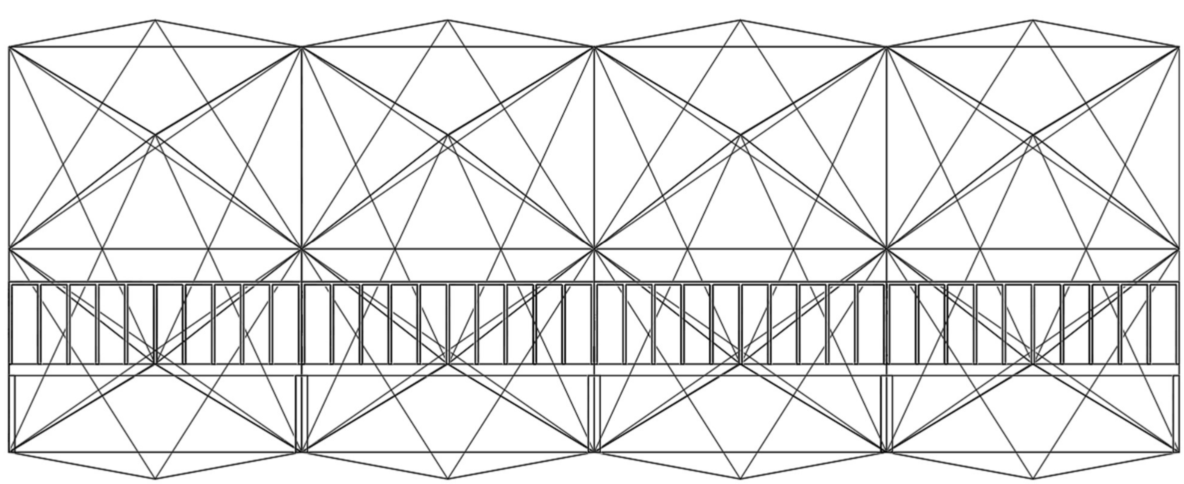

Figure 11 – Structure's lateral view

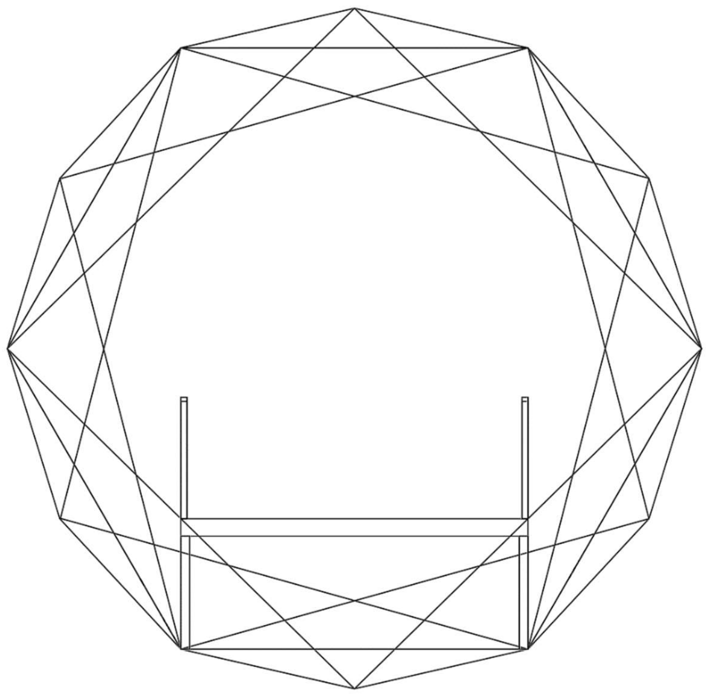

Figure 12 – Structure's front view

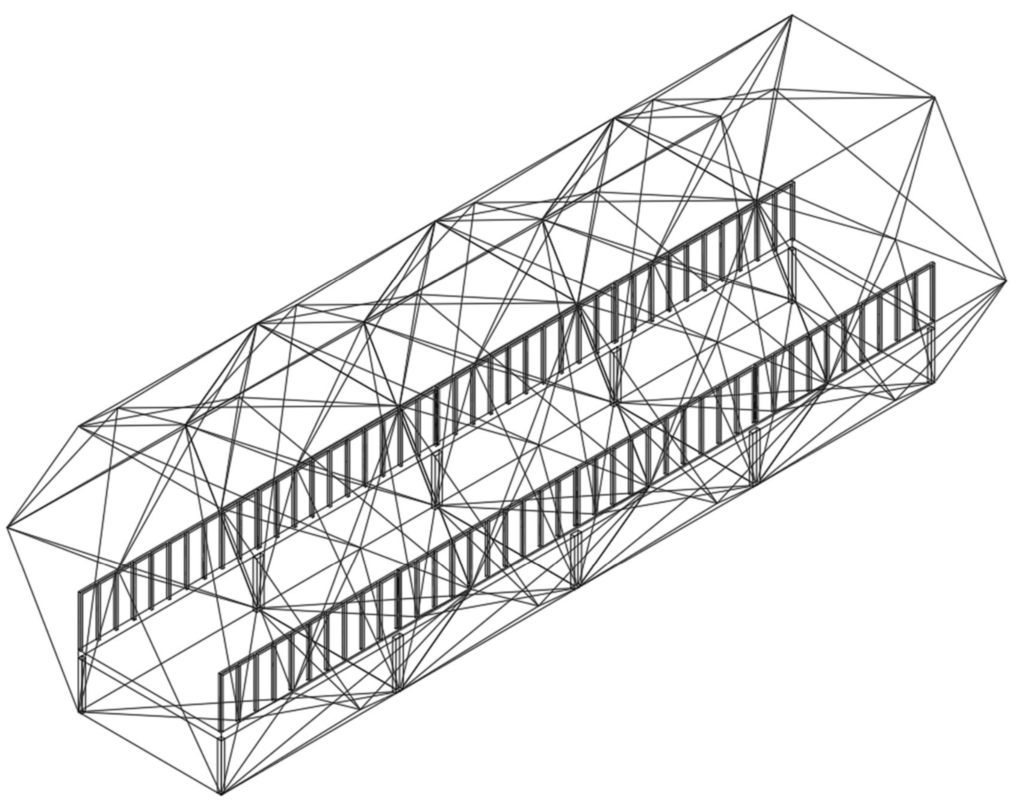

Figure 13 – Structure's 3D view

3.3.2 Topology of the structure

The first step was to define the topology of the structure, in order to obtain a detailed description of the relational structure between all the different elements.

For each module, a total number of 19 nodes, 18 compression bars and 36 compression cables were considered. For the whole structure, a total number of 58 nodes were considered, 72 compression bars and 126 tension cables were considered.

The total number of 19 nodes is derived from the sum of the 6 nodes composing the initial hexagon of the module, 6 nodes composing the final hexagon of the module, 6 nodes on the lateral surfaces of the module and 1 additional fictitious node in the middle of the module (needed for the FE software).

The relational structure for the whole structure is reported in the tables listed below.

Table 2 - Nodes coordinates

Nr. of the node	x [m]	y [m]	z [m]
1	0,00	0,00	0,00
2	2,00	0,00	0,00
3	3,00	1,73	0,00
4	2,00	3,46	0,00
5	0,00	3,46	0,00
6	-1,00	1,73	0,00
7	0,00	0,00	2,50
8	2,00	0,00	2,50
9	3,00	1,73	2,50
10	2,00	3,46	2,50
11	0,00	3,46	2,50
12	-1,00	1,73	2,50
13	1,00	-0,23	1,25
14	2,70	0,75	1,25
15	2,70	2,71	1,25
16	1,00	3,69	1,25
17	-0,70	2,71	1,25
18	-0,70	0,75	1,25
19	1,00	1,25	1,73
20	0,00	0,00	5,00
21	2,00	0,00	5,00

22	3,00	1,73	5,00
23	2,00	3,46	5,00
24	0,00	3,46	5,00
25	-1,00	1,73	5,00
26	1,00	-0,23	3,75
27	2,70	0,75	3,75
28	2,70	2,71	3,75
29	1,00	3,69	3,75
30	-0,70	2,71	3,75
31	-0,70	0,75	3,75
32	1,00	3,75	1,73
33	0,00	0,00	7,50
34	2,00	0,00	7,50
35	3,00	1,73	7,50
36	2,00	3,46	7,50
37	0,00	3,46	7,50
38	-1,00	1,73	7,50
39	1,00	-0,23	6,25
40	2,70	0,75	6,25
41	2,70	2,71	6,25
42	1,00	3,69	6,25
43	-0,70	2,71	6,25
44	-0,70	0,75	6,25
45	1,00	6,25	1,73
46	0,00	0,00	10,00
47	2,00	0,00	10,00
48	3,00	1,73	10,00
49	2,00	3,46	10,00
50	0,00	3,46	10,00
51	-1,00	1,73	10,00
52	1,00	-0,23	8,75
53	2,70	0,75	8,75
54	2,70	2,71	8,75
55	1,00	3,69	8,75
56	-0,70	2,71	8,75
57	-0,70	0,75	8,75
58	1,00	8,75	1,73

The connectivity of the nodes forming the compression bars and the tension cables is reported in the tables contained in Annex A.

The coordinates and the origin (corresponding to the node 1) in the three-dimensional space are considered as described from the drawing reported below.

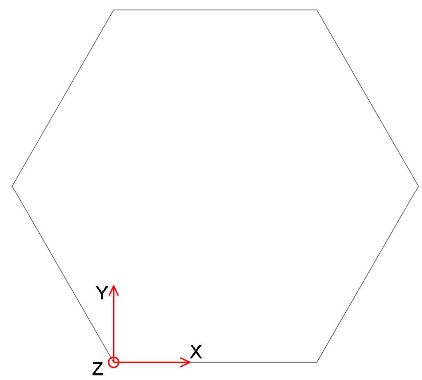

Figure 14 - Origin reference

3.3.3 Form-finding

Once the topology of the structure is defined, it is possible to proceed with the form-finding process. The main goal of form-finding process is to find a stable self-stress state of the structure. It was done creating a Matlab code, reported as annex of this dissertation. In the Matlab code, four additional nodes were considered, increasing the number of nodes from 54 to 58. These are fictitious nodes in the middle of the modules. The following steps were done:

1. The connectivity matrix was built as a 198x58 dimensioned matrix, with 198 as the total number of elements of the bridge and 58 as the total number of nodes, considering also the four fictitious nodes.

2. Starting from the connectivity matrix and the coordinates, the equilibrium matrix was built as a 174x198 matrix, where 174 derives from the sum of the 58 coordinates in the x-direction, the 58 coordinates in the y-direction and the 58 coordinates in the z-direction, while 198 is the total number of elements as usual.

3. The rank of the equilibrium matrix was calculated, and the first rank condition was defined as:

$$rank([A]) < N \tag{2.41}$$

   where N is the total number of elements.

4. The SVD (Singular Value Decomposition) of the equilibrium matrix was done and the force density vectors were introduced, resulting from the pre-loading analysis of the structure.

5. The diagonal square matrix containing the force-density coefficients was built and the force-density matrix was then obtained.

6. Once that the infinitesimal and extensional matrix was built, it was possible to calculate the eigenvalues of the problem, obtaining the following result:

$$eig([\Lambda]) = [0\ 0\ 0\ 0\ 0\ 0\ 0\ 0\ 0\ 0\ 0\ 0\ 0\ 0\ 0\ 1392{,}2\ 1957{,}4\ 5998{,}3] \tag{2.42}$$

   The first fifteen eigenvalues show the rigid body motion, the last three eigenvalues are positive (condition which should be verified as well) and represent the self-stress states.

7. A second rank condition was defined as:

$$rank([D]) < M - dim \tag{2.43}$$

   where M is the total number of nodes and dim is the dimension of the space, which in this case is 3.

3.3.4 Structural analysis

Once the form-finding was done, verifications on the structure have been made. The verifications can be summarized as reported in the following table.

Table 3 - Structural verifications

1a	All the bars remain in compression and all the cables remain in tension after the form-finding and the application of pre-stress before the application of the loads.
1b	All the bars remain in compression and all the cables remain in tension after the form-finding and the application of pre-stress after the application of the loads.

2a	Displacements at the nodes are very small compared to the initial lengths of the elements before the application of the loads.
2b	Displacements at the nodes are very small compared to the initial lengths of the elements after the application of the loads.
3a	The normal force acting on the compression bars is lower than the resisting force after the application of the loads.
3b	The normal force acting on the tension cables is lower than the resisting force after the application of the loads.
4	If, after the application of the loads, the entire structure is stable, the global buckling should not be verified. On the other hand, the local buckling must be verified for each compression bar after the application of the loads.

As it is possible to notice, some verifications should be made before and after loading of the structure. For example, in the case of the verification 1a and 1b it is necessary to verify that the structure remains tensegrity (i.e., to ensure pure compression and/or pure tension inside the structural elements) both before and after the application of the loads.

For what concerns the loads, in the case of this pedestrian bridge, two main loads have been considered: the self-weight of the structure as permanent load and the traffic load as variable load. The prestress load has been already considered in the pre-loading case.

The self-weight of the structure is calculated from the mass matrix representing the structure and a traffic load of 5 kN/m^2 is considered.

All the actions described and indicated above are to be combined linearly with each other through appropriate coefficients that take into account the expected duration of each action, the frequency of its occurrence and the probability of simultaneous presence of several actions.

In particular, the loads were then combined using the fundamental combination at ULS, as reported by equation *(2.44)*.

$$\gamma_{G1} * G_1 + \gamma_{G2} * G_2 + \gamma_P * P + \gamma_{Q1} * Q_{K1} + \gamma_{Q2} * Q_{K2} * \psi_{02} + \gamma_{Q3} * Q_{K3} * \psi_{03} + \cdots \quad (2.44)$$

where G_1 represents the structural permanent loads, G_2 the non-structural permanent loads, P the action due to precompression, Q_{K1} the dominant variable load and $Q_{K2,3,...}$ the other variable loads.

The other elements of the equation are coefficients: γ_{G1} is the partial coefficient of the structure's own weight, γ_{G2} is the partial coefficient of the weights of non-structural elements, γ_{Qi} is the partial coefficient of non-variable actions and $\psi_{0(i+1)}$ is the combination coefficient.

For what concerns our case, only G_1 and Q_{K1} have been considered, and to the coefficients γ_{G1} and γ_{Qi} the values 1,10 and 1,35 have been assigned respectively. The load combination is reported in the table listed below.

Table 4 – Loads' combination

Load	Characteristic value [N]	γ [-]	Design value [N]
Weight	16263,90	1,10	17890,29
Traffic load	75000,00	1,35	101250,00
	Total ULS		119140,29

The first verification consists of a check of the tensegrity condition: all the cables should remain in tension and all the bars in compression both before and after loads have been applied. From a practical point of view, this is true if the following condition is respected:

$$\sigma_{bars} \leq 0 \quad (2.45)$$

$$\sigma_{cables} \geq 0 \quad (2.46)$$

The second verification consists in checking that the displacements at the nodes are lower than the length of the elements. The compression bars have a length of 3,07 meters at minimum and 3,20 meters at maximum, the tension cables 1,62 meters at minimum and 2,00 meters at maximum.

For the verifications 3a, 3b and 4, some information on the materials and on the sections should be provided.

For both tension cables and compression bars, the chosen material is steel S275 with the following characteristics:

$$f_y = 275\ MPa \tag{2.47}$$

$$f_u = 430\ MPa \tag{2.48}$$

The following section areas were considered:

$$A_{bar} = 3000\ mm^2 \tag{2.49}$$

$$A_{cable} = 1500\ mm^2 \tag{2.50}$$

Applying the formulas reported in the previous sections, the resisting normal forces are:

$$N_{t,Rd} = 392857\ N \tag{2.51}$$

$$N_{c,Rd} = 785714\ N \tag{2.52}$$

Table 5 - Structural verifications

1a	$\sigma_{bars,\ \ pre-loading} \leq 0$ $\sigma_{cables,\ \ pre-loading} \leq 0$	VERIFIED
1b	$\sigma_{bars,\ \ post-loading} \leq 0$ $\sigma_{cables,\ \ post-loading} \leq 0$	VERIFIED
2a	$\|\|d_{x,\ \ pre-loading}\|\| \ll l_e$ $\|\|d_{y,\ \ pre-loading}\|\| \ll l_e$ $\|\|d_{z,\ \ pre-loading}\|\| \ll l_e$	VERIFIED

2b	$\lVert d_{x,\ \ post-loading} \rVert \ll l_e$ $\lVert d_{y,\ \ post-loading} \rVert \ll l_e$ $\lVert d_{z,\ \ post-loading} \rVert \ll l_e$	VERIFIED
3a	$N_{c,Ed} \leq N_{c,Rd}$	VERIFIED
3b	$N_{t,Ed} \leq N_{t,Rd}$	VERIFIED
4	$N_{c,Ed} \leq N_{cr}$	VERIFIED

3.3.5 Final remarks

As a conclusion, it is possible to compare the different situation of displacements before and after loading, highlighting that in both cases the structure is largely verified.

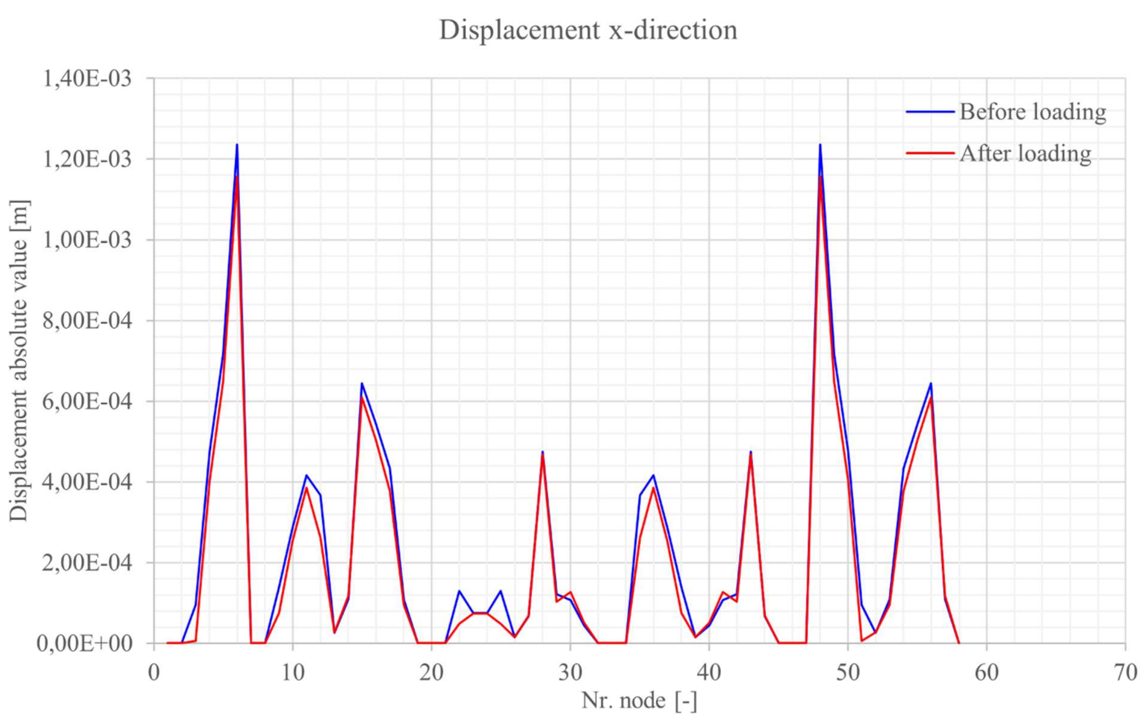

Figure 15 - Displacements x-direction comparison

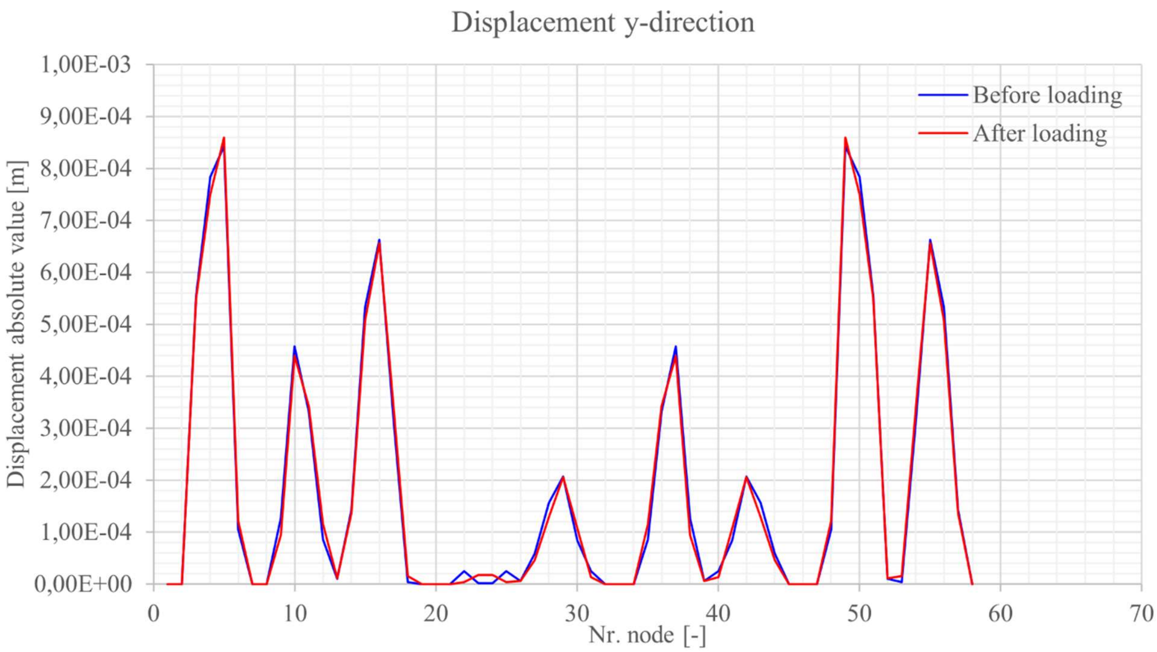

Figure 16 - Displacements y-direction comparison

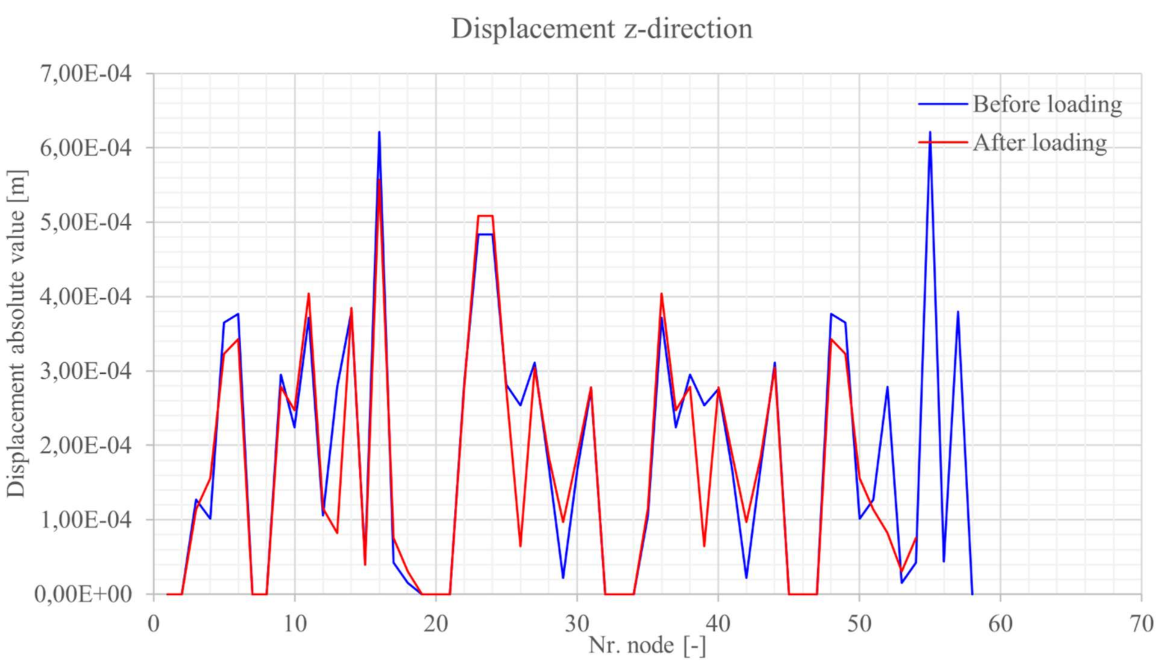

Figure 17 - Displacements z-direction comparison

In particular, it is possible to see that, probably due to the not very high loads, related to the fact the bridge is only pedestrian, there isn't a huge change in the situation before and after loading. The comparison can be done also for the stresses in the compression bars and in the tension cables before and after applying the loads, obtaining the results reported in the following tables.

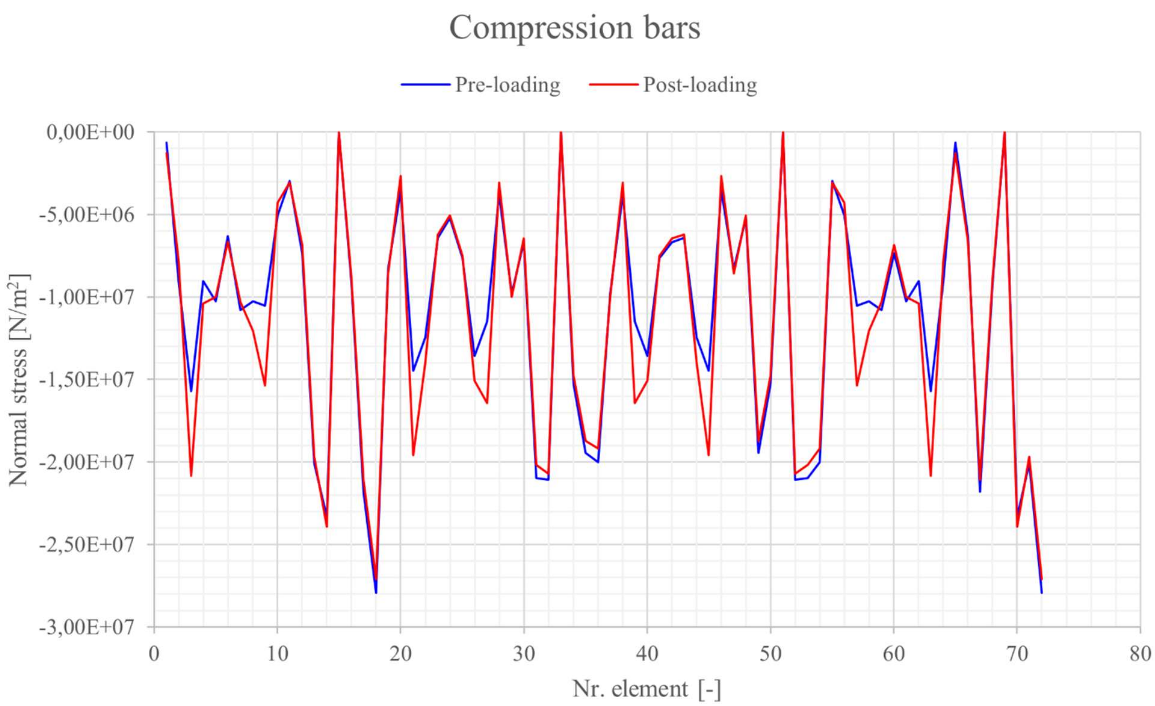

Figure 18 - Normal stress compression bars

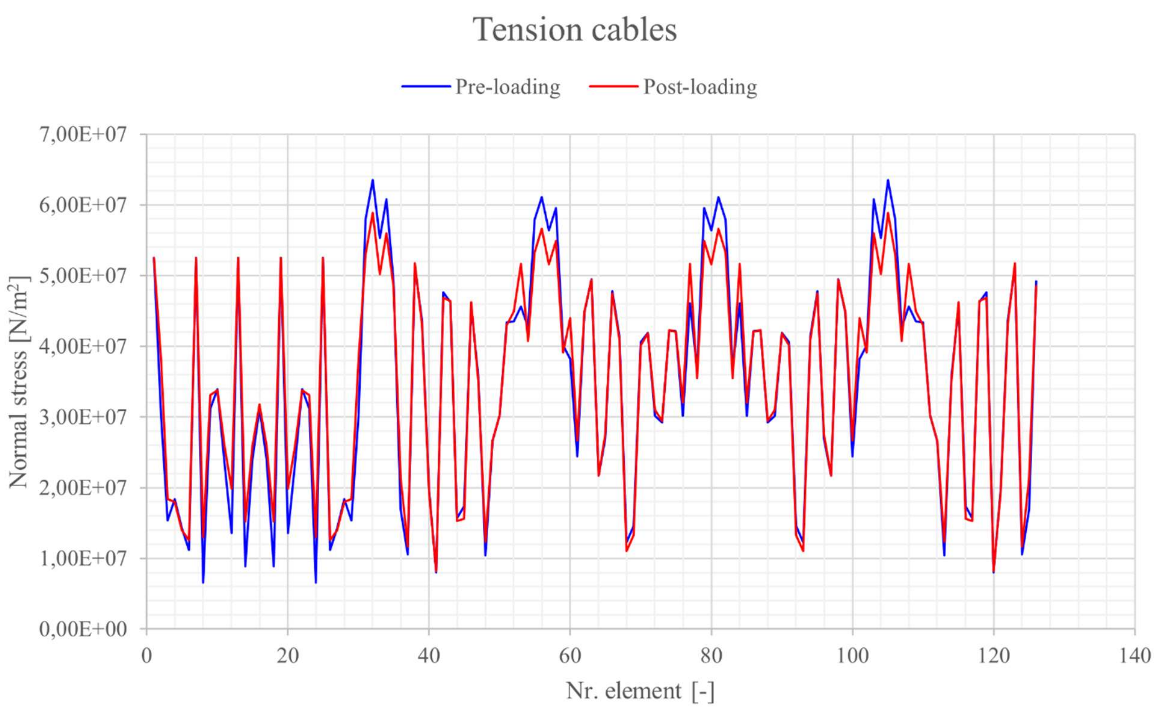

Figure 19 - Normal stress tension cables

Also in the case of stresses, it is possible to highlight the fact that there is no huge difference between the two cases, probably due to the small entity of loads.

The stresses are represented in the finite element model as follows:

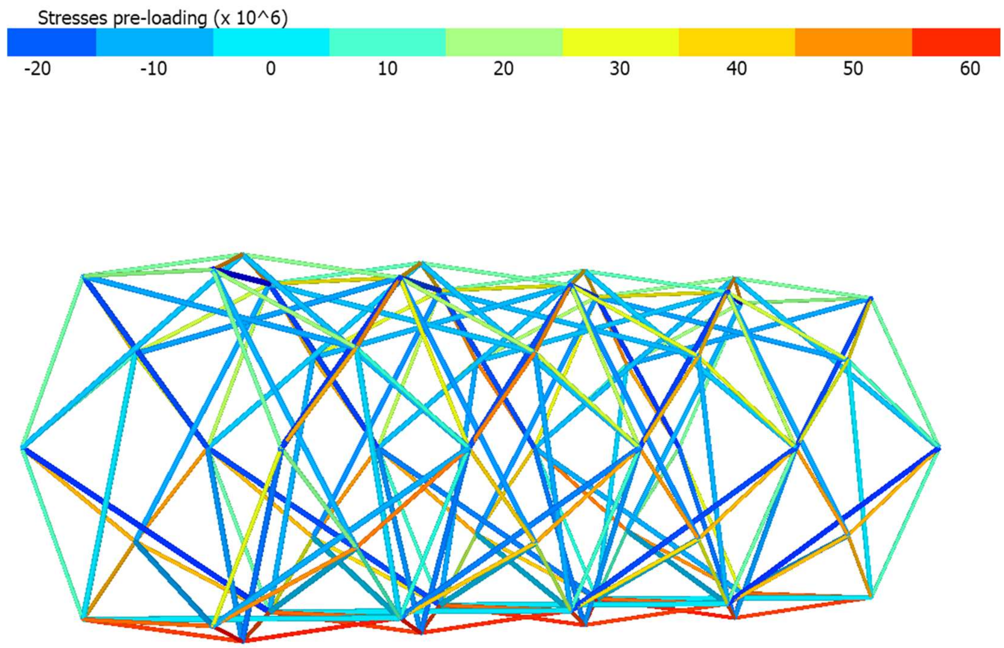

Figure 20 - Pre-loading stresses in FE model

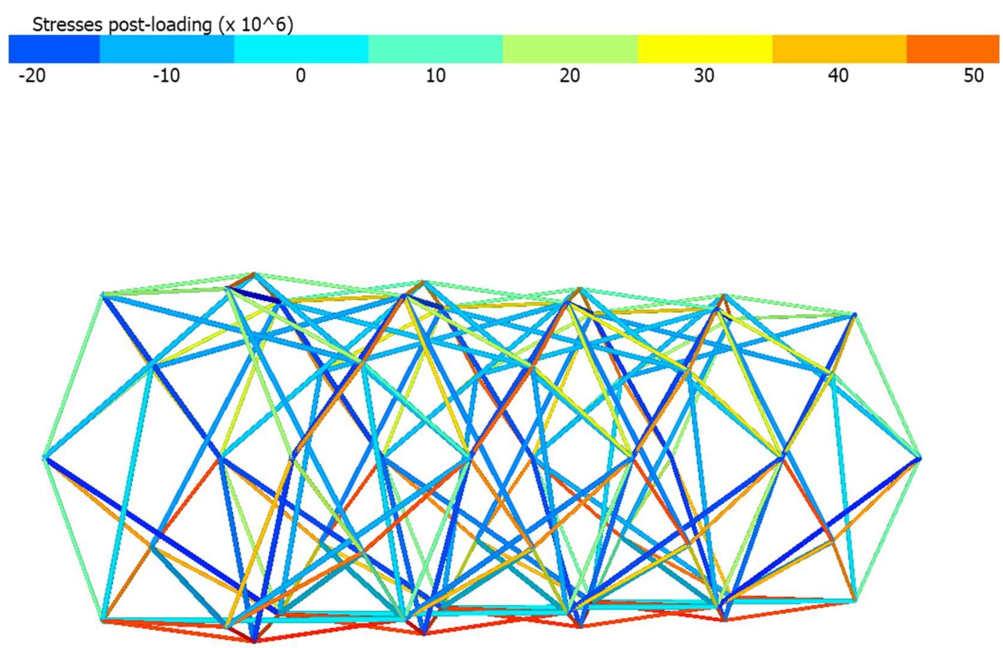

Figure 21 - Post-loading stresses in FE model

4 Dynamic analysis of a tensegrity structure

4.1 Modal analysis

When static analysis is done, the further step is represented by the dynamic analysis. The main purpose of a dynamic analysis is to identify the response of the considered structure to an arbitrary dynamic loading. In particular, the free response of the structure was analysed, obtaining the fundamental frequency of the structure and the mode shapes (i.e., the ways of vibrating of the structure) as main results.

Starting from the equilibrium equation governing the mass i, one can write:

$$-m_i\ddot{u}_i - k_i(u_i - u_{i-1}) + k_{i+1}(u_{i+1} - u_i) = 0 \tag{3.1}$$

Considering two masses, the equilibrium equation can be written for both the masses as:

$$-m_1\ddot{u}_1 - k_1(u_1 - 0) + k_2(u_2 - u_1) = 0 \tag{3.2}$$

$$-m_2\ddot{u}_2 - k_2(u_2 - u_1) + k_3(0 - u_2) = 0 \tag{3.3}$$

The equations *(3.2)* and *(3.3)* represent a system of two equations, which can be rewritten exploiting the mass matrix and the stiffness matrix as:

$$[m]\{\ddot{u}\} + [k]\{u\} = \{0\} \tag{3.4}$$

The solution of the system *(3.4)* is of the form:

$$\{u\} = \{\phi\}e^{j\omega_k t} \tag{3.5}$$

Consequently, the solution contains both a spatial function, represented by $\{\phi\}$, and a temporal function, represented by $e^{j\omega_k t}$.

Deriving the equation *(3.5)*, one has:

$$\{\ddot{u}\} = -\omega_k^2\{\phi\}e^{j\omega_k t} \tag{3.6}$$

Introducing the equation *(3.6)* into the equation *(3.4)*, one obtains:

$$-\omega_k^2[m]\{\phi\}e^{j\omega_k t} + [k]\{\phi\}e^{j\omega_k t} = \{0\} \tag{3.7}$$

The equation *(3.7)* can be rewritten as:

$$([k] - \omega_k^2[m])\{\phi\} = \{0\} \tag{3.8}$$

The equation *(3.8)* represents the so-called eigenvalue problem, that gives as result the natural frequencies and modes of a system.

The eigenvalue problem has a trivial solution, corresponding to equilibrium without motion, which is represented by:

$$\{\phi\} = \{0\} \tag{3.9}$$

Other solutions are found if the following condition is respected:

$$\det([k] - \omega_k^2[m]) = 0 \tag{3.10}$$

Solving the equation *(3.10)*, as many values of ω_k as the number of equations can be found; consequently, substituting the obtained values of ω_k into the equation *(3.8)*, the solution $\{\phi\}$ can be found.

The values of ω_k are also known as eigenvalues, while the vectors ϕ_k are also known as eigenvectors. Consequently, corresponding to the k-th natural vibration frequency ω_k, there is an independent vector ϕ_k, known as natural mode shape of vibration.

If the system has N degrees of freedom, the N natural frequencies and the N mode shapes can be assembled compactly into matrices. Considering the natural mode shape ϕ_k, corresponding to the natural frequency ω_k, and naming its elements as ϕ_{jk}, where *j* represents the degree of freedom, the N eigenvectors can be represented as members of the following square matrix:

$$[\Phi] = \begin{bmatrix} \phi_{11} & \phi_{12} & \cdots & \phi_{1N} \\ \phi_{21} & \phi_{22} & \cdots & \phi_{2N} \\ \vdots & \vdots & \ddots & \vdots \\ \phi_{N1} & \phi_{N2} & \cdots & \phi_{NN} \end{bmatrix} \tag{3.11}$$

The matrix $[\Phi]$ is called the modal matrix for the eigenvalue problem; the eigenvalues ω_k^2 can be also assembled into a diagonal matrix as:

$$[\Omega^2] = \begin{bmatrix} \omega_1^2 & \phi_{12} & \cdots & 0 \\ 0 & 0 & \cdots & 0 \\ \vdots & \vdots & \ddots & \vdots \\ 0 & 0 & \cdots & \omega_N^2 \end{bmatrix} \tag{3.12}$$

The matrix $[\Omega^2]$ is known as the spectral matrix of the eigenvalue problem. By using the modal and spectral matrices, the previous relations can be rewritten as:

$$[k][\Phi] = [m][\Phi][\Omega^2] \tag{3.13}$$

The mode shapes vectors possess the so-called orthogonality property.

Considering two modes r and s with, respectively the natural frequencies ω_r and ω_s, it is possible to write:

$$([k] - \omega_r^2[m])\{\phi\}_r = 0 \tag{3.14}$$

$$([k] - \omega_s^2[m])\{\phi\}_s = 0 \tag{3.15}$$

Pre-multiplying the equation *(3.14)* by $\{\phi\}_s^T$:

$$\{\phi\}_s^T([k] - \omega_r^2[m])\{\phi\}_r = 0 \tag{3.16}$$

Transposing and post-multiplying the equation *(3.15)* by $\{\phi\}_r$:

$$\{\phi\}_s^T([k]^T - \omega_s^2[m]^T)\{\phi\}_r = 0 \tag{3.17}$$

Exploiting the properties of Betti's theorem, for which the transpose of a symmetric matrix is the matrix itself, the equation *(3.17)* becomes:

$$\{\phi\}_s^T([k] - \omega_s^2[m])\{\phi\}_r = 0 \tag{3.18}$$

Finally, subtracting the equations *(3.18)* and *(3.16)*:

$$(\omega_r^2 - \omega_s^2)\{\phi\}_s^T[m]\{\phi\}_r = 0 \tag{3.19}$$

If the two modes r and s are distinct, then $\omega_r \neq \omega_s$, and:

$$\{\phi\}_s^T[m]\{\phi\}_r = 0 \tag{3.20}$$

$$\{\phi\}_s^T[k]\{\phi\}_r = 0 \tag{3.21}$$

Considering all the possible combinations of r and s, the modal model orthogonality can be stated as follows:

$$[M] = [\Phi]^T[m][\Phi] \tag{3.22}$$

$$[K] = [\Phi]^T[k][\Phi] \tag{3.23}$$

where $[K]$ and $[M]$ are diagonal matrices.

The k-th mode of these matrices can be written as:

$$M_k = \phi_k^T m \phi_k \tag{3.24}$$

$$K_k = \phi_k^T k \phi_k \tag{3.25}$$

In general, the eigenvalue problem, determines the natural modes only within a multiplicative factor. Consequently, the mode shapes are usually normalized with respect to some scale factors in order to standardize their elements related to amplitudes in different degrees of freedom.

Typically, the eigenvectors are normalized with respect to the mass matrix, as follows:

$$M_k = \phi_k^T[m]\phi_k = 1 \tag{3.26}$$

Consequently:

$$\{U\} = \frac{\{\Phi\}}{\sqrt{\{\Phi\}^T[m]\{\Phi\}}} \tag{3.27}$$

in such a way that:

$$\{U\}_r^T[m]\{U\}_s = \begin{cases} 0 & r \neq s \\ 1 & r = s \end{cases} \tag{3.28}$$

$$\{U\}_r^T[k]\{U\}_s = \begin{cases} 0 & r \neq s \\ \omega_r^2 & r = s \end{cases} \tag{3.29}$$

and:

$$[U]^T[m][U] = [I] \tag{3.30}$$

$$[U]^T[k][U] = [\Omega] \tag{3.31}$$

where $[U]$ is the mass-normalised modal matrix and $[I]$ is the diagonal identity matrix.

$[\Omega]$ is a diagonal matrix built as follows:

$$[\Omega] = [{}'\omega_{\prime r}^2] \tag{3.32}$$

In general, for tensegrity systems, the equation of motion can be written as:

$$[M]\{\ddot{u}\} + [K]\{u\} = \{F\} \tag{3.33}$$

As mentioned in the previous chapters, the stiffness matrix of a tensegrity system can be expressed as the sum of two different components, the elastic stiffness matrix $[K_E]$ and the geometric stiffness matrix $[K_G]$. Theoretically, also the system higher order stiffness matrix $[K_{NL}]$ should be considered.

From a practical point of view, the Newton-Raphson method should be used since the system is not linear, and this implies an updating of the system at each iteration, which allows to avoid determining the higher order stiffness matrix $[K_{NL}]$.

The displacement at the iteration p is expressed as:

$$\{u_{p+1}\} = \{u_p\} + \{\Delta u_p\} \tag{3.34}$$

$\{\Delta u_p\}$ represents the error estimate, defined as:

$$\{\Delta u_p\} = \{u\} - \{u_p\} \tag{3.35}$$

The iterative procedure is repeated until the convergence is achieved; in general, defining λ as a pre-set tolerance, the convergence criterion is defined as follows:

$$\frac{|u_{p+1} - u_p|}{|u_p|} \leq \lambda \qquad (3.36)$$

Tensegrity systems have a particular geometry, and, because of that, they can be loaded only in presence of a stabilized geometry.

The equation of motion which allows to find the stabilized state, in which the natural frequencies of the system can exist, is given by:

$$[K_{E,p} + K_{G,p}]\{\Delta u_p\} = \{F_p\} - \{R_p\} \qquad (3.37)$$

Where $\{F_p\}$ is the loading vector for the p-th iteration and $\{R_p\}$ is the vector of internal forces.

In the case of the tensegrity bridge, the first 10 mode shapes have been considered; the eigenvalues corresponding to the natural frequencies of the system have been listed in the table below.

Table 6 - Natural frequencies

Mode	Natural frequency [Hz]
1	17,4606
2	34,8383
3	37,8254
4	41,9126
5	47,6161
6	55,2349
7	65,9861
8	75,0899
9	85,5612
10	97,6170

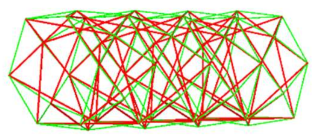

Mode shape 1
$f_1 = 17{,}4606$ *Hz*

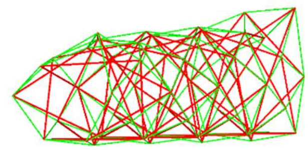

Mode shape 2
$f_2 = 34{,}8383$ *Hz*

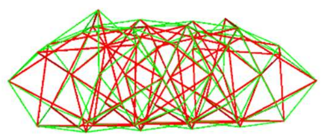

Mode shape 3
$f_3 = 37{,}8254$ *Hz*

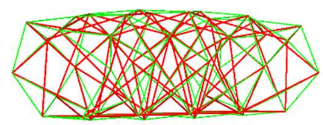

Mode shape 4
$f_4 = 41{,}9126$ *Hz*

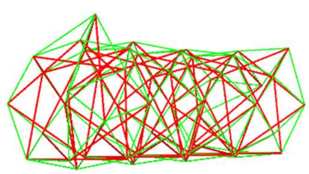

Mode shape 5
$f_5 = 47{,}6161$ *Hz*

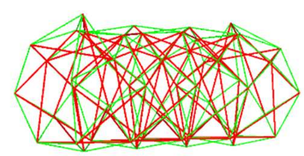

Mode shape 6
$f_6 = 55{,}2349$ *Hz*

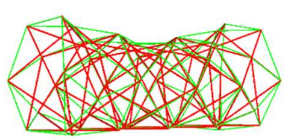

Mode shape 7
$f_7 = 65{,}9861$ *Hz*

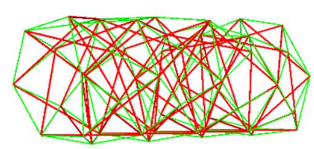

Mode shape 8
$f_8 = 75{,}0899$ *Hz*

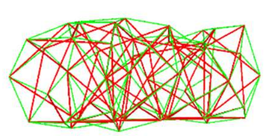

Mode shape 9
$f_9 = 85{,}5612$ *Hz*

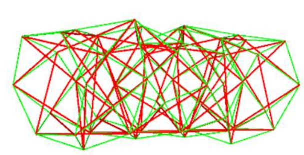

Mode shape 10
$f_{10} = 97{,}6170$ *Hz*

Figure 22 - Mode shapes

4.2 Time-domain response

Once that the modal analysis has been completed, it's possible to proceed with studying the response of the structure in the case of free vibrations. The response has been calculated exploiting the Newmark's method, considering that the structure is non linear.

$$\dot{u}_{i+1} = \dot{u}_i + [(1-\gamma)\Delta t]\ddot{u}_i + [\gamma \Delta t]\ddot{u}_{i+1} \tag{3.38}$$

$$u_{i+1} = u_i + [\Delta t]\dot{u}_i + \left[\left(\frac{1}{2} - \beta\right)\Delta t^2\right]\ddot{u}_i + [\beta \Delta t^2]\ddot{u}_{i+1} \tag{3.39}$$

Since the implicit formulation is difficult to use, it is preferred to convert it in an explicit formulation: therefore, it would be possible to express the final acceleration in terms of other response quantities. In particular, in our case, the values of β and γ are defined as follows:

$$\beta = \frac{1}{4} \tag{3.40}$$

$$\gamma = 0.5 \tag{3.41}$$

The effective load at the instant t_{i+1} is related to the displacement by the so-called effective stiffness through the following relationship:

$$\tilde{k}_c u_{i+1} = \tilde{p}_{(i+1)c} \tag{3.42}$$

The effective stiffness $\tilde{k}_c$ has the following form:

$$\tilde{k}_c = k + \frac{2c}{\Delta t} + \frac{4m}{\Delta t^2} \tag{3.43}$$

On the other hand, the effective load $\tilde{p}_{(i+1)c}$ is defined as:

$$\tilde{p}_{(i+1)c} = p_i + c\left(\frac{2}{\Delta t}u_i + \dot{u}_i\right) + m\left(\frac{4}{\Delta t^2}u_i + \frac{4}{\Delta t}\dot{u}_i + \ddot{u}_i\right) \tag{3.44}$$

The acceleration is so obtained solving the dynamic equilibrium as:

$$\ddot{u}_{i+1} = \frac{1}{m}(p_{i+1} - c\dot{u}_{i+1} - ku_1) \tag{3.45}$$

In the finite element software, the Newmark's method has been implemented as follows:

1. Definition of the initial conditions:
   1.1 Definition of the mass matrix, stiffness matrix and damping matrix, considering that:
      - the mass matrix and the stiffness matrix have been previously defined for the purpose of the modal analysis.
      - the damping matrix is defined as three times the mass matrix.

   1.2 Definition of the time step as:

$$\Delta t = 0{,}001\ s \tag{3.46}$$

   1.3 Definition of the initial conditions:

$$x(0) = 0 \tag{3.47}$$

$$\dot{x}(0) = 0 \tag{3.48}$$

2. Definition of the parameters β and γ as previously pointed out.
3. Definition of the integration coefficients:

$$a_0 = \frac{4}{\Delta t^2} \tag{3.49}$$

$$a_1 = \frac{2}{\Delta t} \tag{3.50}$$

$$a_2 = \frac{4}{\Delta t} \tag{3.51}$$

$$a_3 = a_4 = 1 \tag{3.52}$$

$$a_5 = 0 \tag{3.53}$$

$$a_6 = a_7 = \frac{\Delta t}{2} \tag{3.54}$$

4. Calculation of the effective stiffness matrix

$$[K_{eff}] = [K] + a_0[M] + a_1[C] \tag{3.55}$$

5. Defining N = 8000, while i < N:
   5.1 Calculate the effective force vector as:

$$R = [M](\ddot{u} + a_2\dot{u} + a_0 u) + [C](\dot{u} + a_1 u) \tag{3.56}$$

   5.2 Solve for the displacements as:

$$u = u(K_{eff}, R) \tag{3.57}$$

   5.3 Calculate the velocities and accelerations at time t, exploiting the two equations above mentioned.

A critical aspect concerning the Newmark's method is represented by the choice of the time step: in general, the time step depends on how the applied load varies through the time, on how complex the stiffness and damping properties are and on the fundamental period of the structure. In the case of the considered structure, the loading history can be considered relatively simple, then the time step will depend only on the fundamental period of vibration of the structure. The choice of the time step is strictly related to two fundamental requirements of Newmark's method and, more in general, of direct integration methods: stability and accuracy.

A numerical procedure is said to stable if it takes to a bounded solution with a time step shorter than some stability limit; the same procedure can be defined unconditionally stable if it takes to bounded solutions for each time step chosen. Accuracy means that the time step should be chosen small enough to provide an accurate solution for each mode of vibration of the structure. In some cases, the time step chosen to verify the accuracy requirement is so small, that implies a verification of the stability requirement. In the case of Newmark's method, the stability requirement is given by:

$$\frac{\Delta t}{T} < \frac{1}{\pi\sqrt{2}} \frac{1}{\sqrt{\gamma - 2\beta}} \tag{3.58}$$

Considering the above-mentioned values of β and γ, one has:

$$\frac{\Delta t}{T} < \infty \tag{3.59}$$

This means that in this particular case the Newmark's method is stable for every value of Δt; on the other hand, the accuracy criterion needs still to be verified.

The accuracy requirement writes as:

$$\frac{\Delta t}{T} < 0{,}1 \tag{3.60}$$

The fundamental period for each mode shape is reported in the table listed below.

Table 7 - Fundamental periods

Mode	Fundamental period [s]	0,1T [s]
1	0,057272	0,005727
2	0,028704	0,002870
3	0,026437	0,002644
4	0,023859	0,002386
5	0,021001	0,002100
6	0,018104	0,001810
7	0,015155	0,001515
8	0,013317	0,001332
9	0,011688	0,001169
10	0,010244	0,001024

Alternatively, it's also possible to decrease the time step until it is not possible anymore to notice changes in the response of the structure. In the case of this structure, the initial chosen time step was $\Delta t = 0{,}005\ s$, which was then decreased to $\Delta t = 0{,}001\ s$. Decreasing it again, it's clear that the structure response doesn't change anymore. Consequently, the chosen time step is given by:

$$\Delta t = 0{,}001\ s \tag{3.61}$$

In the following graphs is reported the response of the structure for different time steps, and then the response of the structure in the case of the chosen time step.

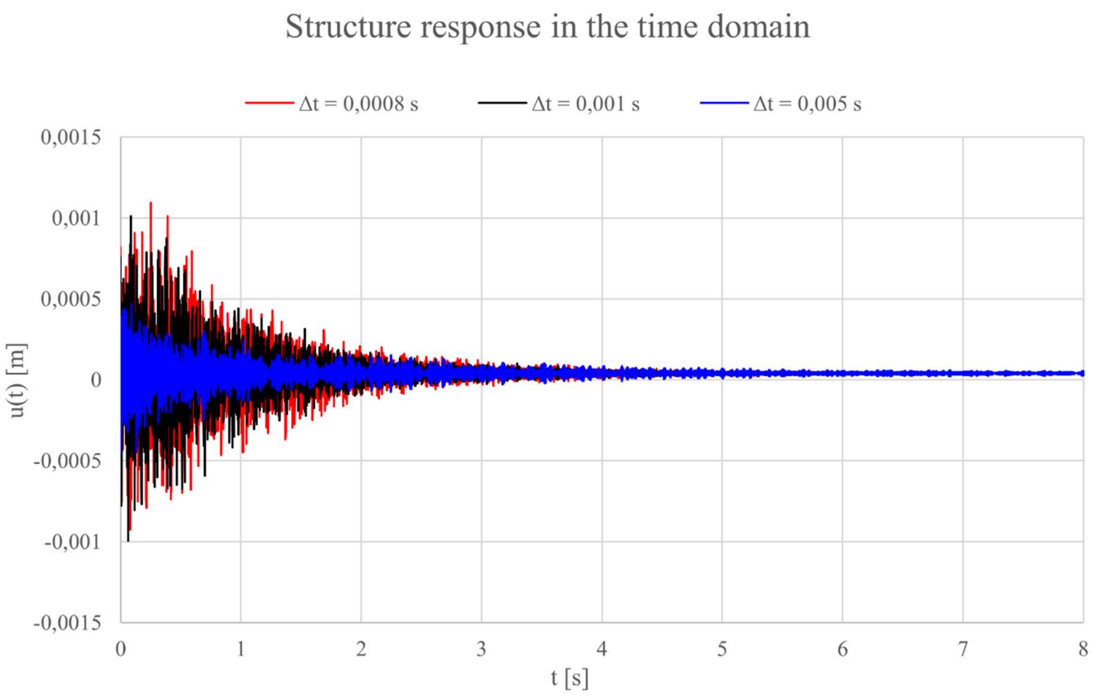

Figure 23 - Time domain structure's response comparison

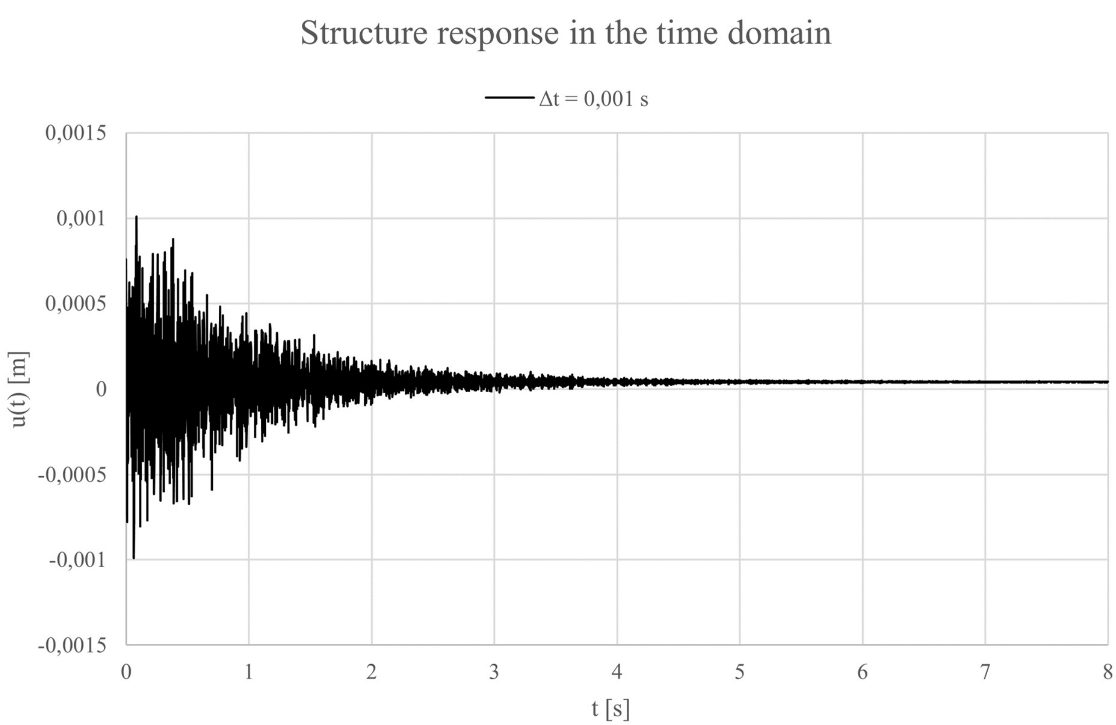

Figure 24 - Time domain structure's response

4.3 Frequency-domain response

In most of structural dynamics applications, it's preferable to consider a frequency-domain representation of the response than a time-domain representation. In this case, the so-called frequency response function should be calculated exploiting the Fourier's transform.

The Fourier transform is defined in the field of signals theory; a signal is a real or complex function of time that is physically realizable. Considering a complex signal defined on the interval $t \in [-\frac{T}{2}; \frac{T}{2}]$, its Fourier expansion is defined as:

$$x(t) = \sum_{-\infty}^{+\infty} \mu_n e^{jn\frac{2\pi}{T}t} \tag{3.62}$$

where μ_n is the Fourier's coefficient. It can be written as:

$$\mu_n = \frac{1}{T}\int_{-T/2}^{T/2} x(t)e^{-jn\frac{2\pi}{T}t}dt \tag{3.63}$$

Substituting the Fourier's coefficient defined by *(3.63)* into the Fourier expansion defined by *(3.62)*, one has:

$$x(t) = \frac{1}{T}\sum_{-\infty}^{+\infty}\left[\int_{-\frac{T}{2}}^{\frac{T}{2}} x(t')e^{-jn\frac{2\pi}{T}t'}dt'\right]e^{jn\frac{2\pi}{T}t} \tag{3.64}$$

The fundamental period T can be rewritten as:

$$T = \frac{n}{f_n} \tag{3.65}$$

And consequently:

$$\Delta f = f_n - f_{n-1} = f_0 = \frac{1}{T} \tag{3.66}$$

Where f_0 represent the fundamental frequency, defined as the inverse of the fundamental period.

The equation *(3.64)* becomes:

$$x(t) = \sum_{-\infty}^{+\infty} \left[\int_{-\frac{T}{2}}^{\frac{T}{2}} x(t') e^{-j2\pi f_n t'} dt' \right] e^{j2\pi f_n t} \Delta f \tag{3.67}$$

The next step is to pass from a discrete analysis to a continuous analysis, considering that:

$$T \to +\infty \tag{3.68}$$

$$\Delta f \to df \tag{3.69}$$

$$f_n \to f \tag{3.70}$$

The equation *(3.67)*, now defined on the interval $t \in (-\infty; +\infty)$, can be rewritten as:

$$x(t) = \int_{-\infty}^{+\infty} \left[\int_{-\infty}^{+\infty} x(t') e^{-j2\pi ft}\ dt' \right] e^{j2\pi ft} df \tag{3.71}$$

And:

$$x(t) = \int_{-\infty}^{+\infty} X(f) e^{j2\pi ft} df \tag{3.72}$$

The Fourier's transform is then defined as:

$$X(f) = \int_{-\infty}^{+\infty} x(t) e^{-j2\pi ft} dt \tag{3.73}$$

The equation *(3.73)* is often written as:

$$X(f) = F[x(t)] \tag{3.74}$$

where F represents the Fourier transform operator.

The main advantage of the Fourier transform is that it extends the Fourier analysis of a signal from a finite existence domain to an infinite existence domain, and it allows to easily pass from a time-domain to a frequency domain and vice-versa.

On the other hand, the use of the Fourier transform contains two main problems: the definition of the integral over an infinite domain and the continuity of the variables f and t. Consequently, another quantity has to be introduced, known as discrete Fourier transform (DFT).

The DFT allows to define the Fourier transform for finite sets of data, i.e., signals whose value is known only at defined time instants separated by a specific sampling time.

Before defining the DFT is then necessary to transform the continuous signal in a periodic one; this is done in two main steps:

1. Truncate the signal in such a way it has a finite duration:

$$0 < t < T \tag{3.75}$$

   where T represents the period of the signal.
2. Sample the signal with a sampling frequency defined as:

$$f_c = \frac{1}{t_c} \tag{3.76}$$

Once that sampling time and sampling frequency have been set, the sampled signal, which is nothing more than the sum of the parts of a real signal by means of a measurement grid, can be interpreted as a sequence of generalized δ Dirac's functions:

$$x_\delta(t) = \sum_{-\infty}^{+\infty} t_c x(nt_c)\delta(t - nt_c) = t_c x(t) \sum_{-\infty}^{+\infty} \delta(t - nt_c) \tag{3.77}$$

By Fourier-transforming the equation *(3.77)*, one has:

$$X_\delta(f) = \sum_{-\infty}^{+\infty} X(f - nf_c) \tag{3.78}$$

The δ Dirac's function is defined as:

$$\delta(t - nt_c) = \begin{cases} 1 & if\ nt_c < t < (n+1)t_c \\ 0 & otherwhise \end{cases} \tag{3.79}$$

Considering the following number of samples:

$$N = \frac{T}{t_c} \tag{3.80}$$

For a periodic signal, the Fourier's coefficient writes:

$$\mu_k = \frac{1}{T}\int_{-T/2}^{T/2} x(t)e^{-jk\frac{2\pi}{T}t}dt \approx \frac{1}{T}\sum_{n=0}^{N-1} x(nt_c)e^{-jk\frac{2\pi}{T}nt_c}t_c = \frac{t_c}{T}\sum_{n=0}^{N-1} x(nt_c)e^{-jk\frac{2\pi}{T}nt_c} \tag{3.81}$$

The equation *(3.81)* can be rewritten as:

$$\frac{1}{N}\sum_{n=0}^{N-1} x(nt_c)e^{-jk\frac{2\pi}{N}n} = \bar{x}(kf_c) \tag{3.82}$$

$\bar{x}(kf_c)$ is defined as the DFT of the discrete periodic signal $x(nt_c)$.

If on one hand the DFT reduces the problem from a continuous to a discrete one, on the other hand it implies a very high computational complexity.

Is therefore required the use of a simpler quantity: the fast Fourier transform (FFT) needs hence to be introduced.

The FFT is a fast optimized algorithm which allows to compute the DFT of a periodic signal with a lower computational complexity.

For the DFT the computational complexity is of the order of N^2 (N inner products with length N). If (and only if) N is an integer of power 2, it is possible to reduce the computational complexity to N·log(N) by means of the FFT, where log(N) is the logarithm on base 2 of N.

In the case study of this dissertation, the time-domain response has been calculated in the sub-chapter 4.2. The calculation of the frequency-domain response of the structure to free vibrations has been calculated using the finite element software SlangTNG, though the FFT command.

Defining $u(t)$ as the response in the time domain and $a(t)$ the input signal in the time domain, it is possible to obtain the correspondent values of these two quantities in the frequency domain exploiting the FFT as:

$$U(f) = F[u(t)] \tag{3.83}$$

$$A(f) = F[a(t)] \tag{3.84}$$

The response of the structure in the frequency domain is a complex number, which should be divided in its real and imaginary part to be properly represented. In the graphs below the real and the imaginary part of the response of the structure in case of free vibrations in the frequency domain are reported.

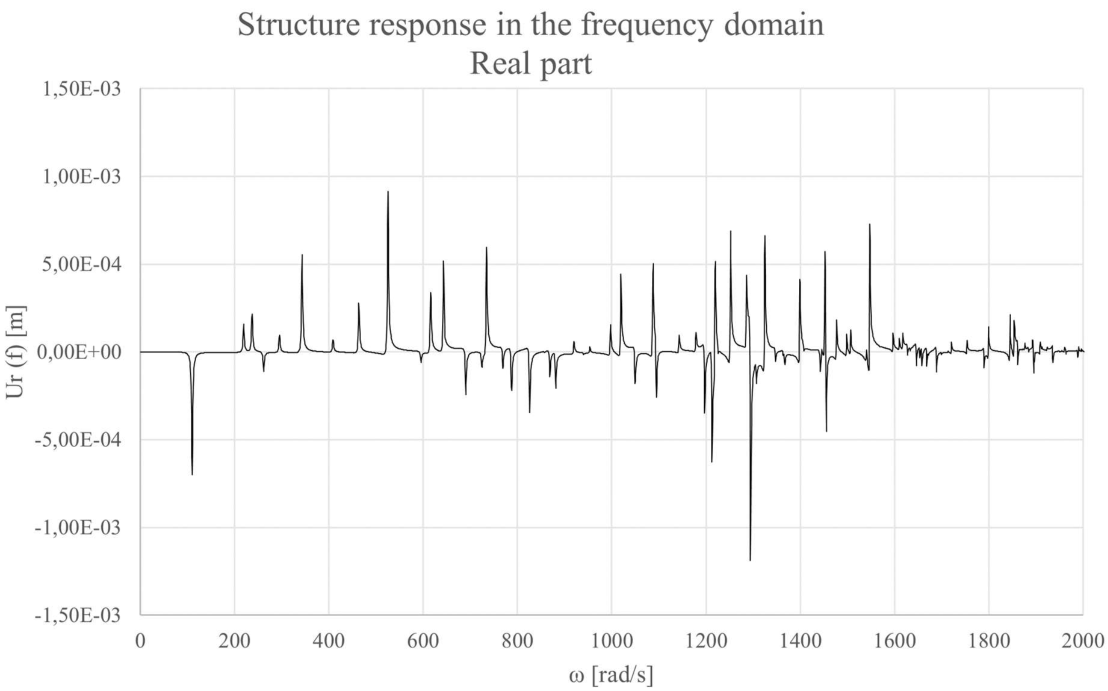

Figure 25 - Frequency domain structure's response (real part)

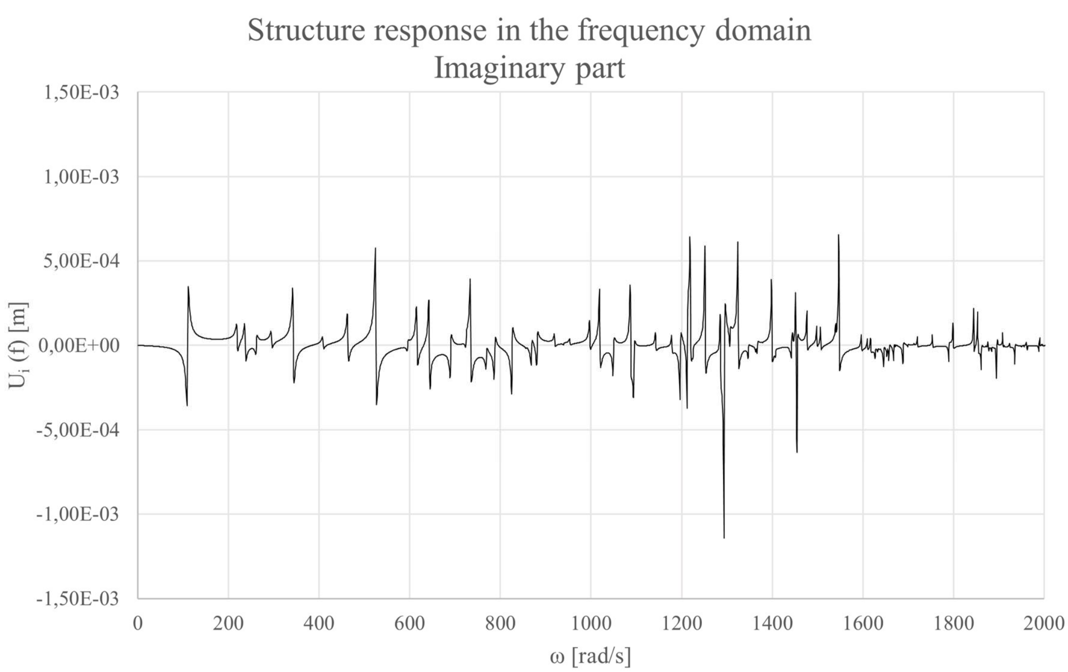

Figure 26 - Frequency domain structure's response (imaginary part)

In the frequency domain, the dynamic response can be written as:

$$U(f) = H(f)A(f) \tag{3.85}$$

where $U(f)$ is the response in the frequency domain and $A(f)$ is the input signal in the frequency domain.

$H(f)$ is the so-called frequency response function, and it is defined by the ratio between the output in the frequency domain and the input in the frequency domain.

$$H(f) = \frac{U(f)}{A(f)} \tag{3.86}$$

In the graphs below the real and the imaginary part of the frequency response function of the structure in the case of free vibrations are reported.

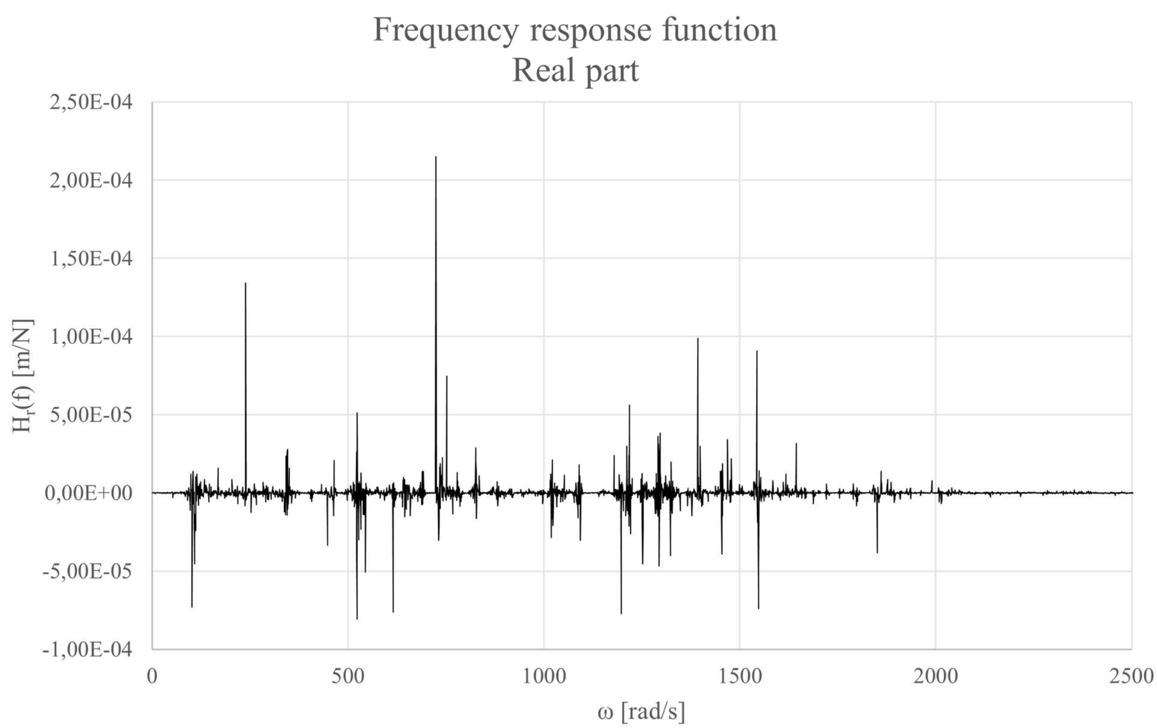

Figure 27 - Real part of FRF

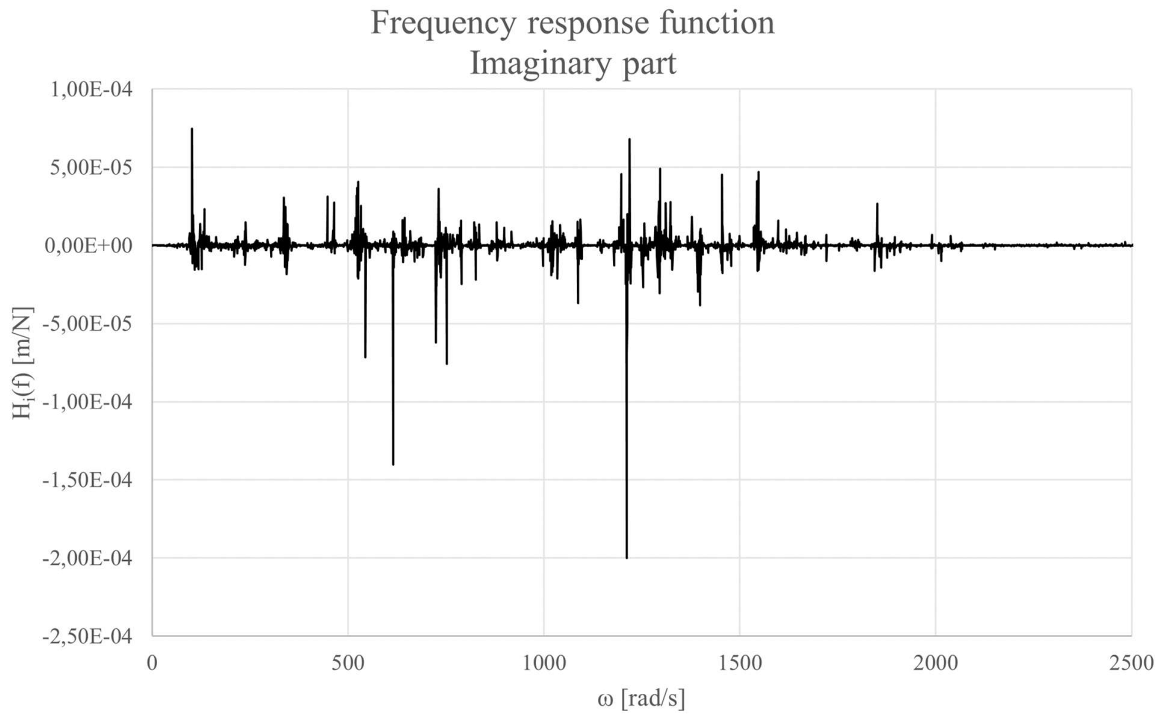

Figure 28 - Imaginary part of FRF

Since the frequency response function is a complex number decomposed in its real and imaginary parts, it's possible to translate the information given by these quantities into magnitude and phase.

In the case of this dissertation, a magnitude/phase representation has been chosen, considering that:

$$H(f) = H_R(f) + jH_I(f) \tag{3.87}$$

The equation *(3.87)* can be rewritten as:

$$H(f) = |H(f)|e^{j\theta(\omega)} \tag{3.88}$$

where $|H(f)|$ is the magnitude of the FRF and θ is the phase of the FRF.

In the case of the case study, the magnitude, and the phase of the FRF are reported in the graphs below.

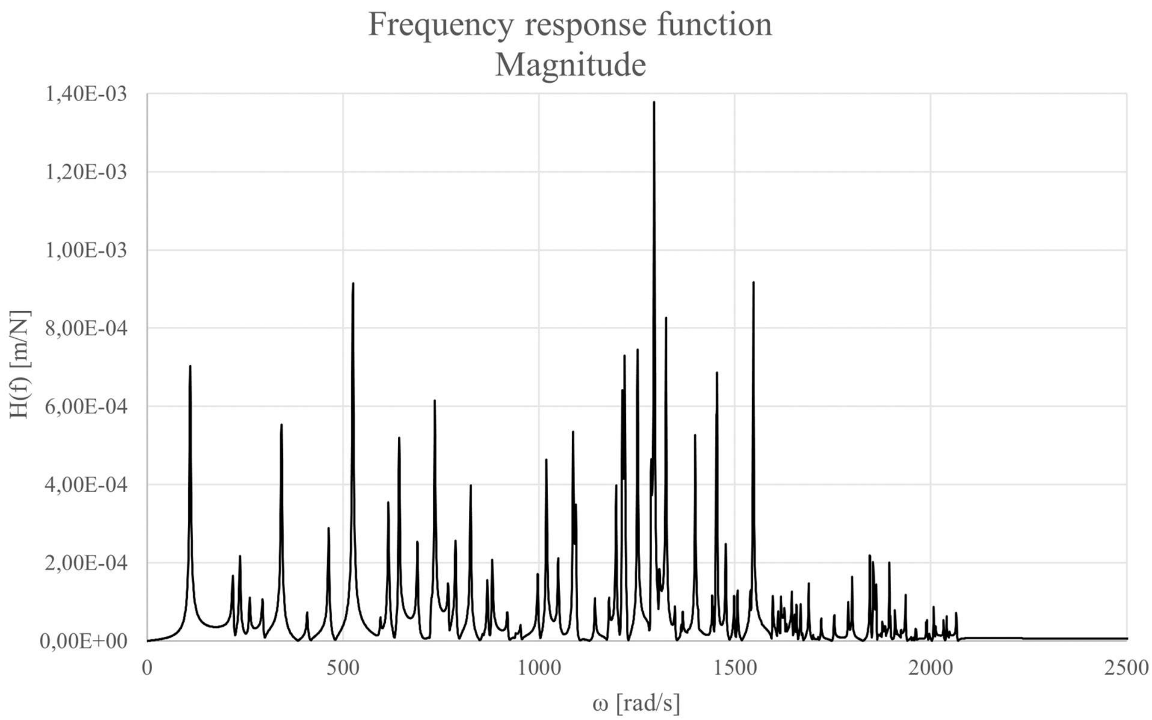

Figure 29 - Magnitude of FRF

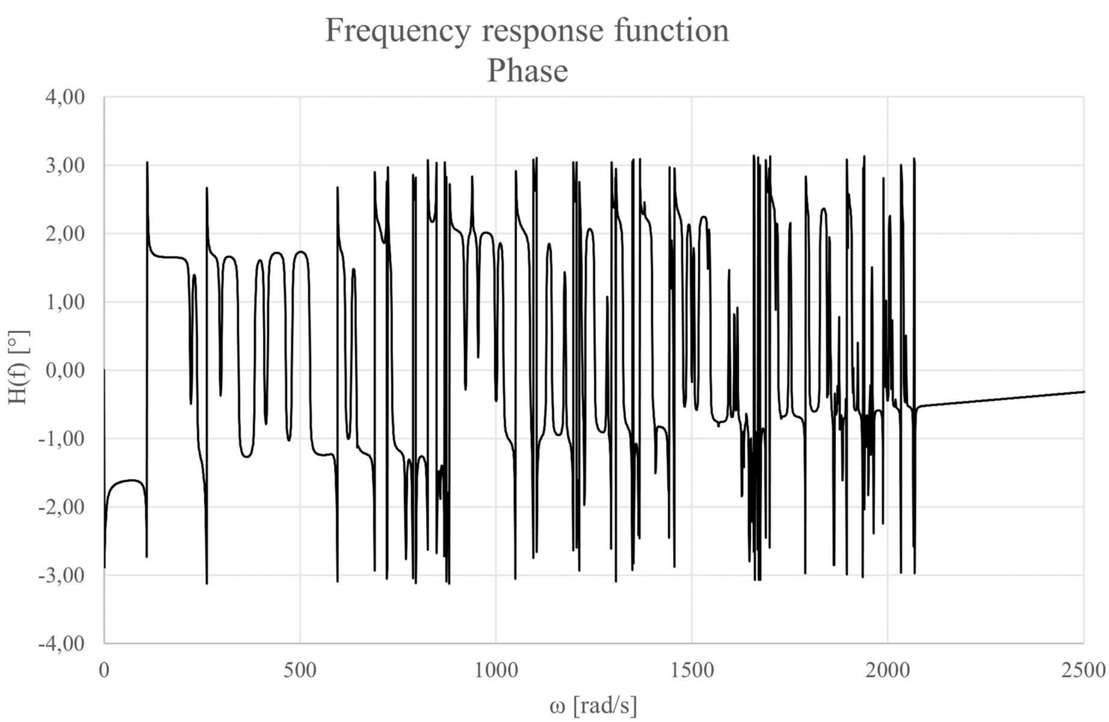

Figure 30 - Phase of FRF

5 Vibration-based structural health monitoring on structure's FE model

5.1 Theoretical background of structural health monitoring

Structural health monitoring can be defined as the discipline which "*aims to give, at every moment during the life of a structure, a diagnosis of the "state" of the constituent materials, of the different parts, and of the full assembly of these parts constituting the structure as a whole*".

Structural health monitoring is based on damage identification, i.e., the individuation of any kind of damage within the structure.

In 1993, Rytter proposed a 4 steps damage identification methodology:

1. Detection of damage, which allows to understand if any type of damage exists within the structure.
2. Localization of damage, in order to understand where the damage is located within the structure.
3. Assessment of damage, consisting in an estimation of the quantity of damage.
4. Consequence of damage.

According to Huston, a further step should be added, and the fourth step should be referred to more as prognosis of the damage than consequence of damage; consequently, the previously mentioned scheme becomes:

1. Detection of damage.
2. Localization of damage.
3. Assessment of damage.
4. Prognosis, in order to understand the possible future types of damage and the remaining service life of the structure.
5. Remediation, individuating the possible actions to take against the development of further damages.

From a practical point of view, structural health monitoring consists in placing sensors in a structure in order to monitor its health state.

In this thesis, the main focus will be on the second step of localization of the damage with consequent placement of sensors. In particular tensegrities, when subjected to external loads, experience a change in their form and this implies a need for a structural health monitoring.

There are many reasons why structural health monitoring and damage identification are fundamental in civil engineering structures. Indeed, structural health monitoring is not needed only in case of safety-critical applications, i.e., applications related to the human life or extreme cases, such as the complete failure of the structure, but also in case of non-safety-critical applications, such as maintenance of the structure, structural performance evaluation and expected lifetime prediction.

Nevertheless, in the case of non-safety-critical applications, it could be difficult to justify the need for structural health monitoring; the usefulness of this discipline is not obvious for example when the damage in the structure is not visible by a human eye. Moreover, the structures should be designed in such a way to avoid their sudden failure: if the failure of the structure is not imminent, then the placement of structural health monitoring instruments, such as sensors, could be difficult to justify, due to the fact that there are no immediate and visible benefits.

The difficulty to justify the need for structural health monitoring is defined by Davison as the "*predictive maintenance dilemma*".

Houston proposes 4 different criteria for assessing when SHM is useful:

1. The structural problem should be important, i.e., the damage should have a certain impact on the health of the structure (for example, it does not make sense to investigate cracks that have no impact on the structure).
2. The structural problem should be fixable or preventable, if detected in a sufficient early stage of development.
3. Structural measurements and data processing should be easy: sensors networks should provide measurements that are easy to interpret.
4. The measurements should correlate well with the underlying problem, with a minimum of confounding issues: it's the case of temperature effects on the structure, which should be taken into account, besides the mechanical processes which can affect the health of the structure.

In order to design properly a structural health monitoring system, the definition of the tasks is fundamental. In general, there can be different types of tasks, for example the purpose of the structural health monitoring system (such as providing the expected lifetime of the structure, an early warning of a sudden collapse or information on maintenance activities scheduling), the measurands to be measured (i.e., the quantities that need to be detected, such as displacements or velocities), or the types of condition to be monitored.

In the case of this dissertation, the main task of the structural health monitoring will be driven by the types of condition to be monitored; the main assumption is indeed the unknown origin of the damage in the structure.

In general, damage can origin from different types of situations, such as fatigue, cracking, corrosion, degradation of material properties, sudden temperature changes.

This dissertation will be focused on three different types of damage condition:

1. Relaxation of steel tension cables.
2. Effect of the temperature gradients on the elements of the structure.
3. Corrosion of the cross-section of the steel elements of the structure.

When the health monitoring of a structure is based on its vibrational properties, it is possible to refer to it as vibration based structural health monitoring (or vibrational health monitoring). The basic idea of vibration based SHM is to identify the damage through the changes in the dynamic behaviour of the structure.

The dynamic behaviour of a structure, as pointed out in the chapter 4 of this dissertation, is characterized either by single-valued parameters (such as fundamental frequencies) and plots (such as frequency response function plots), which are therefore used ad damage indicators.

A damage indicator can be defined as "*a dynamic quantity which can be used to identify the existence of damage in the structure*".

In the case of this dissertation, the natural, or fundamental, frequencies of the structure will be analysed in order to identify the type of damage and, consequently, the location of the damage. According to Rytter, natural frequencies are the most used type of damage indicator due to the fact they are easy to determine with a relatively high level of accuracy.

The natural frequencies for different types of damage will be then analysed and compared in the case of the considered tensegrity bridge in the following subchapters.

5.2 Damage cases

5.2.1 First case study: relaxation of the tension cables

Loss of pre-stress/pre-strain represents a very common phenomenon in the case of steel elements, which should be detected early in order to avoid any possible catastrophic failure of the element.

The loss of pre-stress/pre-strain can be categorized in two different groups:

1. Initial losses of prestress (or instantaneous losses), consisting in the losses of prestress taking place immediately after pre-stressing of the member. This initial loss can have different origins, such as an elastic deformation of the element or an elongation of the tendon.
2. Time-dependent losses (or final losses of pre-stress), due to the relaxation or creep of the pre-stressing steel or temperature changes.

Relaxation can be defined as the loss of pre-stress/pre-strain due to environmental forces or natural deterioration.

In the case of tensegrity structures, an initial strain is applied to the tension elements in order to build up the concept of tensegrity, i.e., all the elements should be either in pure compression or in pure tension. Throughout the time, the strain can reduce progressively, causing a lengthening of the tension elements, and, therefore, inducing relaxation.

A different change of pre-strain was considered for different tension cables, as reported in the following table.

Table 8 - Cases of relaxation

Nr. case	Description	Pre-strain values
1	Healthy situation	$\varepsilon_{hex} = 2{,}5*10^{-4}$ $\varepsilon_{lat} = 2{,}5*10^{-4}$
2	Loss of pre-strain in the tension cables composing the hexagon module	$\varepsilon_{hex} = 1*10^{-4}$ $\varepsilon_{lat} = 2{,}5*10^{-4}$
3	Loss of pre-strain in the lateral tension cables	$\varepsilon_{hex} = 2{,}5*10^{-4}$ $\varepsilon_{lat} = 1*10^{-4}$
4	Loss of pre-strain in all the tension cables	$\varepsilon_{hex} = 1*10^{-4}$ $\varepsilon_{lat} = 1*10^{-4}$
5	Loss of pre-strain in the tension cables composing the hexagon module	$\varepsilon_{hex} = 1*10^{-5}$ $\varepsilon_{lat} = 2{,}5*10^{-4}$
6	Loss of pre-strain in the lateral tension cables	$\varepsilon_{hex} = 2{,}5*10^{-4}$ $\varepsilon_{lat} = 1*10^{-5}$
7	Loss of pre-strain in all the tension cables	$\varepsilon_{hex} = 1*10^{-5}$ $\varepsilon_{lat} = 1*10^{-5}$
8	Loss of pre-strain in the tension cables composing the hexagon module	$\varepsilon_{hex} = 1*10^{-6}$ $\varepsilon_{lat} = 2{,}5*10^{-4}$

9	Loss of pre-strain in the lateral tension cables	$\varepsilon_{hex} = 2{,}5*10^{-4}$ $\varepsilon_{lat} = 1*10^{-6}$
10	Loss of pre-strain in all the tension cables	$\varepsilon_{hex} = 1*10^{-6}$ $\varepsilon_{lat} = 1*10^{-6}$
11	Loss of pre-strain in the cables T16, T50, T77, T95	$\varepsilon = 2{,}5*10^{-4}$ $\varepsilon_{sel} = 1*10^{-8}$
12	Loss of pre-strain in the cables T16, T50, T77, T95	$\varepsilon = 1*10^{-4}$ $\varepsilon_{sel} = 1*10^{-8}$

A graphical representation of the interested cables is reported in the following images; only a few cases will be reported as example: in particular, the cases 1, 2, 3, 4, 11.

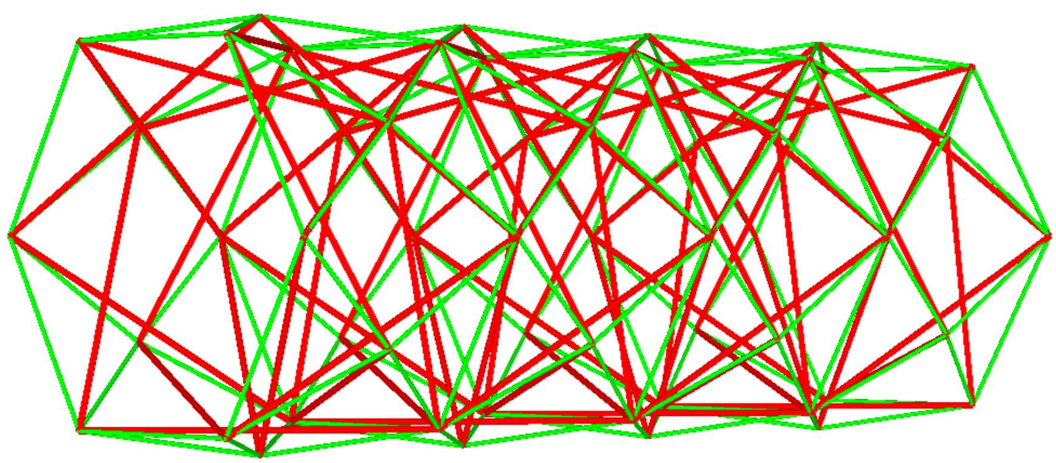

Figure 31 - Relaxation case 1

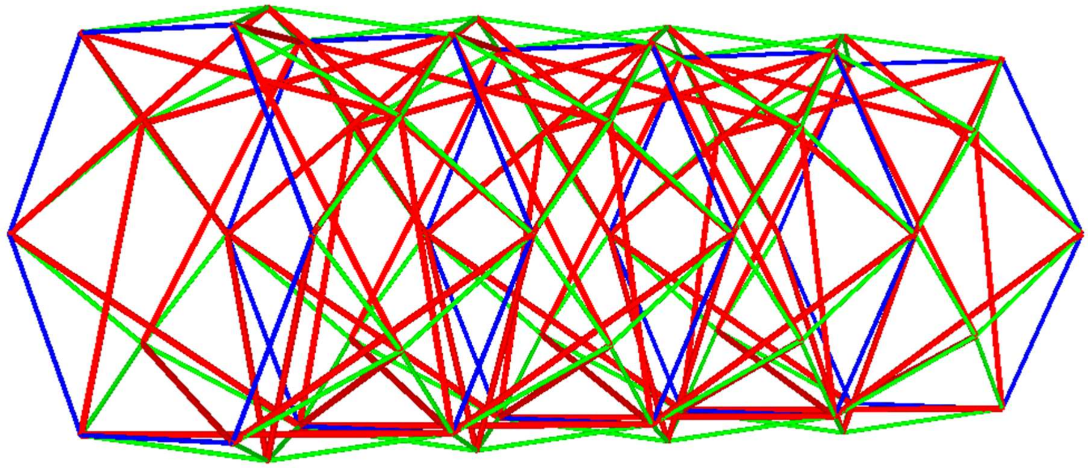

Figure 32 - Relaxation case 2

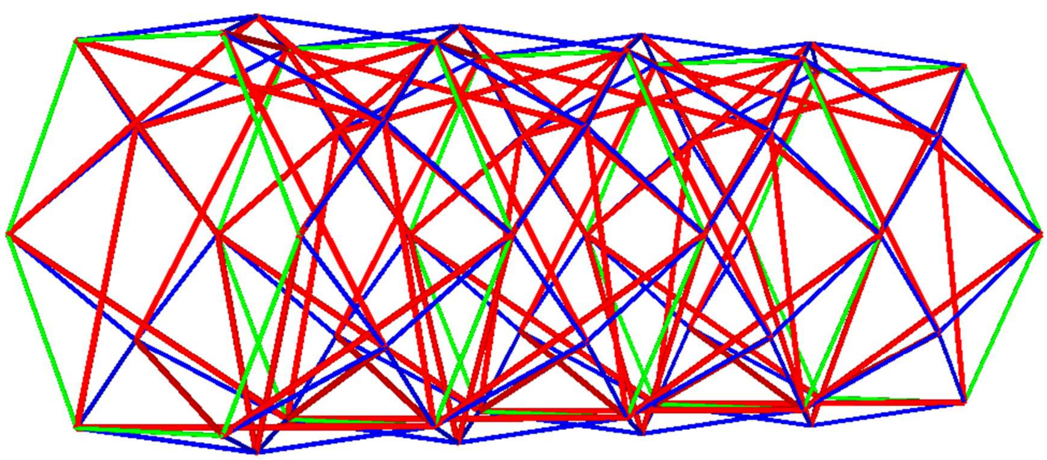

Figure 33 - Relaxation case 3

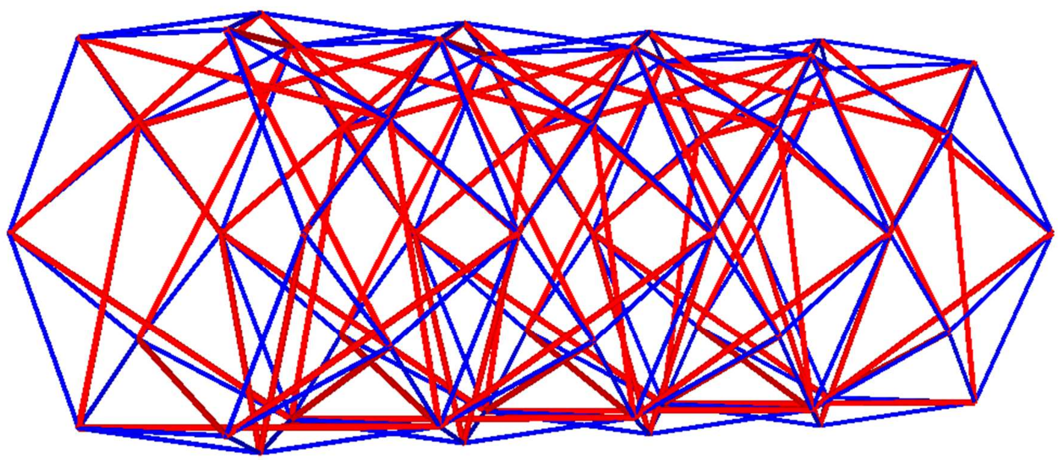

Figure 34 - Relaxation case 4

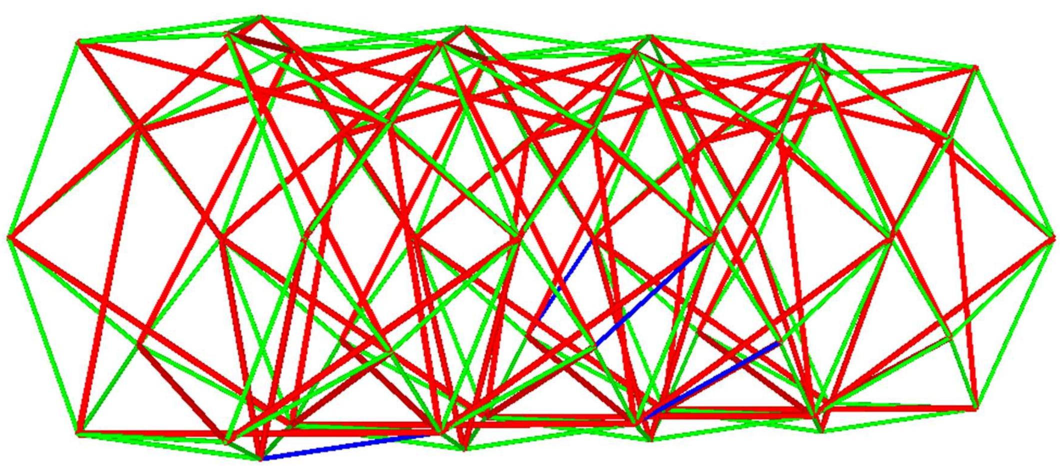

Figure 35 - Relaxation case 11

After the definition of the cases, the first step was to calculate the response of the structure both in time and frequency domain for the different cases of relaxation. Then the frequency response function was calculated, of which only the magnitude and the phase will be reported.

To have a better visualization, the 11 cases have been grouped in 4 different sets. The case of the healthy structure will be pictured in each graph to understand the comparison between healthy and damaged structure.

Table 9 – Relaxation: sets' definition

Nr. case	Nr. set
2	1
3	
4	
5	2
6	
7	
8	3
9	
10	
11	4
12	

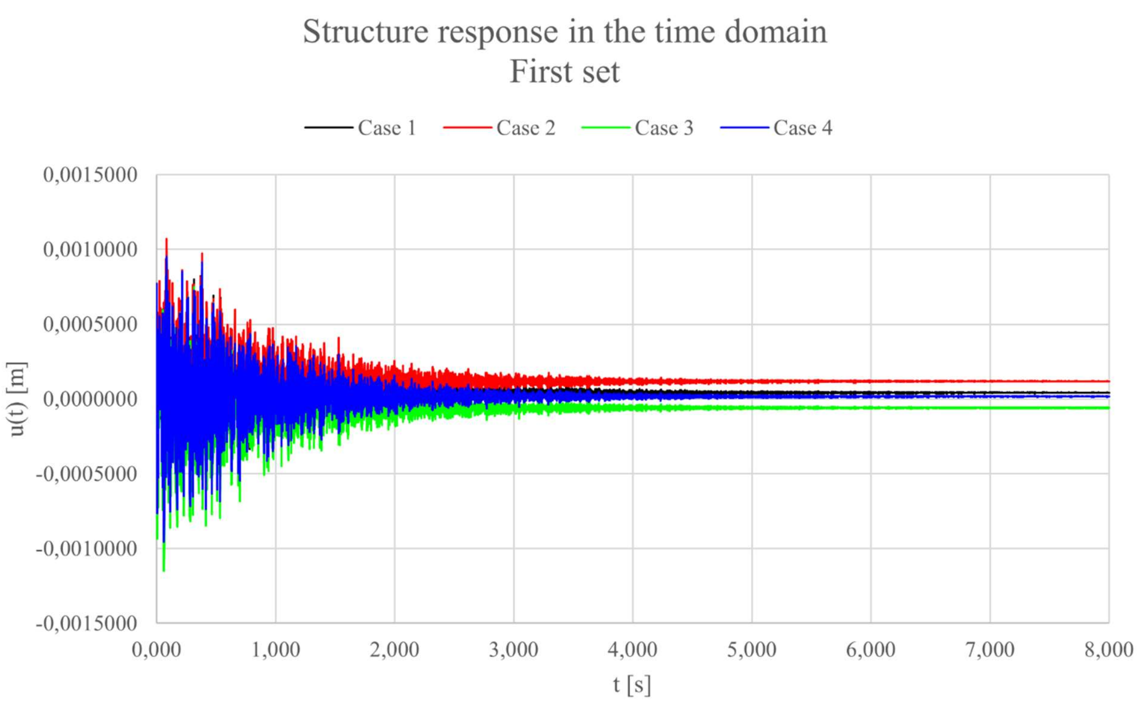

Figure 36 - Relaxation: time domain response (first set)

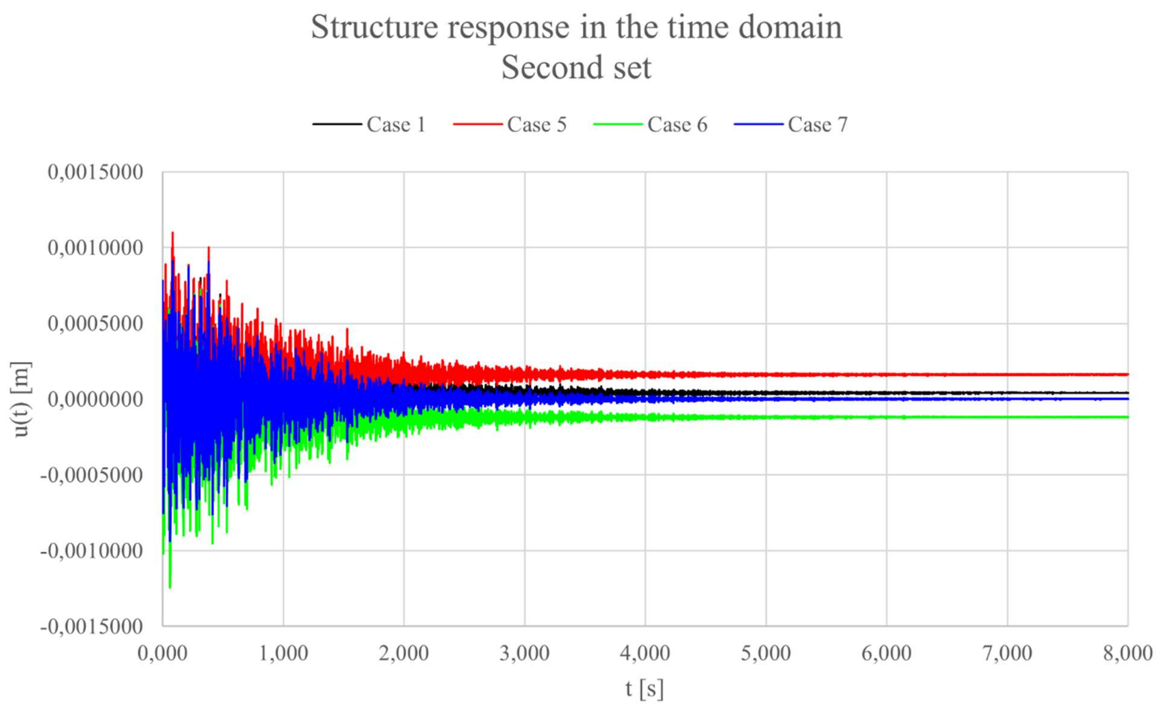

Figure 37 - Relaxation: time domain response (second set)

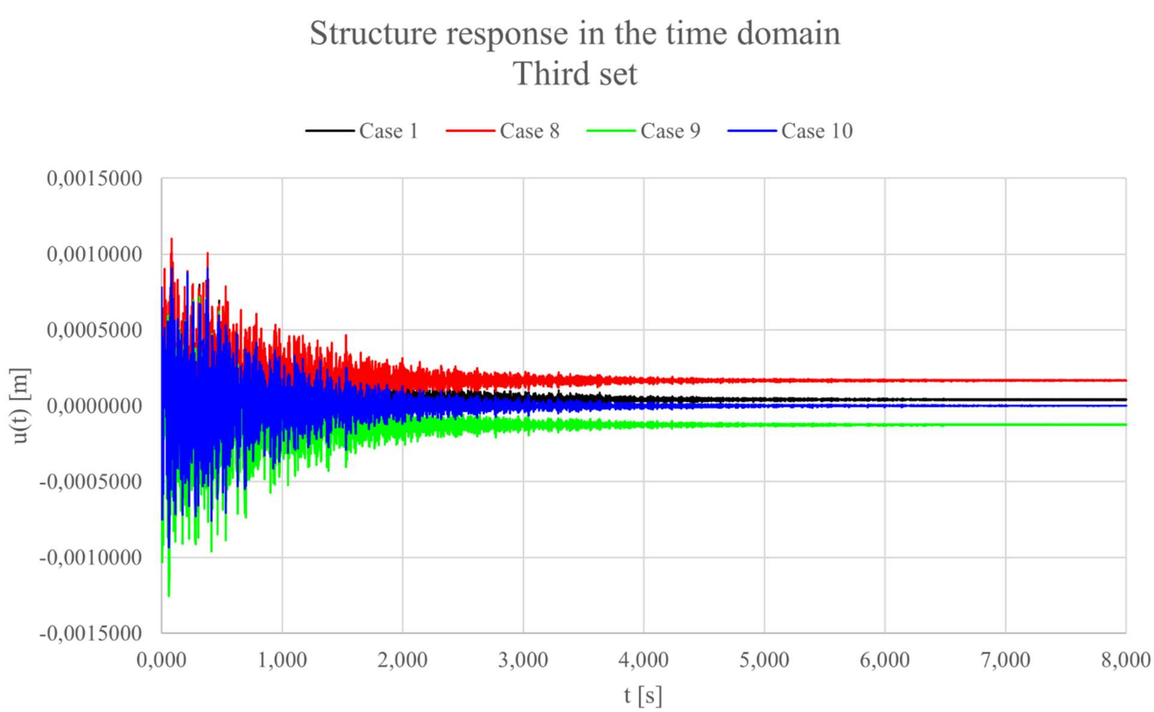

Figure 38 - Relaxation: time domain response (third set)

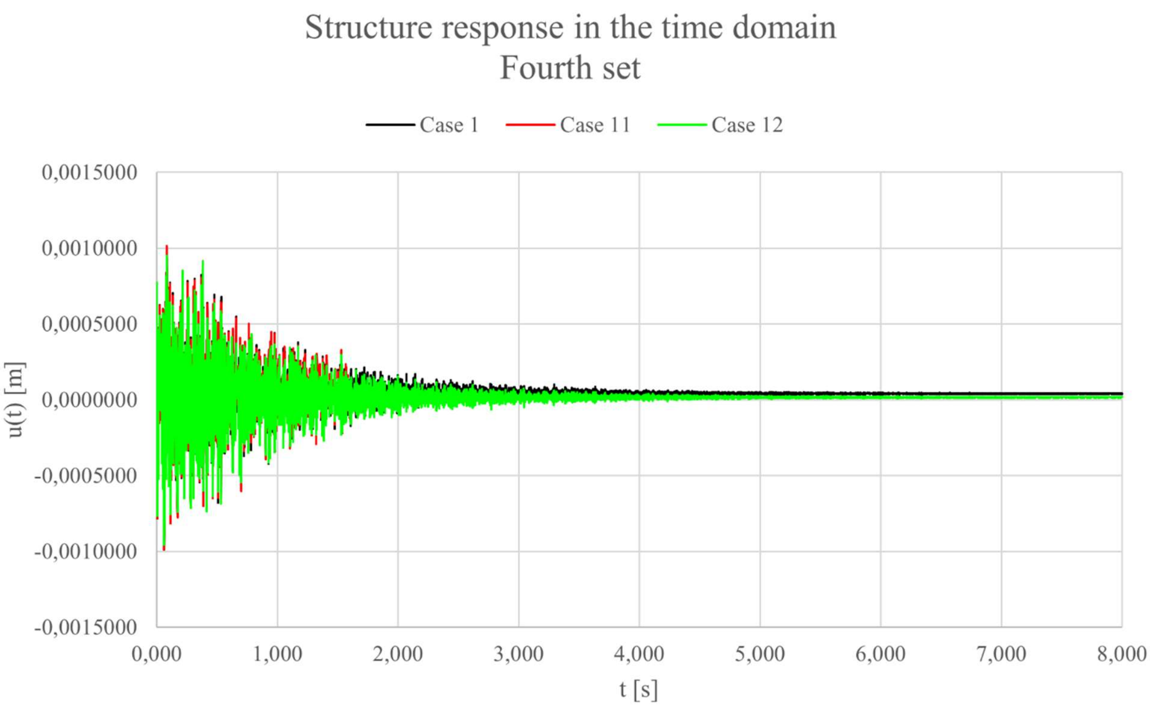

Figure 39 - Relaxation: time domain response (fourth set)

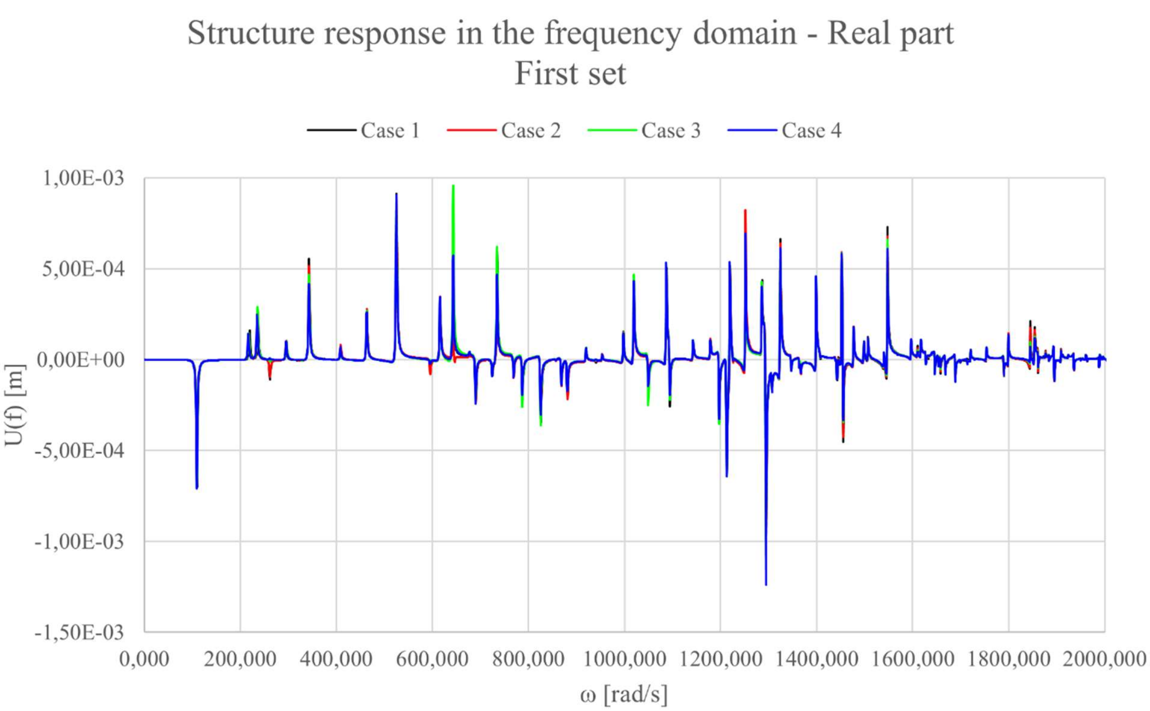

Figure 40 - Relaxation: real part of frequency domain response (first set)

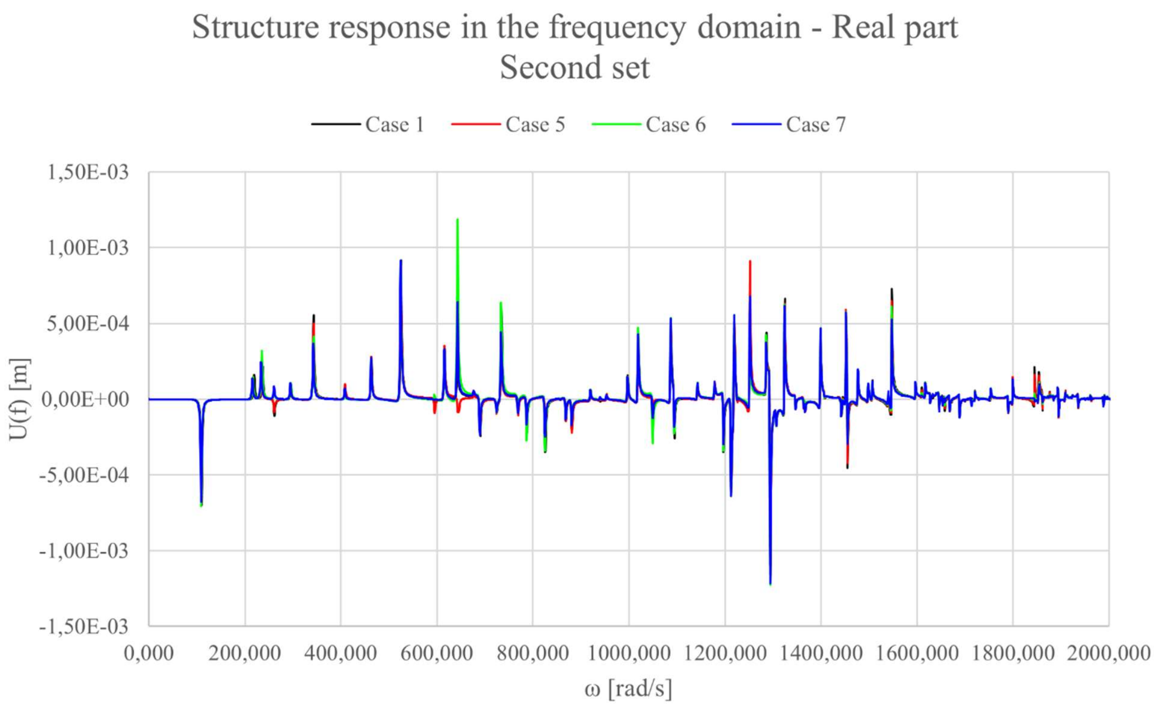

Figure 41 - Relaxation: real part of frequency domain response (second set)

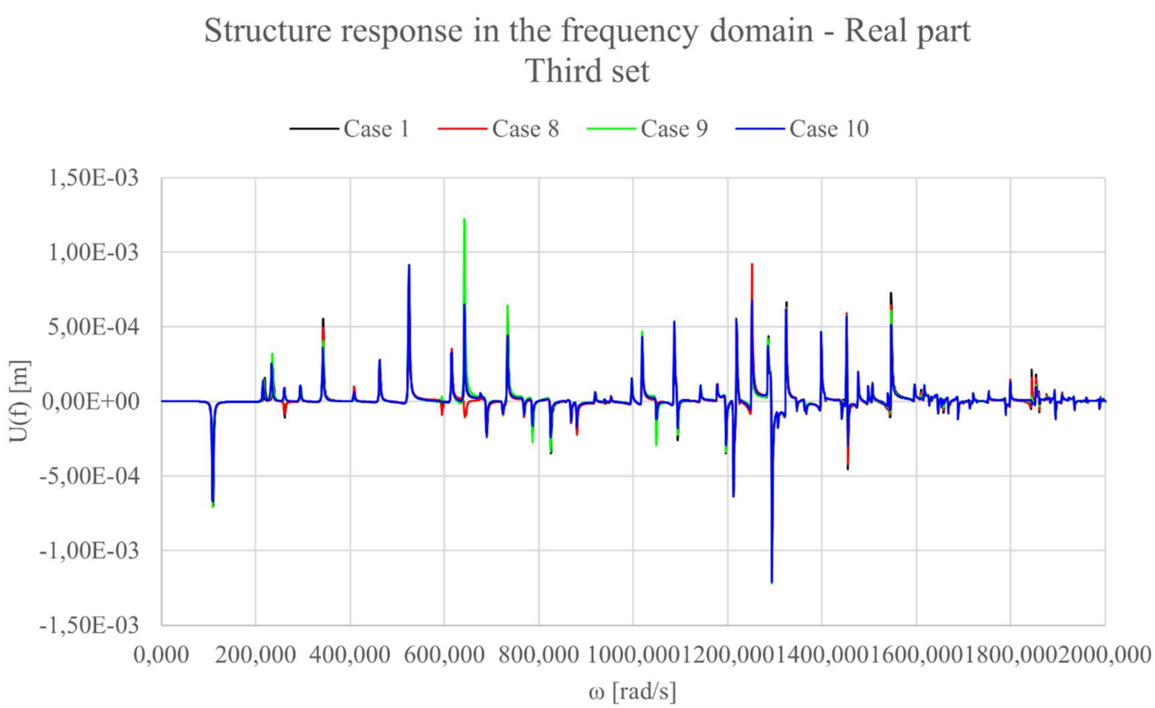

Figure 42 - Relaxation: real part of frequency domain response (third set)

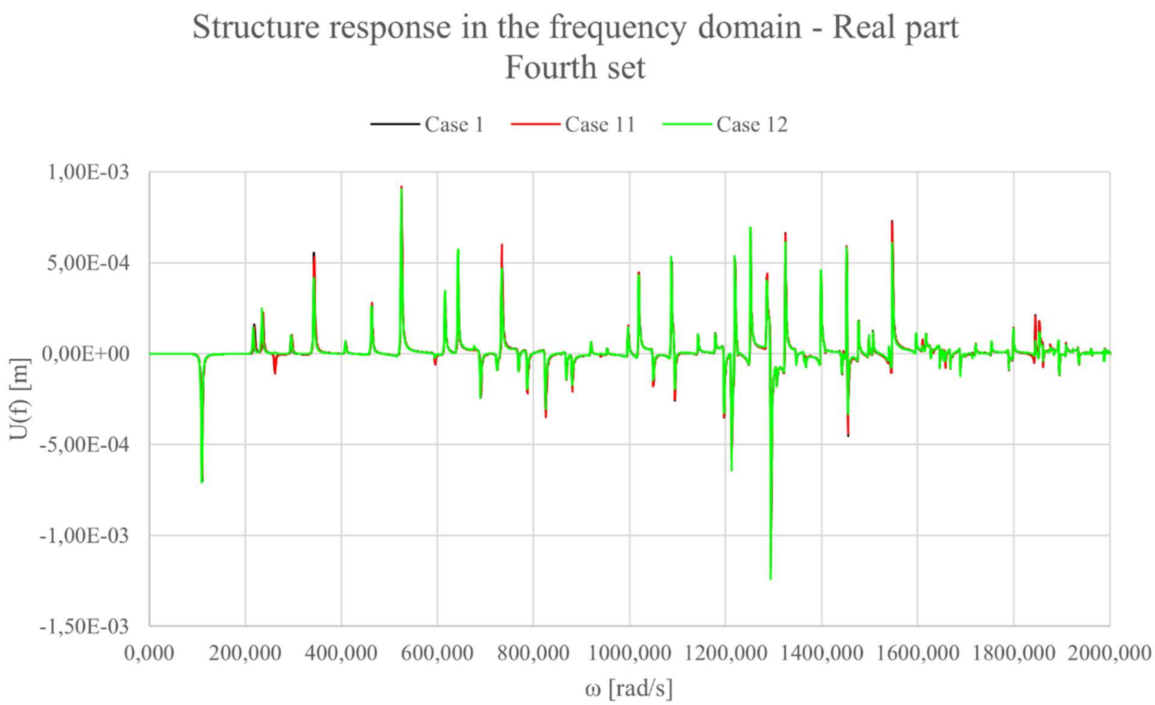

Figure 43 - Relaxation: real part of frequency domain response (fourth set)

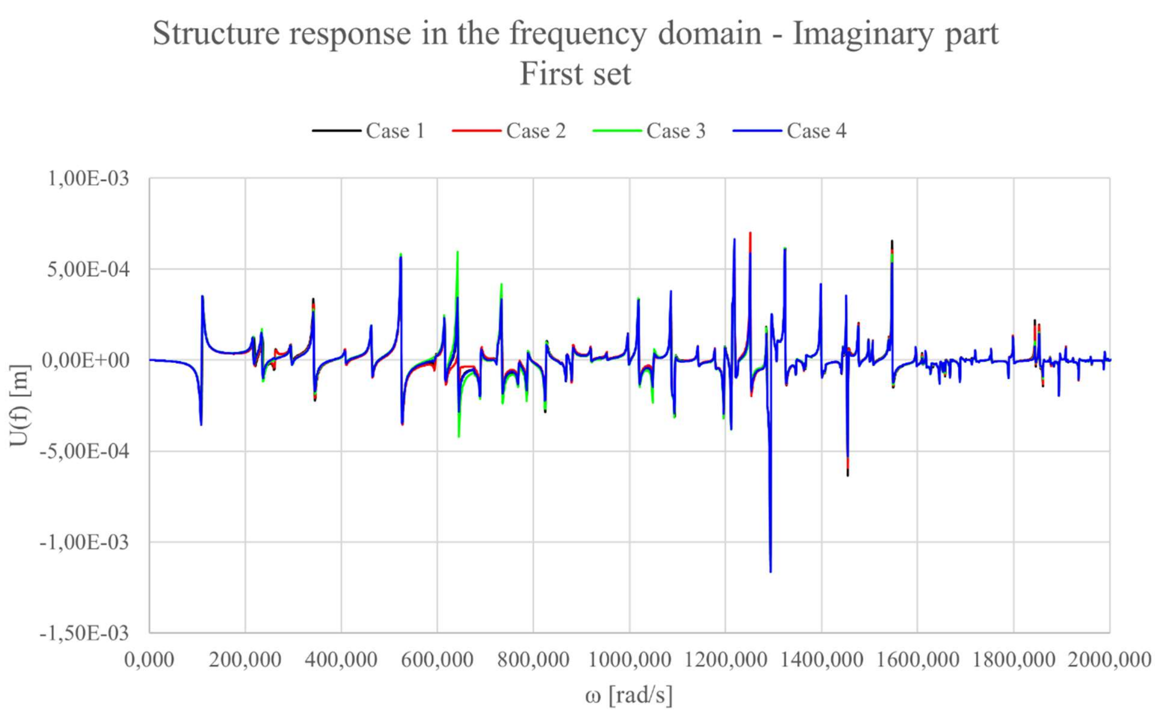

Figure 44 - Relaxation: imaginary part of frequency domain response (first set)

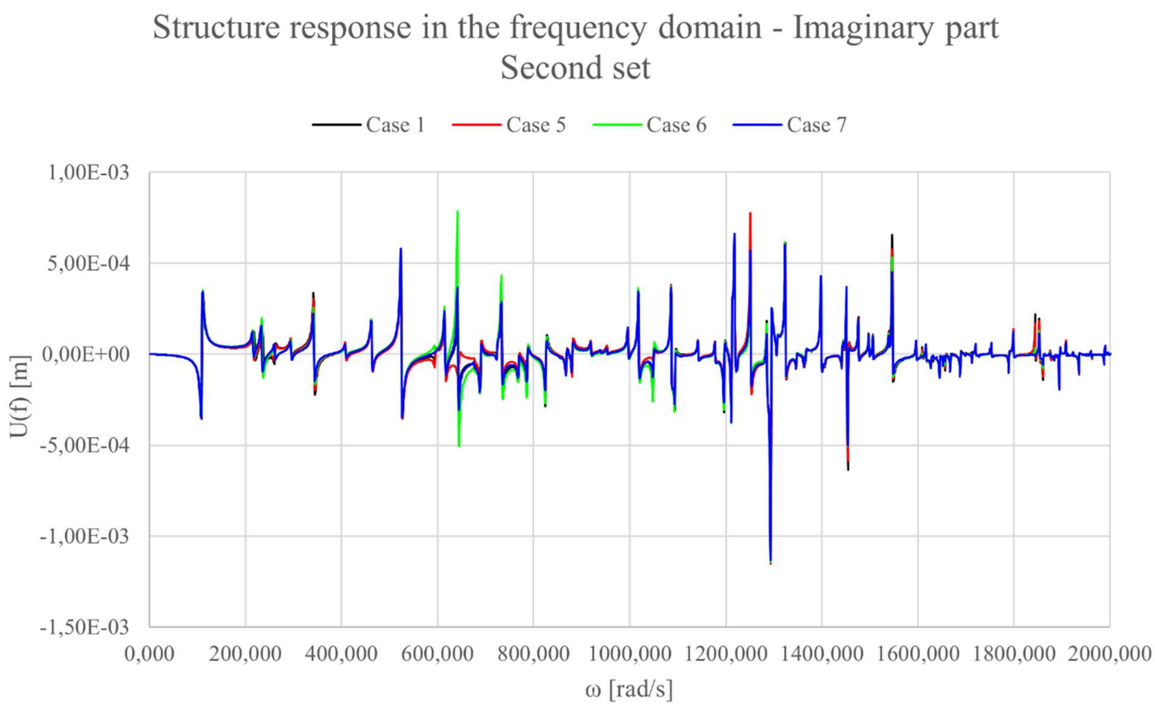

Figure 45 - Relaxation: imaginary part of frequency domain response (second set)

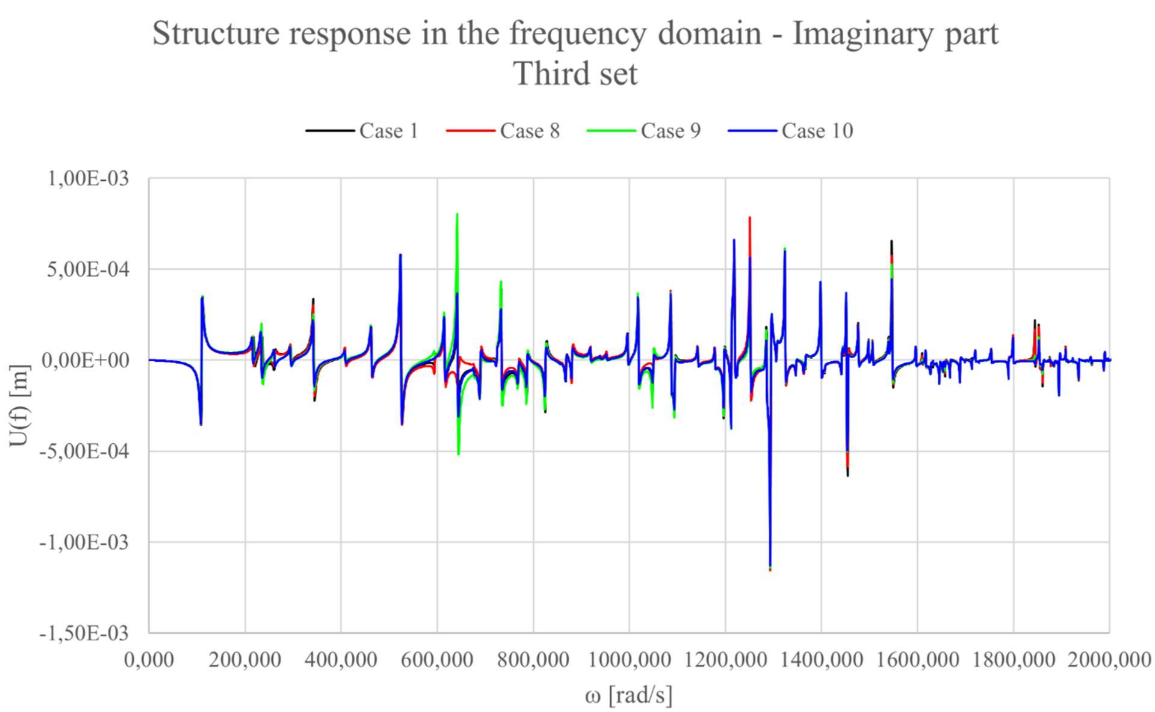

Figure 46 - Relaxation: imaginary part of frequency domain response (third set)

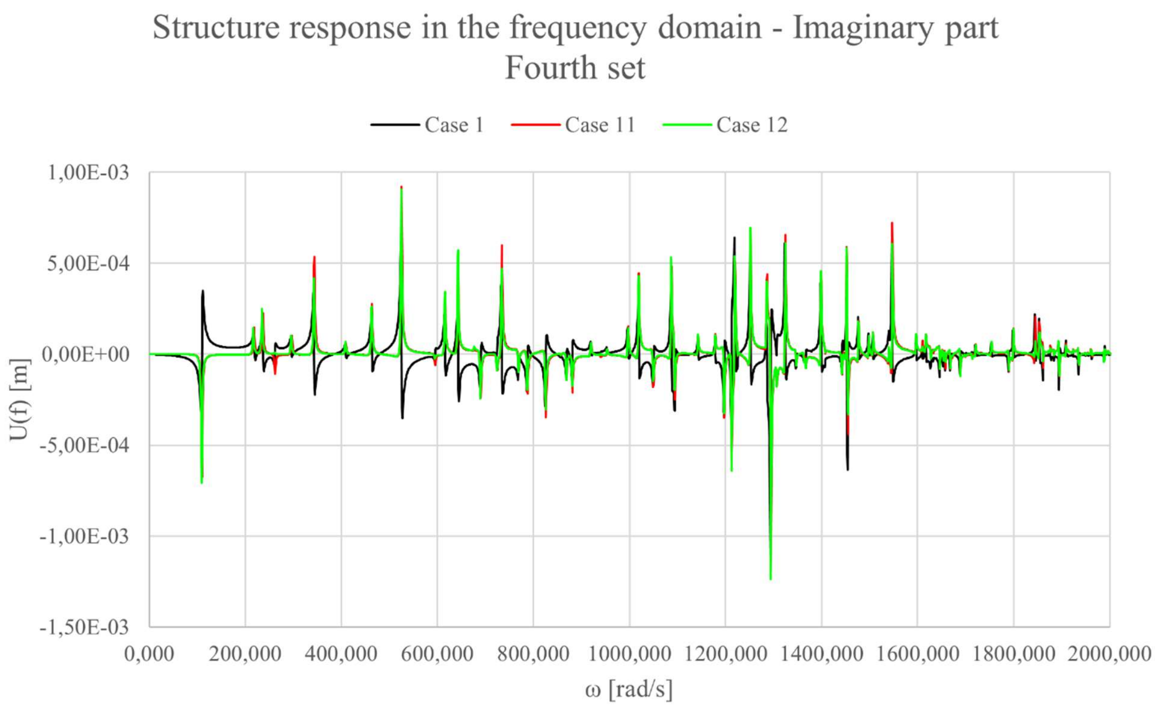

Figure 47 - Relaxation: imaginary part of frequency domain response (fourth set)

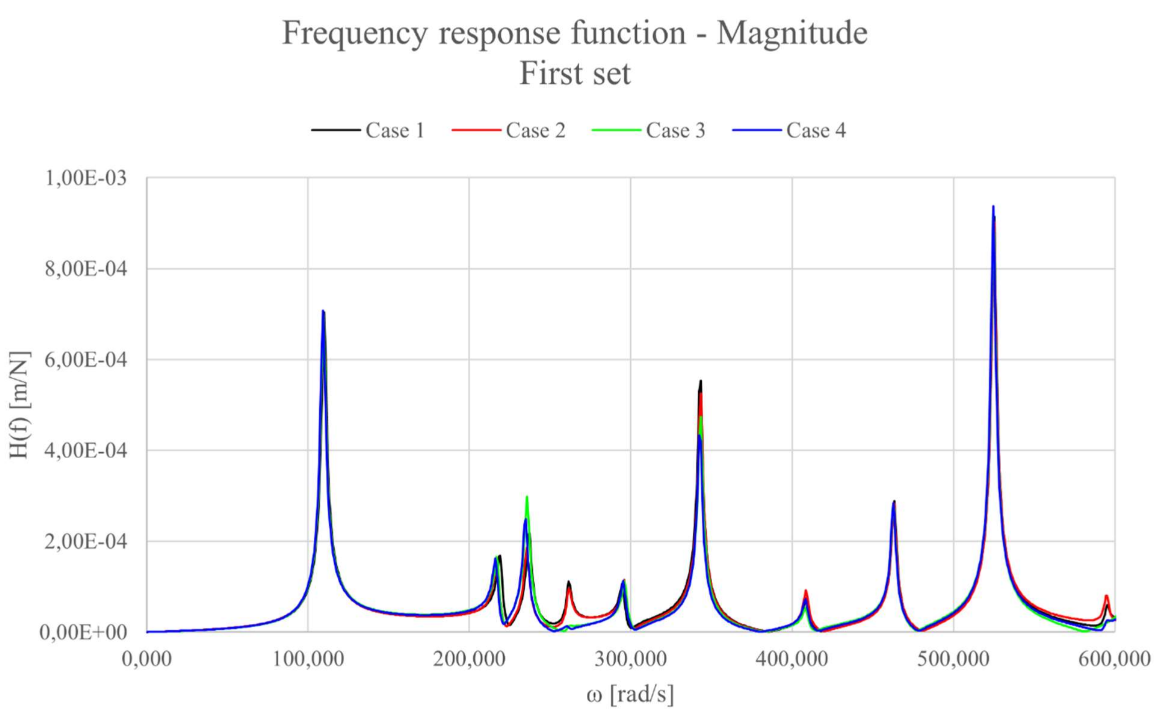

Figure 48 - Relaxation: magnitude of FRF (first set)

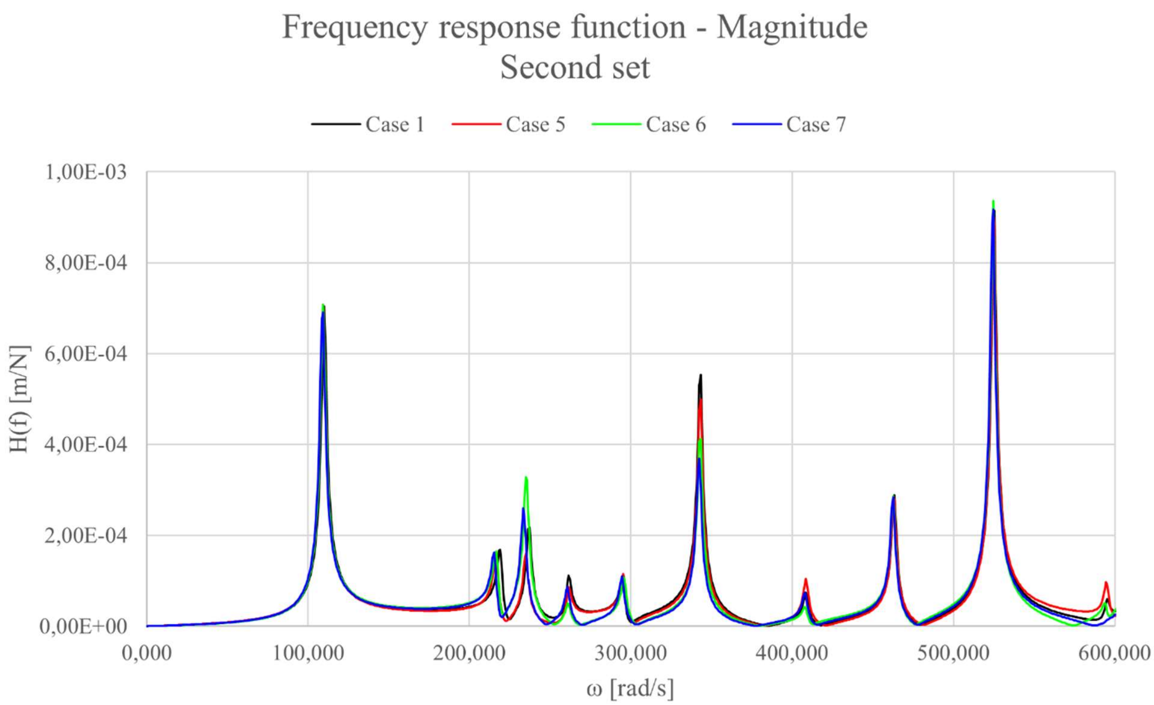

Figure 49 - Relaxation: magnitude of FRF (second set)

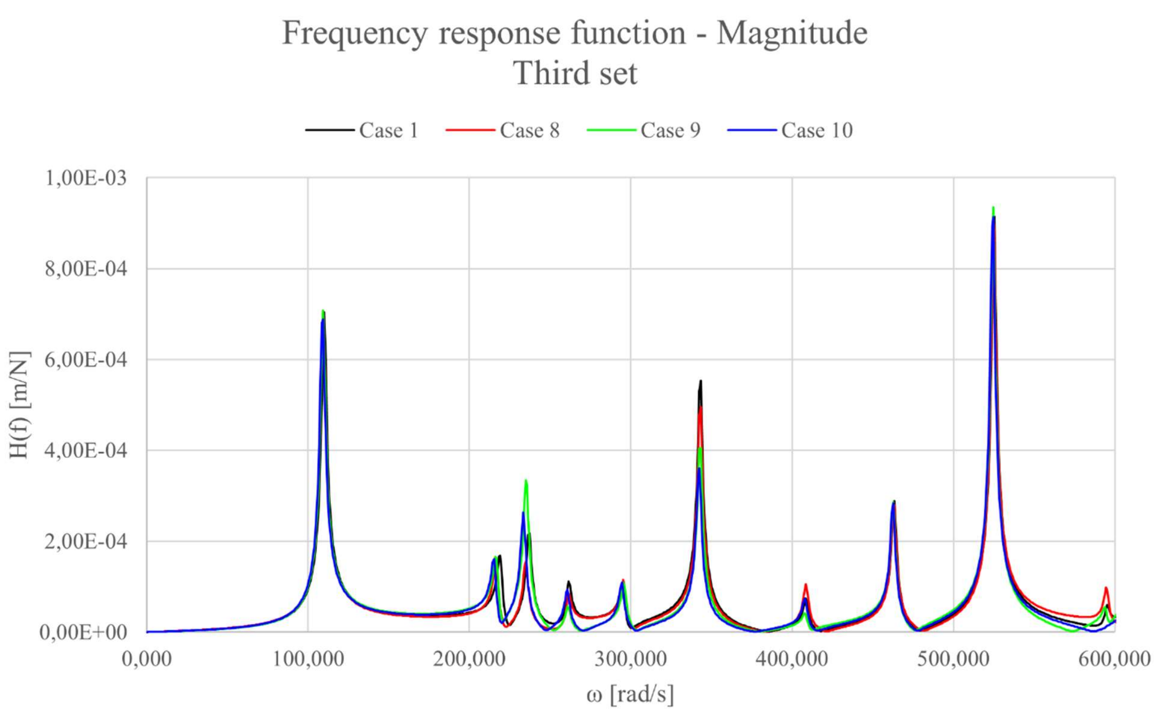

Figure 50 - Relaxation: magnitude of FRF (third set)

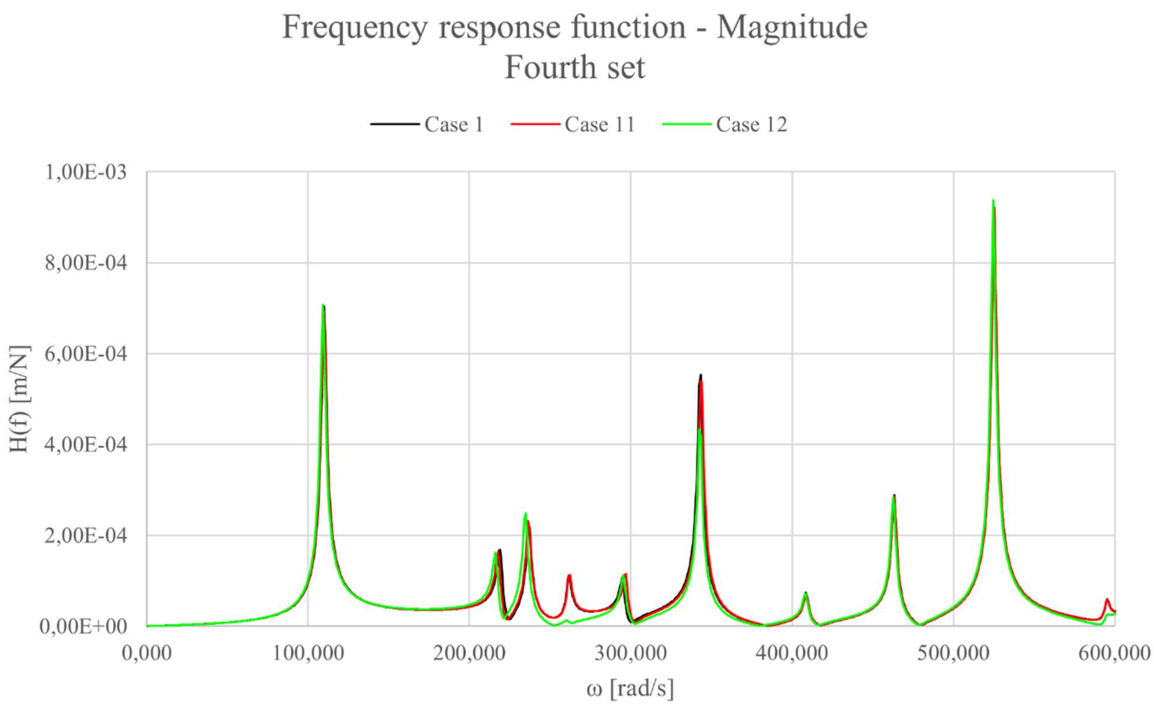

Figure 51 - Relaxation: magnitude of FRF (fourth set)

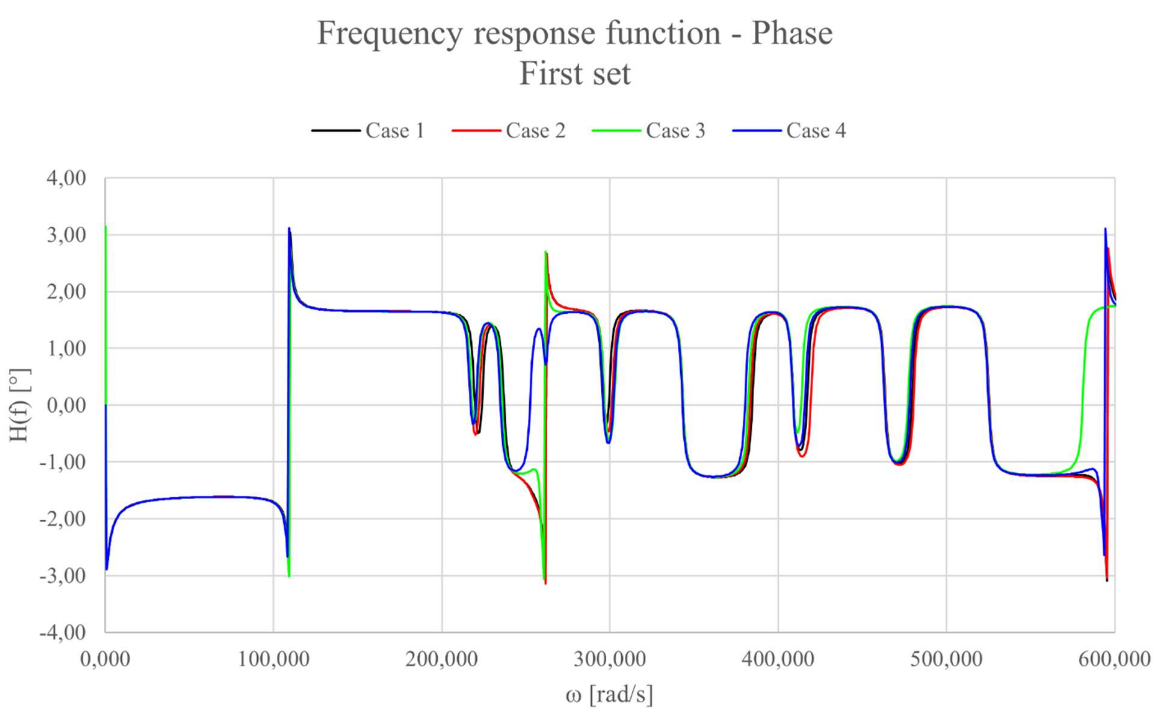

Figure 52 - Relaxation: phase of FRF (first set)

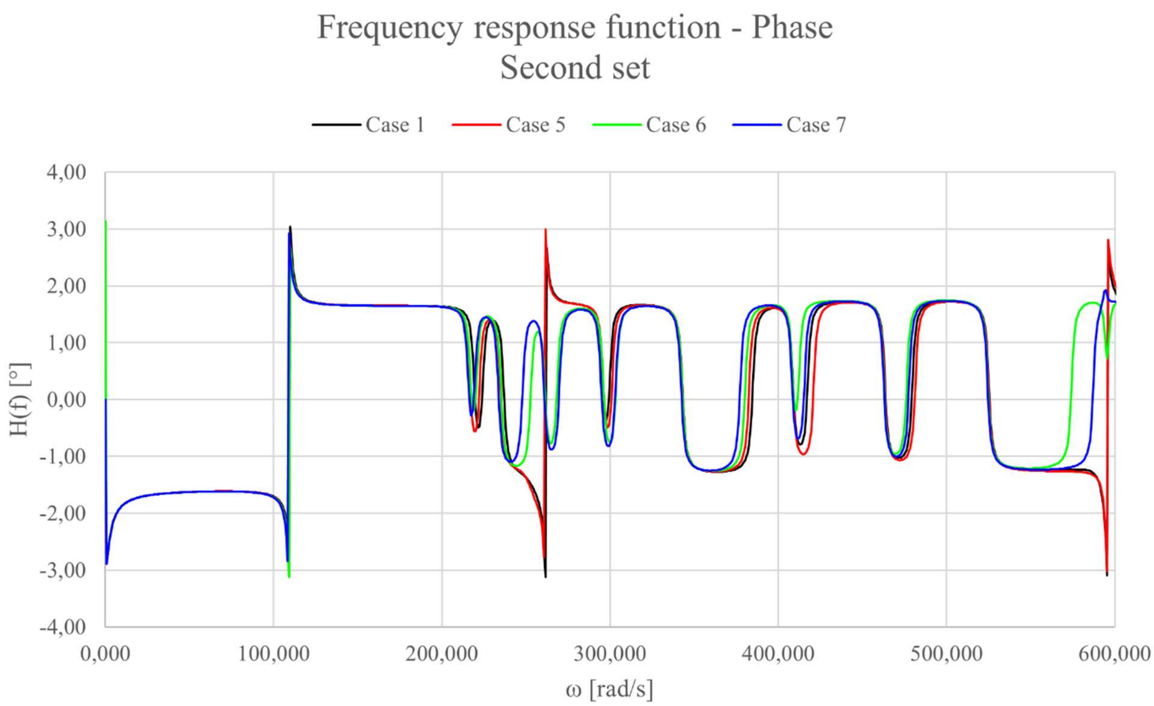

Figure 53 - Relaxation: phase of FRF (second set)

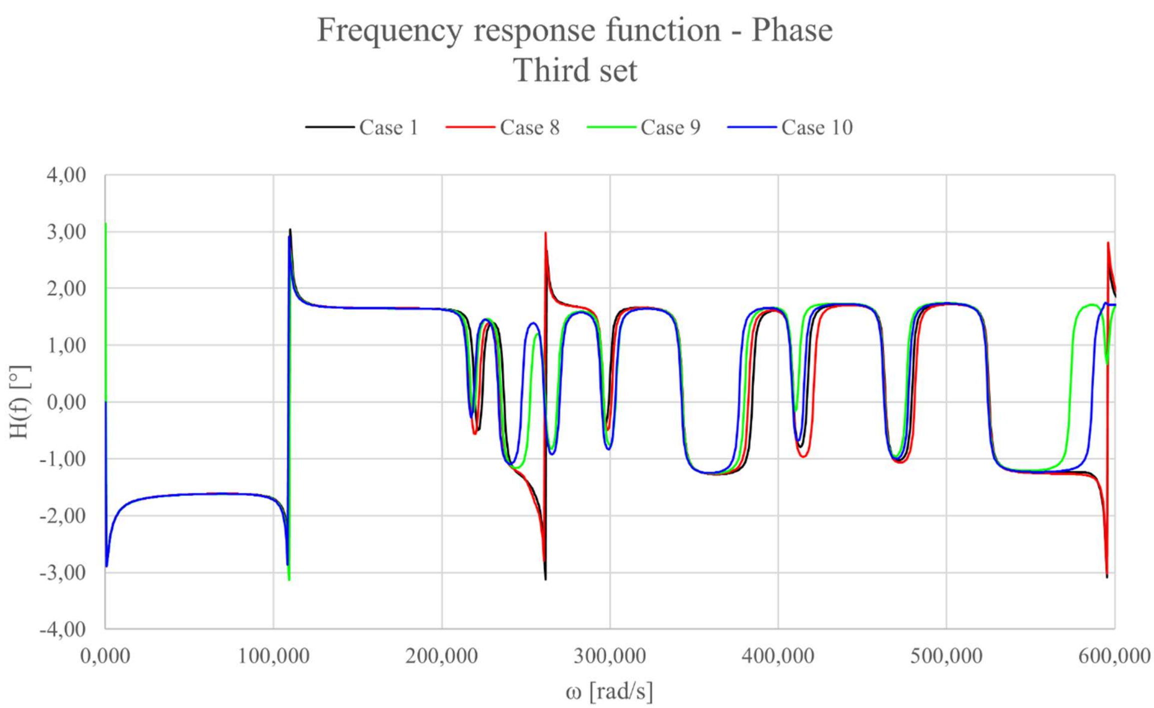

Figure 54 - Relaxation: phase of FRF (third set)

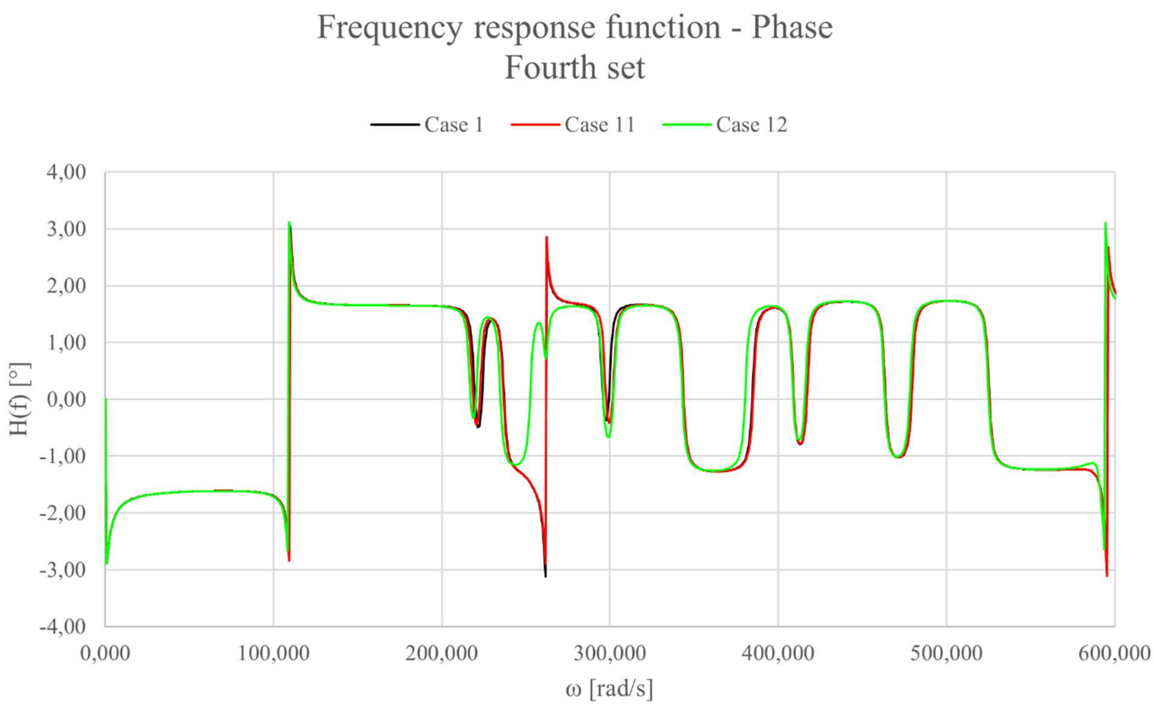

Figure 55 - Relaxation: phase of FRF (fourth set)

Then the natural frequencies can be extracted from the frequency response function, exploiting their correspondence to the peaks of the frequency response function from a graphical point of view.

The natural frequencies for the different cases of relaxation are reported in the table listed below.

Table 10 - Relaxation: fundamental frequencies

Nr. case	f_1 [Hz]	f_2 [Hz]	f_3 [Hz]	f_4 [Hz]	f_5 [Hz]
1	17,4730	34,8007	37,6914	41,6516	46,8811
2	17,4138	34,5046	37,4700	41,6707	47,0652
3	17,4082	34,5041	37,5076	47,0947	-
4	17,3687	34,3749	37,3349	46,9734	-

5	17,3922	34,4230	37,3706	41,6522	46,9992
6	17,3817	34,4209	37,4266	41,5477	47,0433
7	17,3228	34,2096	37,1567	41,4632	46,8463
8	17,3898	34,4163	37,3585	41,6502	46,9888
9	17,3787	34,4144	37,4193	41,5468	47,0385
10	17,3186	34,1937	37,1383	41,4586	46,8334
11	17,4460	34,6319	37,6424	41,7008	47,1877
12	17,3687	34,3749	37,3349	46,9734	-

5.2.2 Second case study: changes in the pre-strain due to temperature gradients

Environmental effects play an important role in damage detection in civil engineering structures and, sometimes, they have a bigger effect than the one of structural origin.

In general, temperature variations cause the contraction or the expansion of the considered element, described by the so-called thermal expansion coefficient. In the case of a steel structure, such as the case study of this dissertation, the thermal expansion coefficient will affect the pre-strain more than the elastic modulus.

Moreover, tensegrity structures have a non-linear behaviour, and this implies that the relaxation of all the tension elements composing the structures will be non-linear too. So, for simplicity, a uniform relaxation only in the longitudinal direction for all the tension cables has been considered.

Considering an increment or decrement of temperature ΔT, also called temperature gradient, the change in temperature can be always defined as:

$$T = T_0 + \Delta T \qquad (4.1)$$

where T_0 represent the initial temperature and T represents the final temperature.

At the temperature T_0 the element is characterized by an initial length L_0 and, when subjected to a temperature gradient, the same element will lengthen or shorten of a quantity ΔL, defined as:

$$\Delta L = L_0(T_0)\alpha\Delta T \tag{4.2}$$

Consequently, the length of the element at the temperature T will be defined as:

$$L = L_0(T_0)[1 + \alpha\Delta T] \tag{4.3}$$

Therefore, the lengthening or shortening of the element is directly related to thermal expansion coefficient **α**, which describes how the element changes when it is subjected to a temperature variation. Its unit of measure is K^{-1} (in the S.I.) or $C^{\circ,\,-1}$.

For this case study, the following thermal expansion coefficient has been considered:

$$\alpha = 1{,}2 * 10^{-5}\ C^{\circ-1} \tag{4.4}$$

A thermal expansion coefficient of this order will cause a change in the pre-strain of the order of mm. The different considered cases have been reported in the table listed below.

Table 11 – Cases of temperature effects

Nr. case	Description	Pre-strain values
1	Healthy situation	$\varepsilon = 2{,}5*10^{-4}$
2	Lengthening of the elements due to ΔT	$\varepsilon = 1*10^{-4}$
3	Lengthening of the elements due to ΔT	$\varepsilon = 5*10^{-5}$
4	Lengthening of the elements due to ΔT	$\varepsilon = 1*10^{-5}$
5	Lengthening of the elements due to ΔT	$\varepsilon = 5*10^{-6}$
6	Lengthening of the elements due to ΔT	$\varepsilon = 1*10^{-6}$

The same procedure previously used in the case of relaxation due to loss of pre-strain has been used also in the case of temperature effects. The results are reported in the graphs reported below.

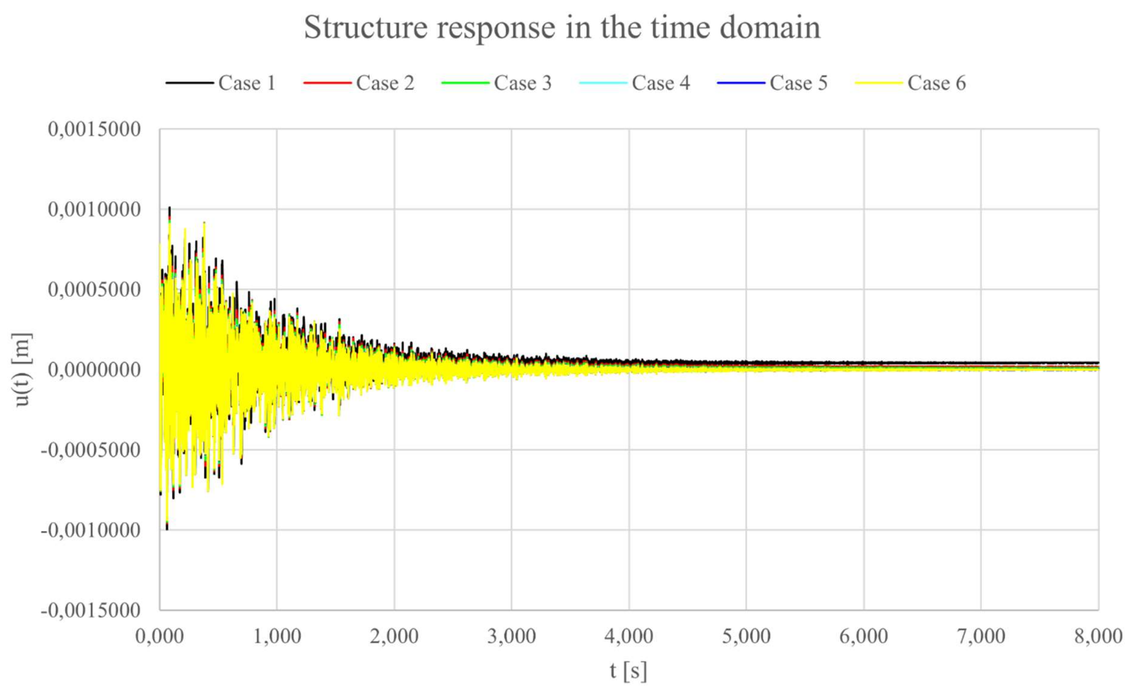

Figure 56 - Temperature effects: time domain response

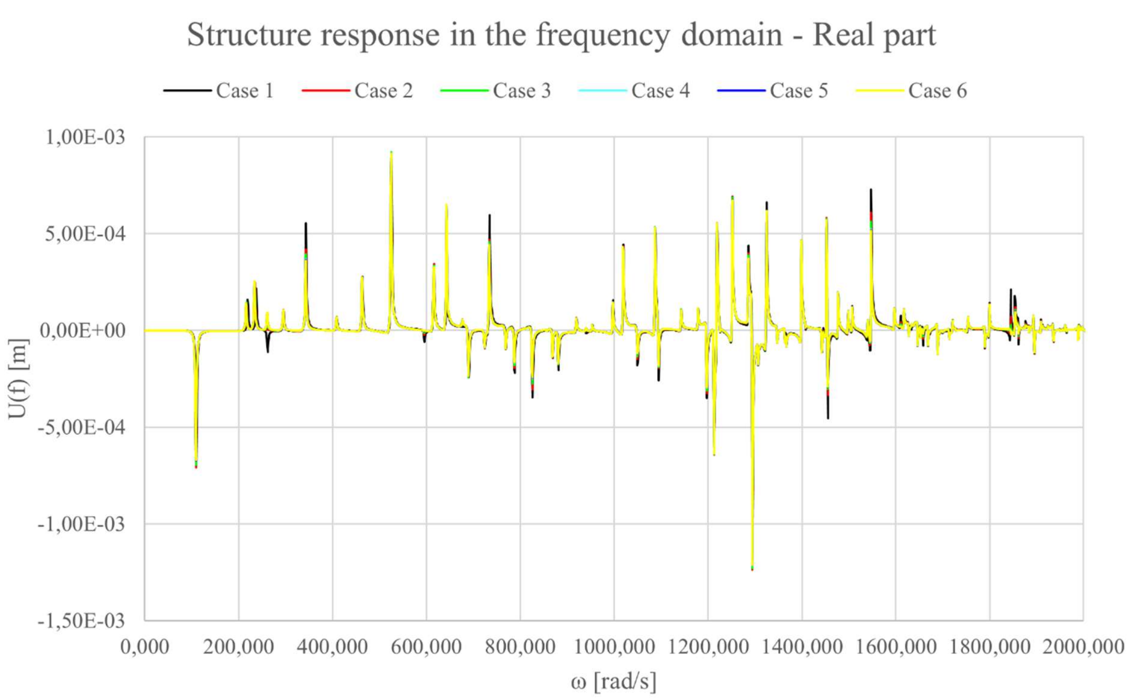

Figure 57 - Temperature effects: real part of frequency domain response

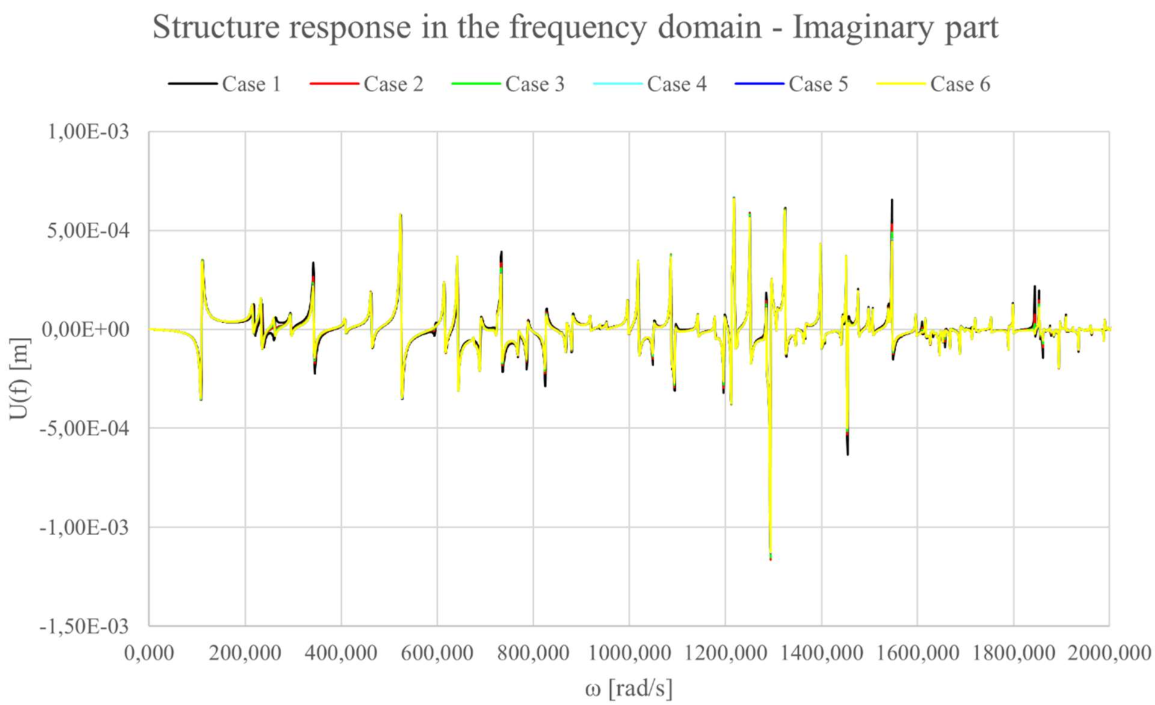

Figure 58 - Temperature effects: imaginary part of frequency domain response

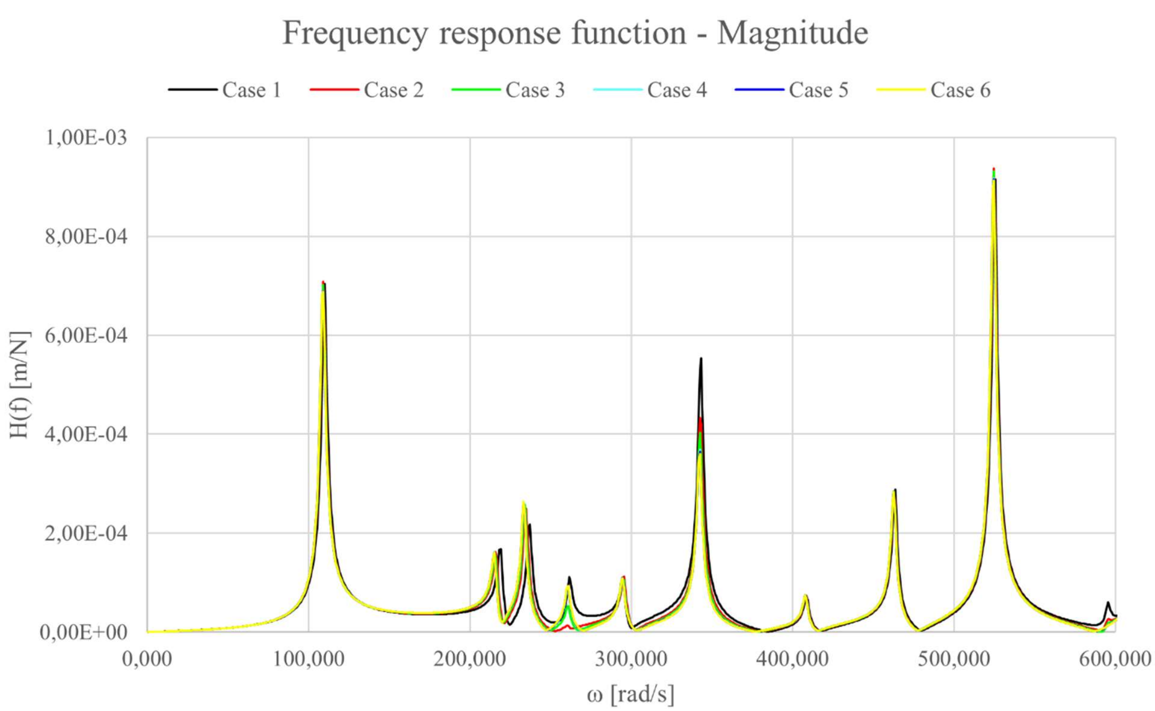

Figure 59 - Temperature effects: magnitude of FRF

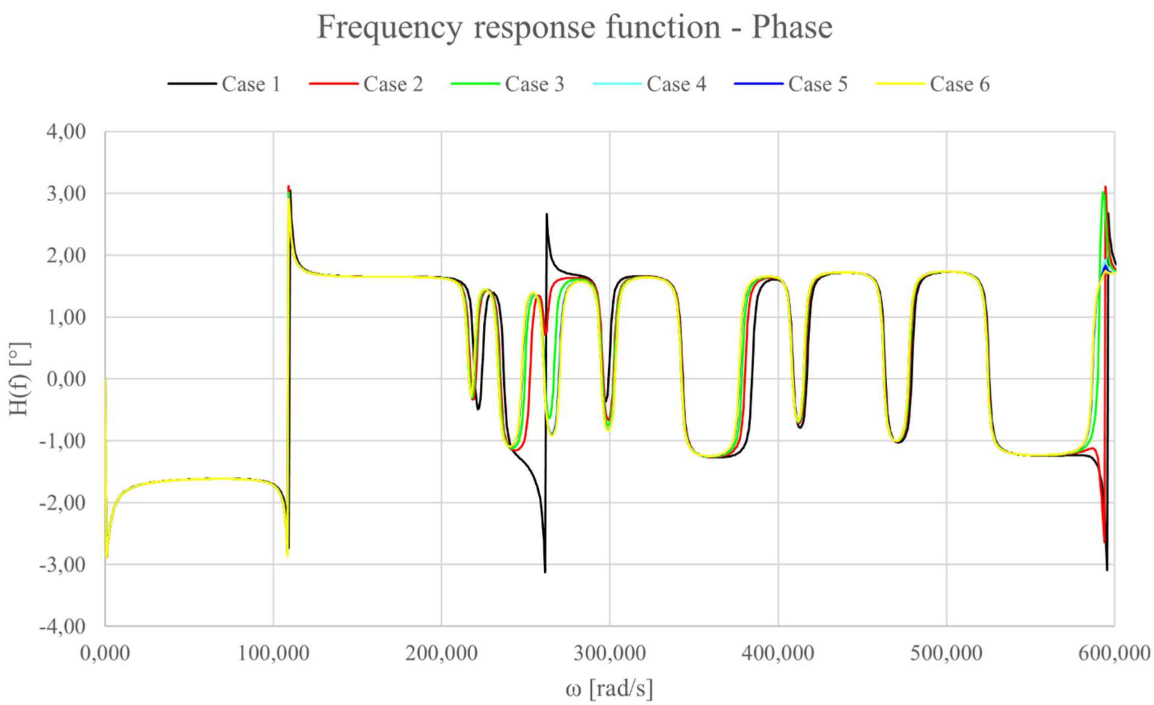

Figure 60 - Temperature effects: phase of FRF

Table 12 - Temperature effects: fundamental frequencies

Nr. case	f_1 [Hz]	f_2 [Hz]	f_3 [Hz]	f_4 [Hz]	f_5 [Hz]
1	17,4730	34,8007	37,6914	41,6516	46,8811
2	17,3687	34,3749	37,3349	46,9734	-
3	17,3419	34,2843	37,2341	41,4783	46,9073
4	17,3228	34,2096	37,1567	41,4632	46,8463
5	17,3205	34,2005	37,1467	41,4607	46,8389
6	17,3186	34,1937	37,1383	41,4586	46,8334

5.2.3 Third case study: corrosion of the steel elements

One of the most common damage phenomena in metallic materials is represented by corrosion. Corrosion is strictly correlated to the micro-environment in which the structure is built; for example, if the metallic element is exposed to air with a very high level of moisture, there is a good probability for corrosion to happen.

The most common type of corrosion is wet corrosion, that has an electrochemical nature: the process is characterized by two different chemical reactions, an anodic and a cathodic one, which have to happen concurrently and in presence of an electrolyte (i.e., water). When the metallic element is in contact with the electrolyte, which allows the ionized species to be transferred, an anodic reaction involving the metal occurs, resulting in the oxidation of the metal and, consequently, in the release of electrons.

The electrons will be then transferred by the electrolyte to the cathodic zone of the metal, where a reduction reaction will occur. If one of the two reactions is slowed or stopped, also the other reaction will be slowed or stopped: it is therefore fundamental that both the reactions occur contemporarily.

There can be different types of wet corrosion; in the case of this dissertation, the uniform corrosion is considered, which means that the corrosion process will be uniform all over the metallic element. The main consequence of uniform corrosion is represented by a reduction in the bearing cross-section area of the element.

Since the tension cables and the compression bars are made of steel S275, they can both experience corrosion: different cases of reduction of the cross-sectional area for all the elements have been therefore considered.

All the cases are reported in the table listed below.

Table 13 - Cases of corrosion

Nr. case	A_{bars} [cm^2]	A_{cables} [cm^2]
1	30,00	15,00
2	30,00	13,66
3	28,09	15,00

4	28,09	13,66
5	30,00	13,01
6	27,16	15,00
7	27,16	13,01
8	30,00	12,38
9	26,24	15,00
10	26,24	12,38
11	30,00	8,920
12	21,08	15,00
13	21,08	8,920

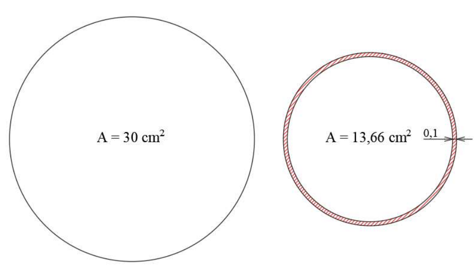

Case 2

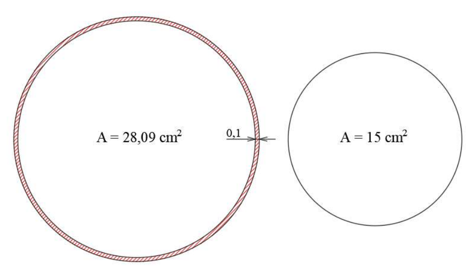

Case 3

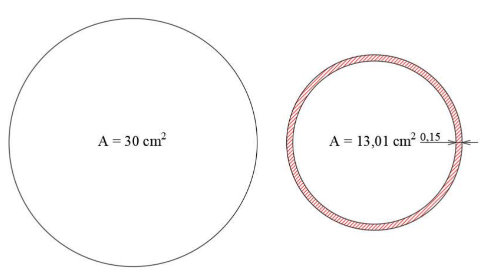

Case 5

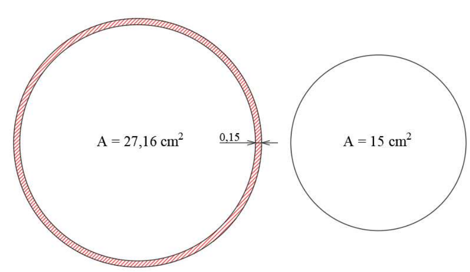

Case 6

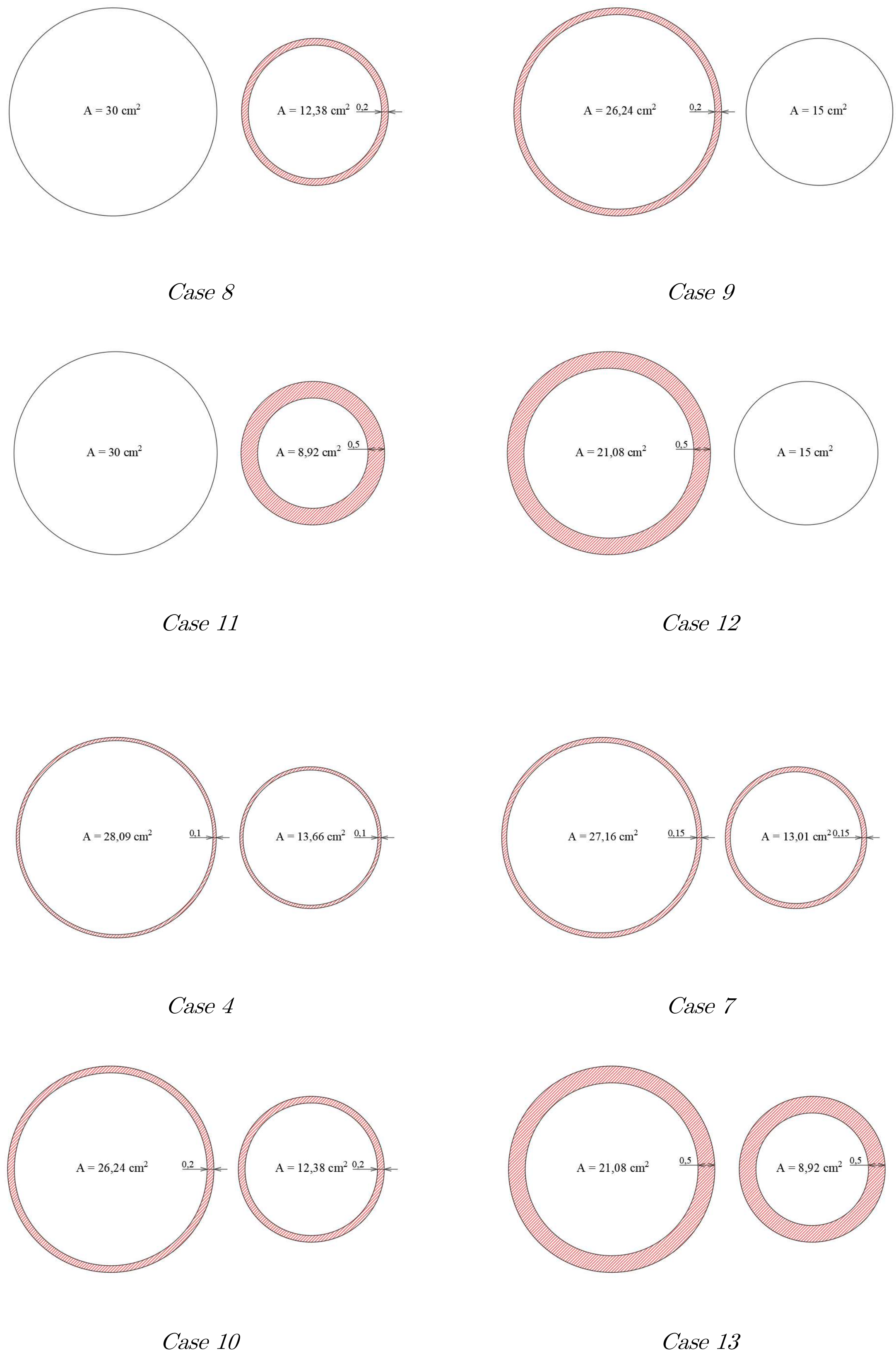

Figure 61 - Corrosion cases

In order to have a better visualization of the results, the different cases of corrosion have been grouped in different sets.

Table 14 - Corrosion: sets' definition

Nr. case	Nr. set
2	1
3	
4	
5	2
6	
7	
8	3
9	
10	
11	4
12	
13	

The same procedure previously used in the case of relaxation due to loss of pre-strain and to temperature effects has been used also in the case of corrosion. The healthy situation is reported in all the graphs.

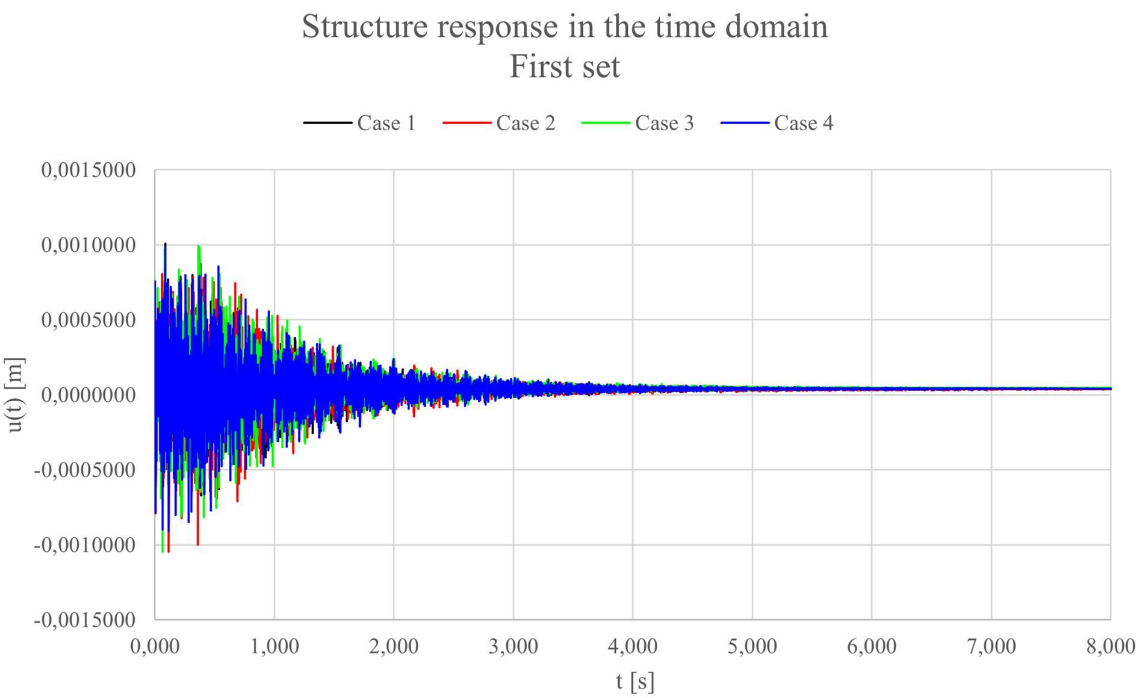

Figure 62 - Corrosion: time domain response (first set)

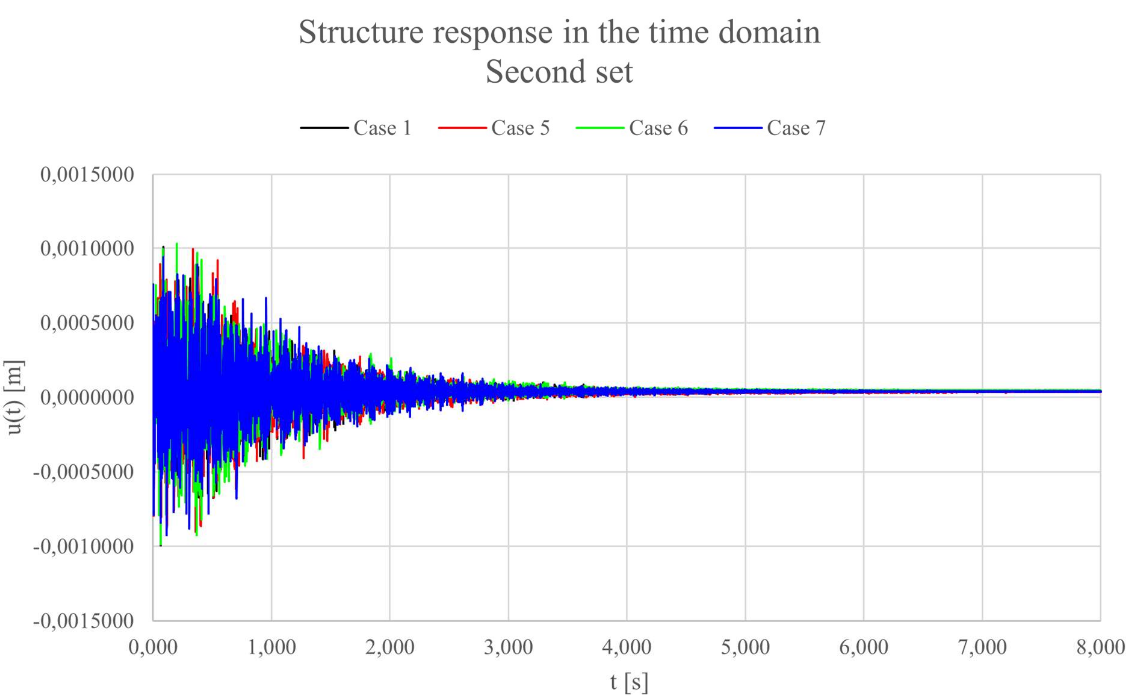

Figure 63 - Corrosion: time domain response (second set)

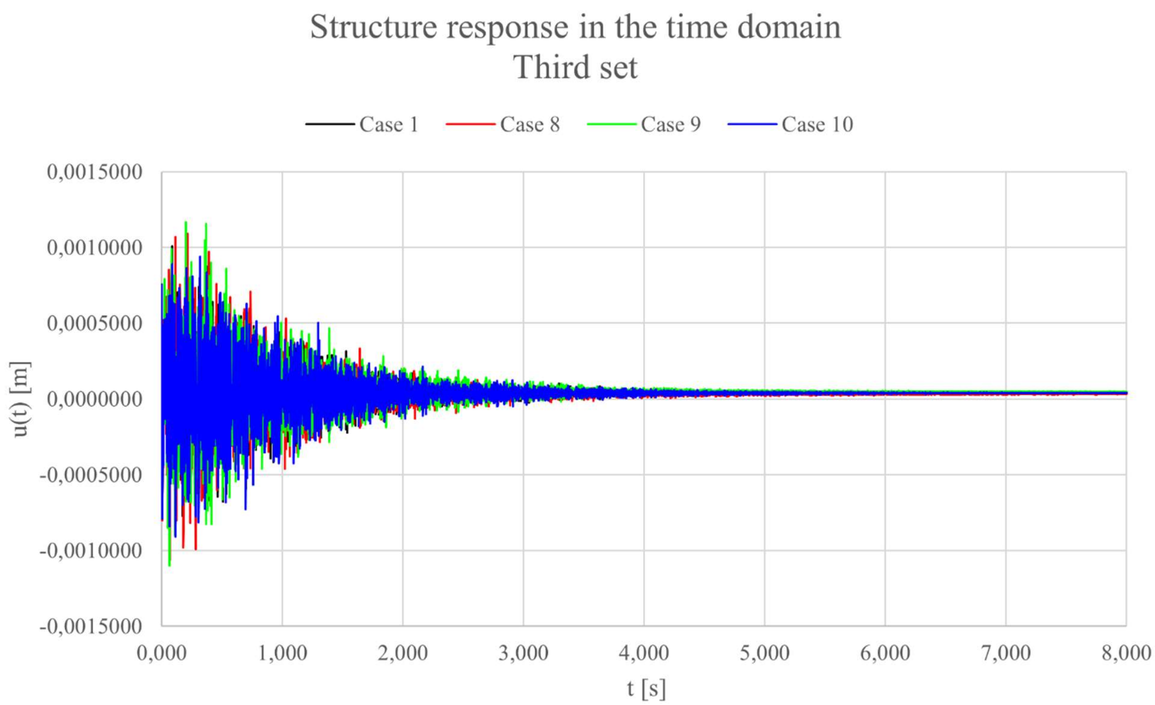

Figure 64 - Corrosion: time domain response (third set)

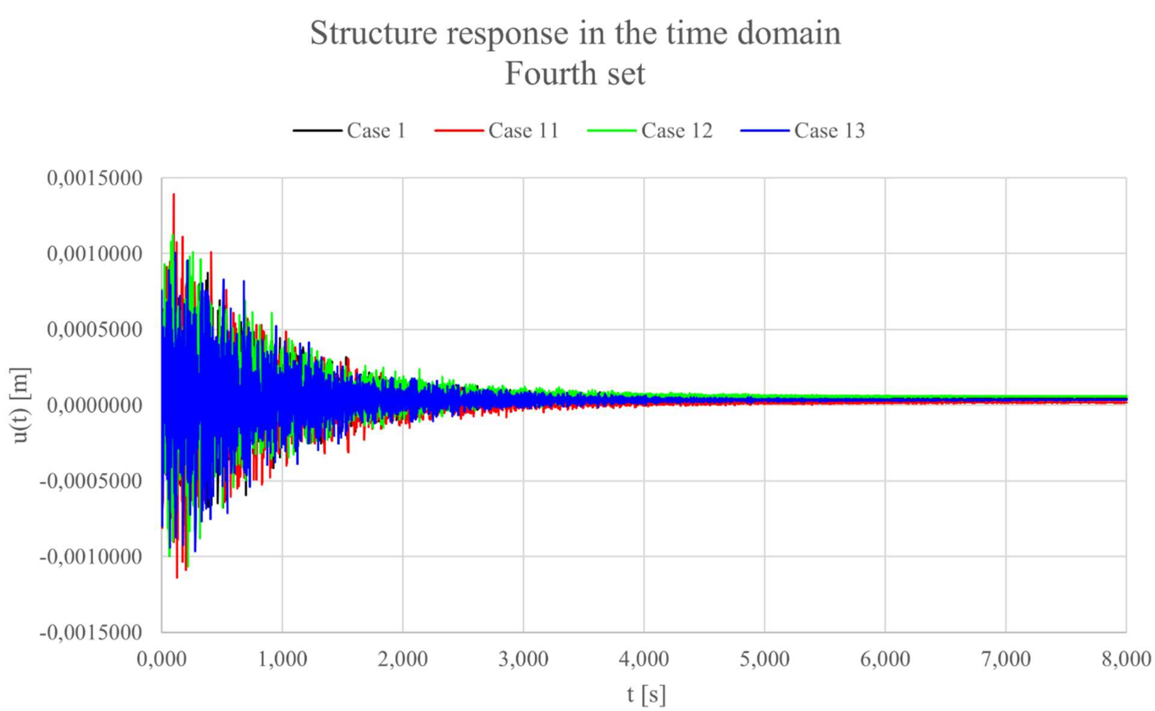

Figure 65 - Corrosion: time domain response (fourth set)

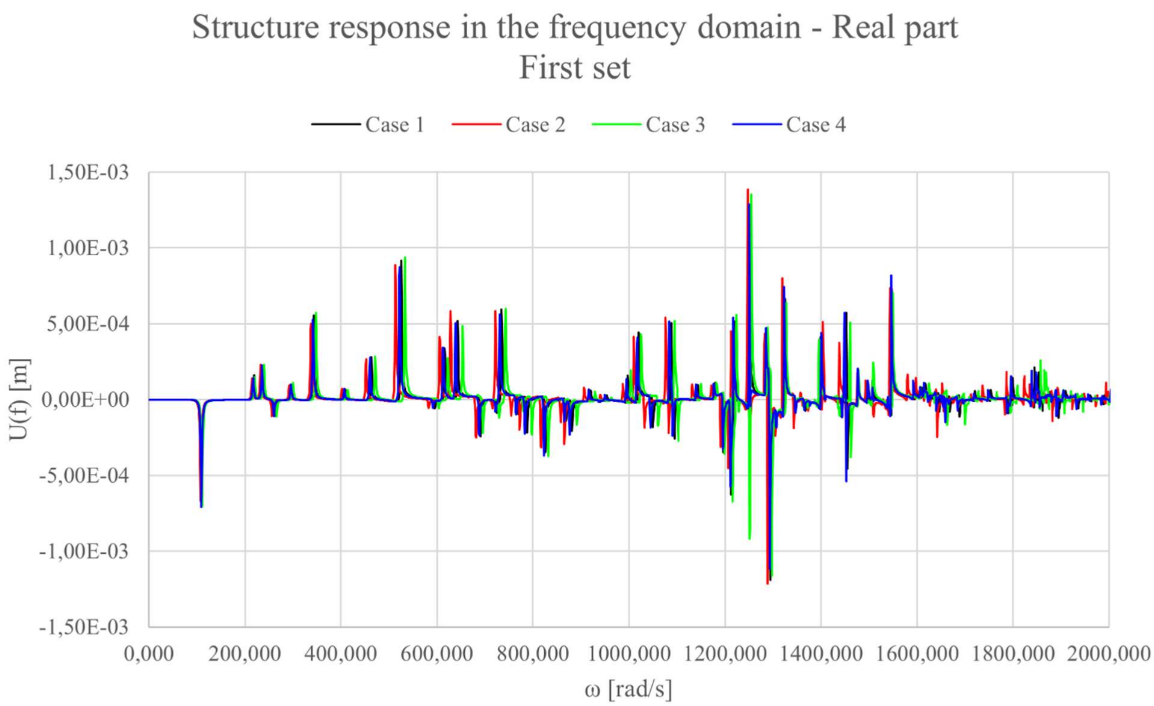

Figure 66 - Corrosion: real part of frequency domain response (first set)

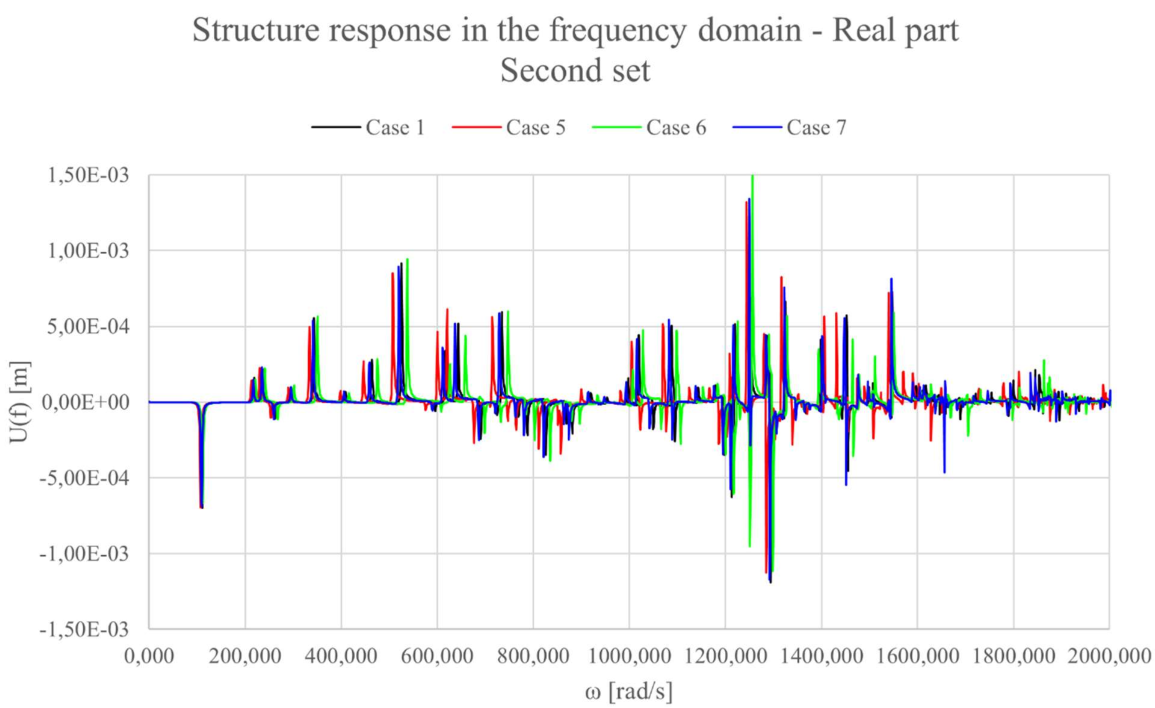

Figure 67 - Corrosion: real part of frequency domain response (second set)

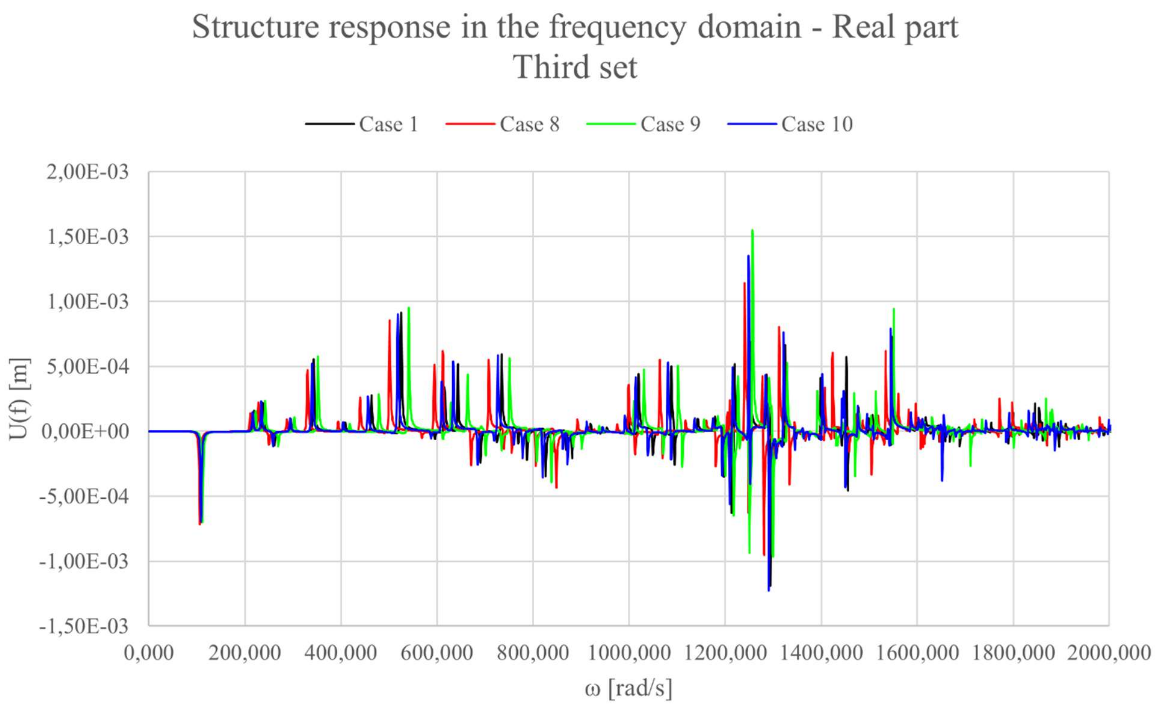

Figure 68 - Corrosion: real part of frequency domain response (third set)

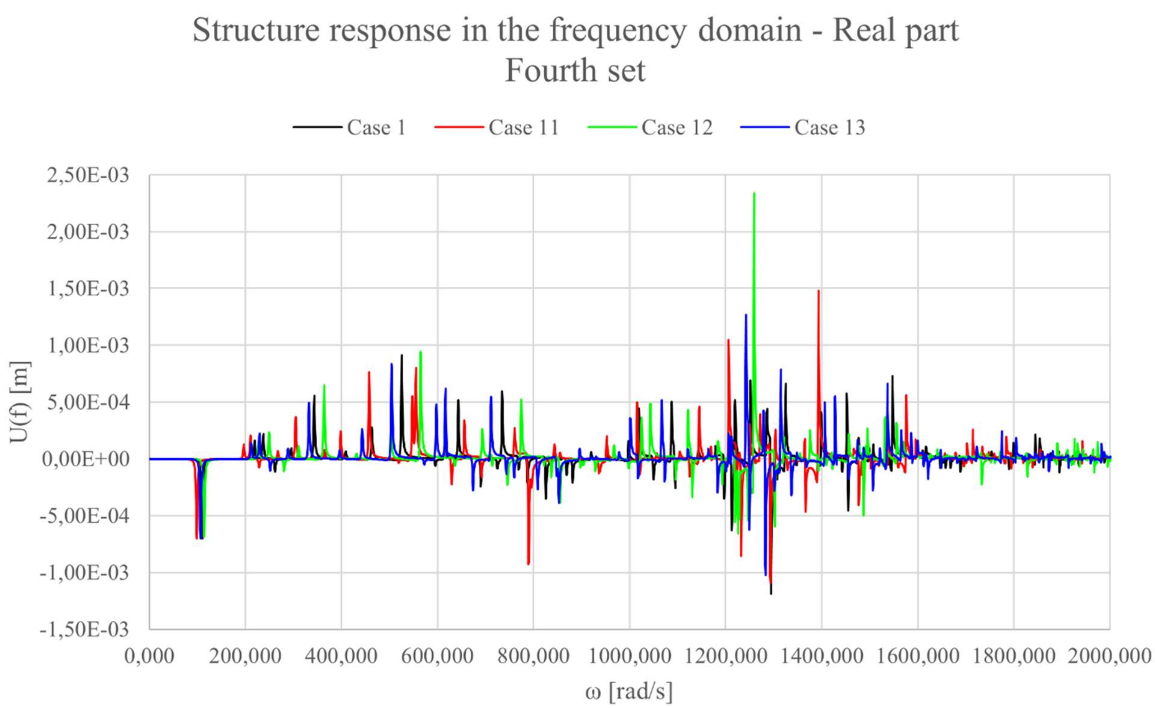

Figure 69 - Corrosion: real part of frequency domain response (fourth set)

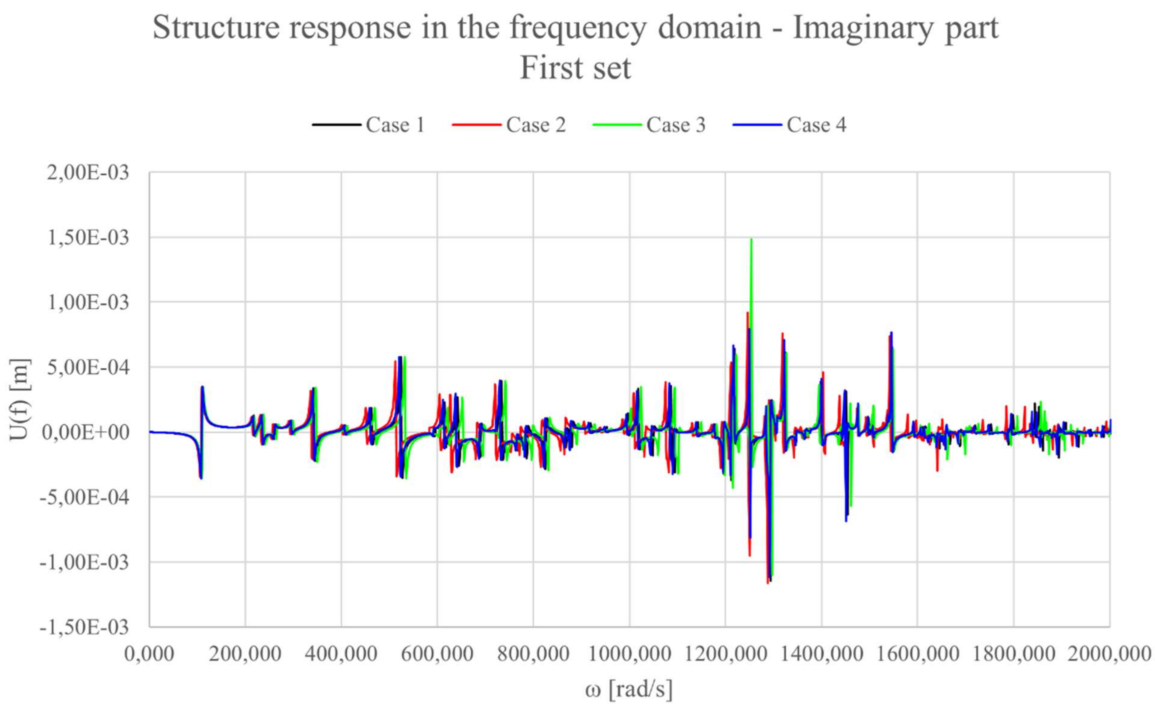

Figure 70 - Corrosion: imaginary part of frequency domain response (first set)

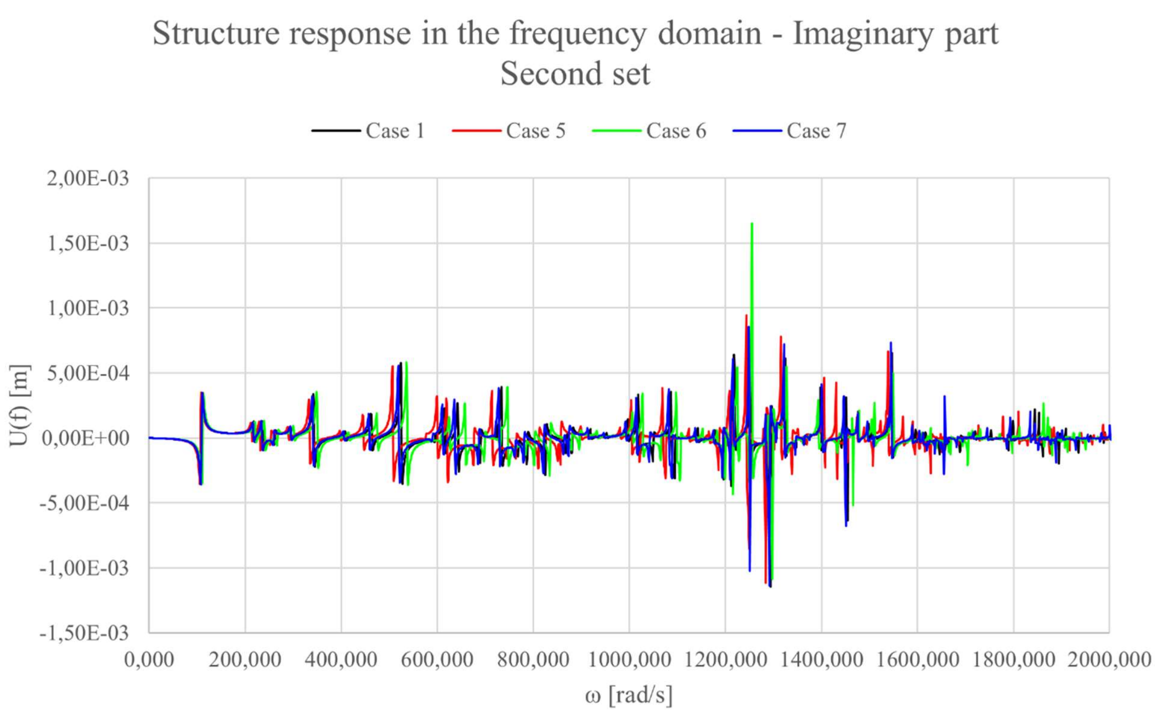

Figure 71 - Corrosion: imaginary part of frequency domain response (second set)

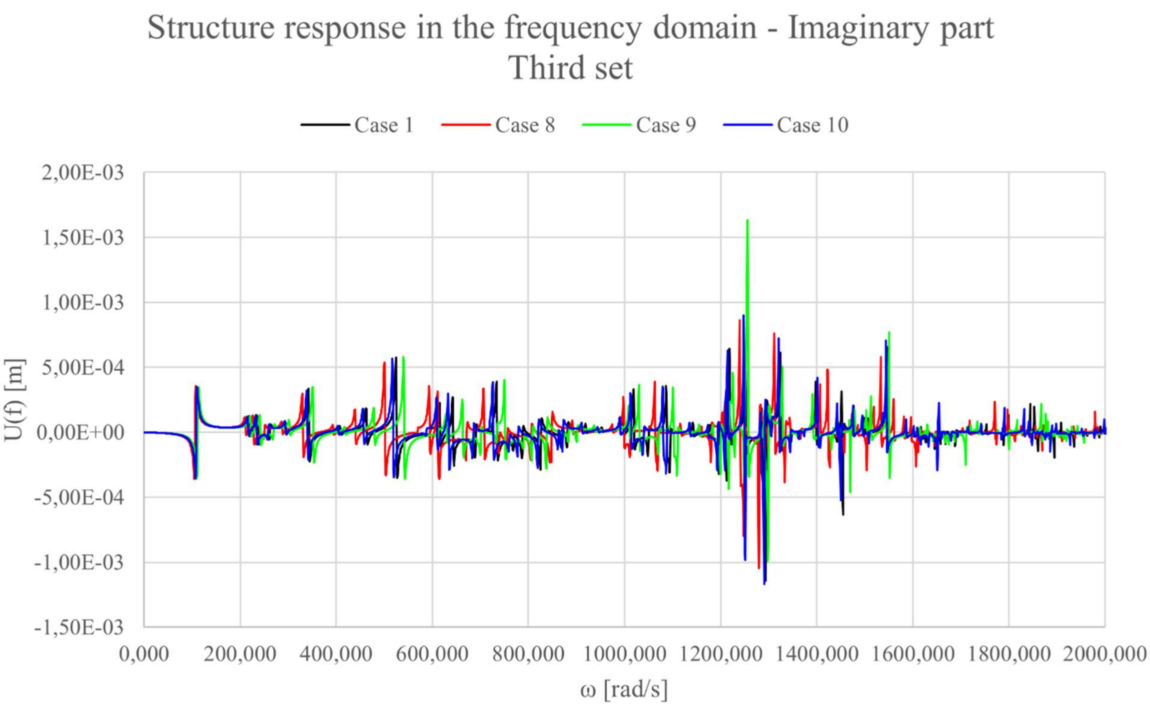

Figure 72 - Corrosion: imaginary part of frequency domain response (third set)

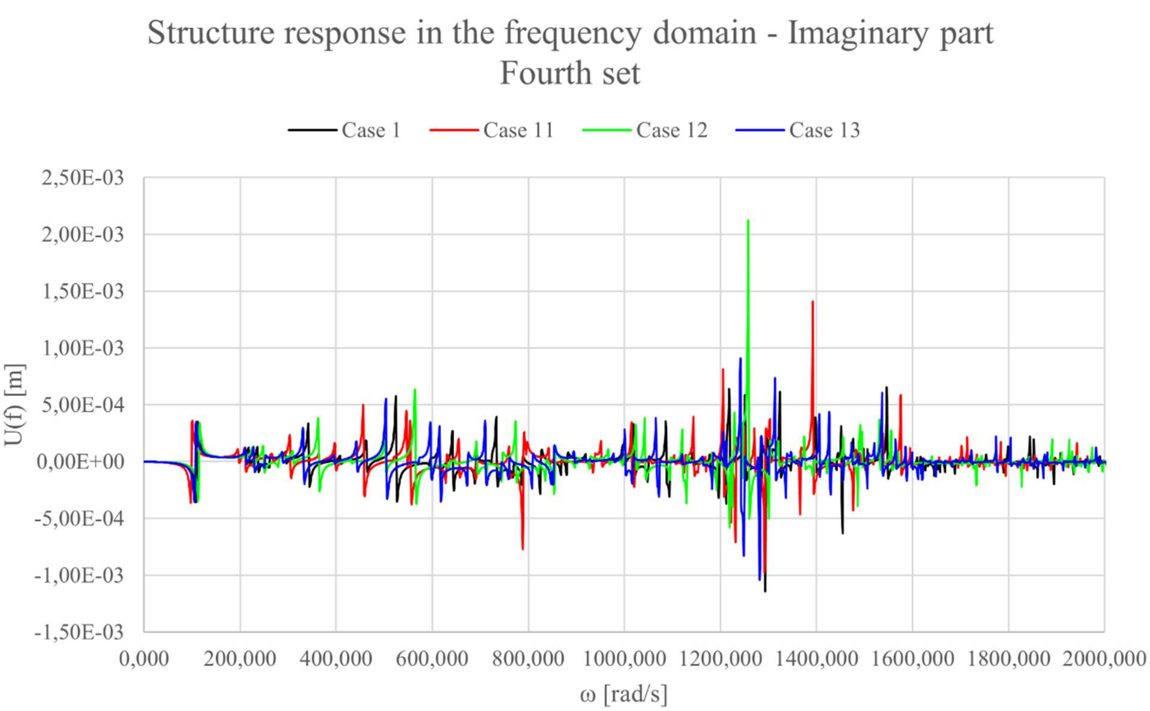

Figure 73 - Corrosion: imaginary part of frequency domain response (fourth set)

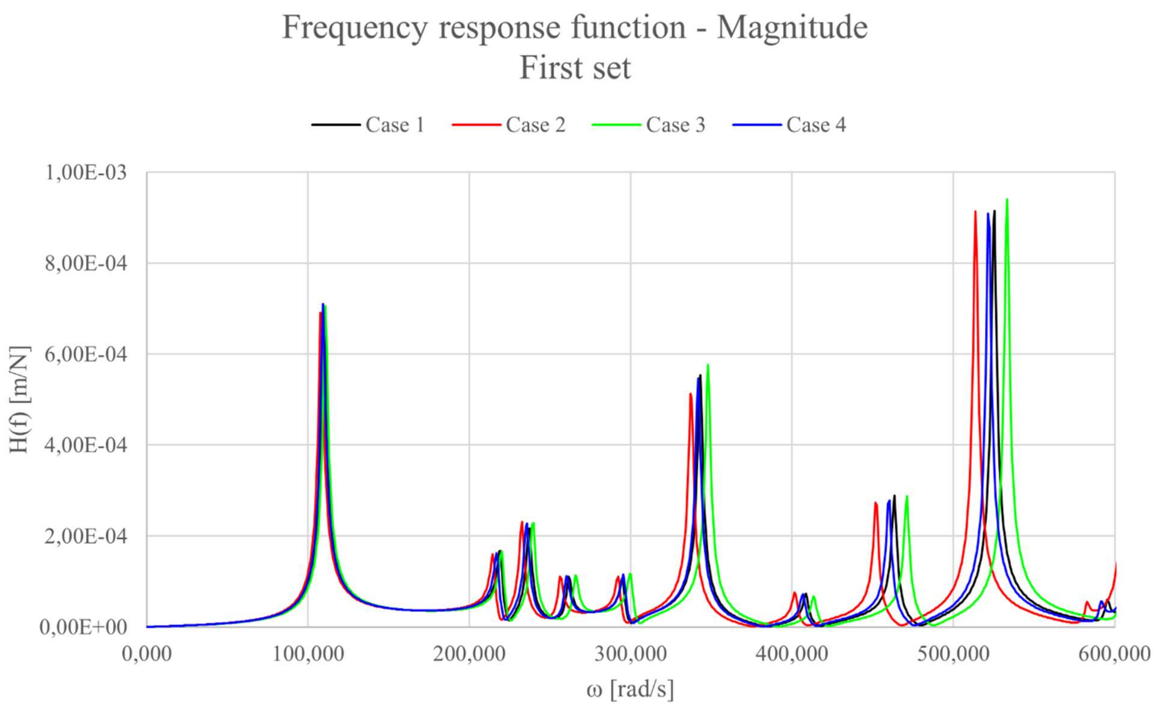

Figure 74 - Corrosion: magnitude of FRF (first set)

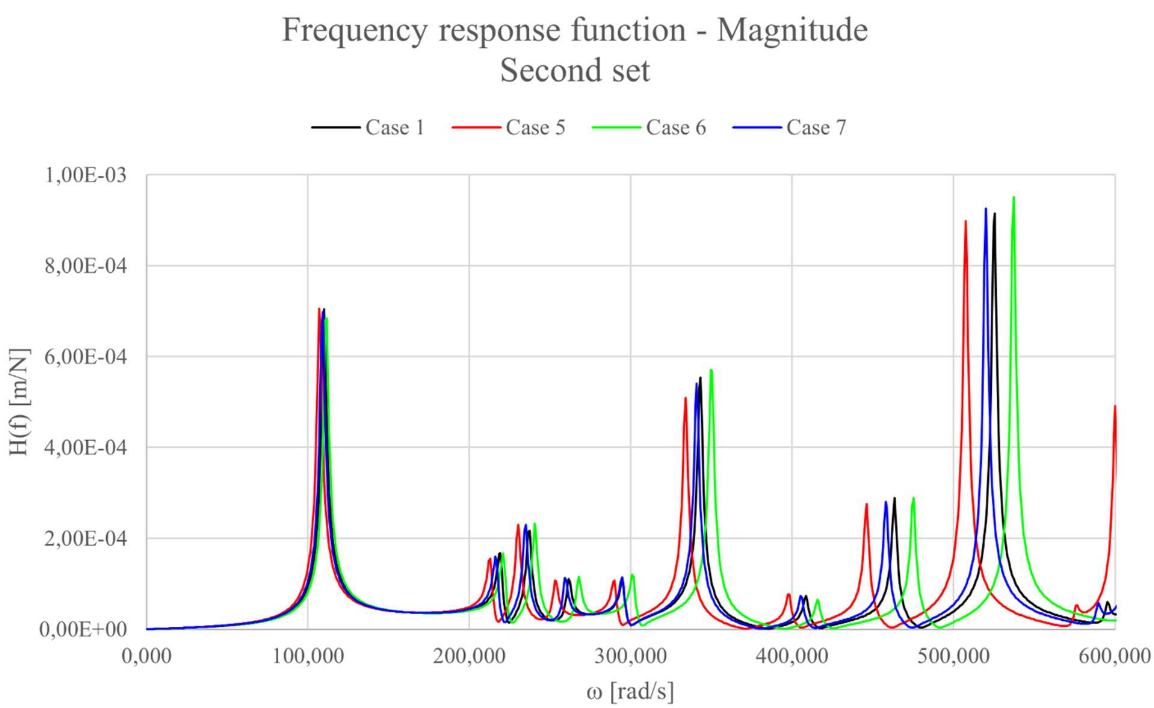

Figure 75 - Corrosion: magnitude of FRF (second set)

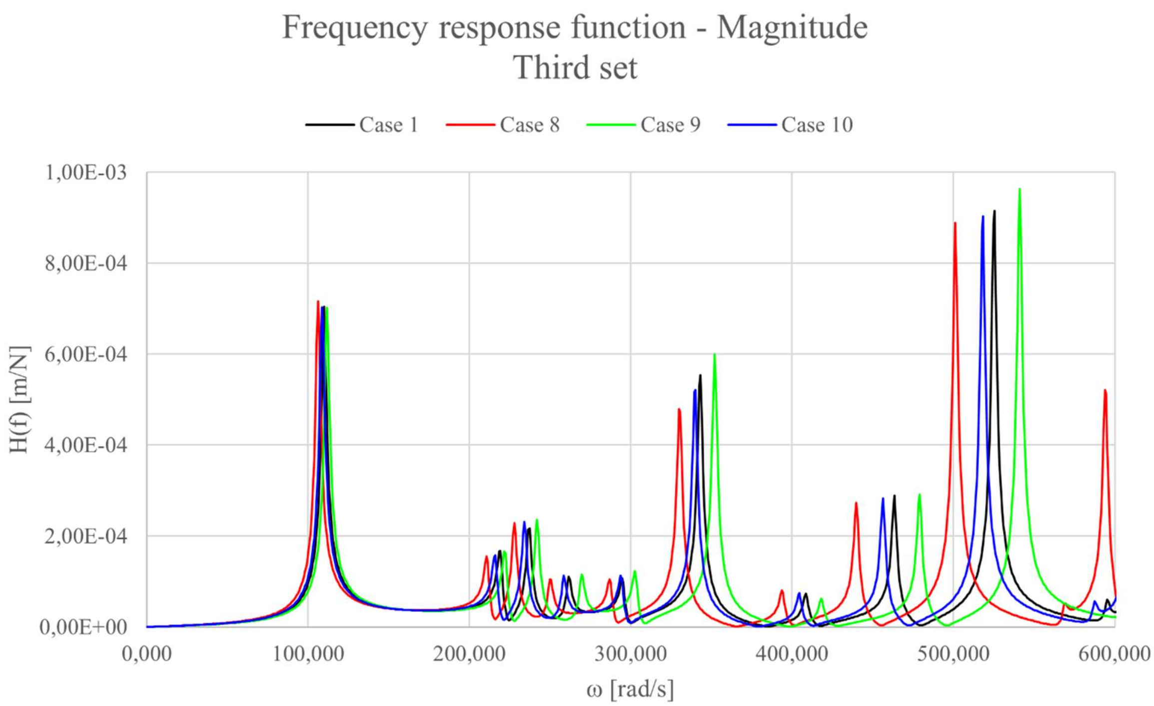

Figure 76 - Corrosion: magnitude of FRF (third set)

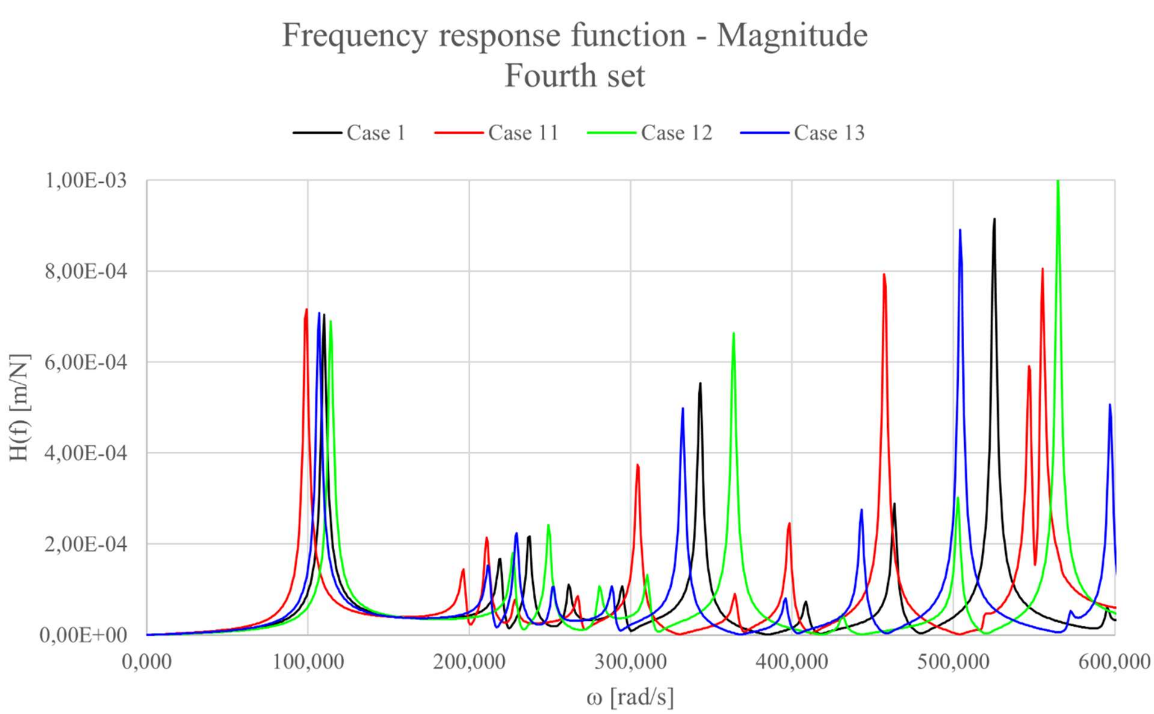

Figure 77 - Corrosion: magnitude of FRF (fourth set)

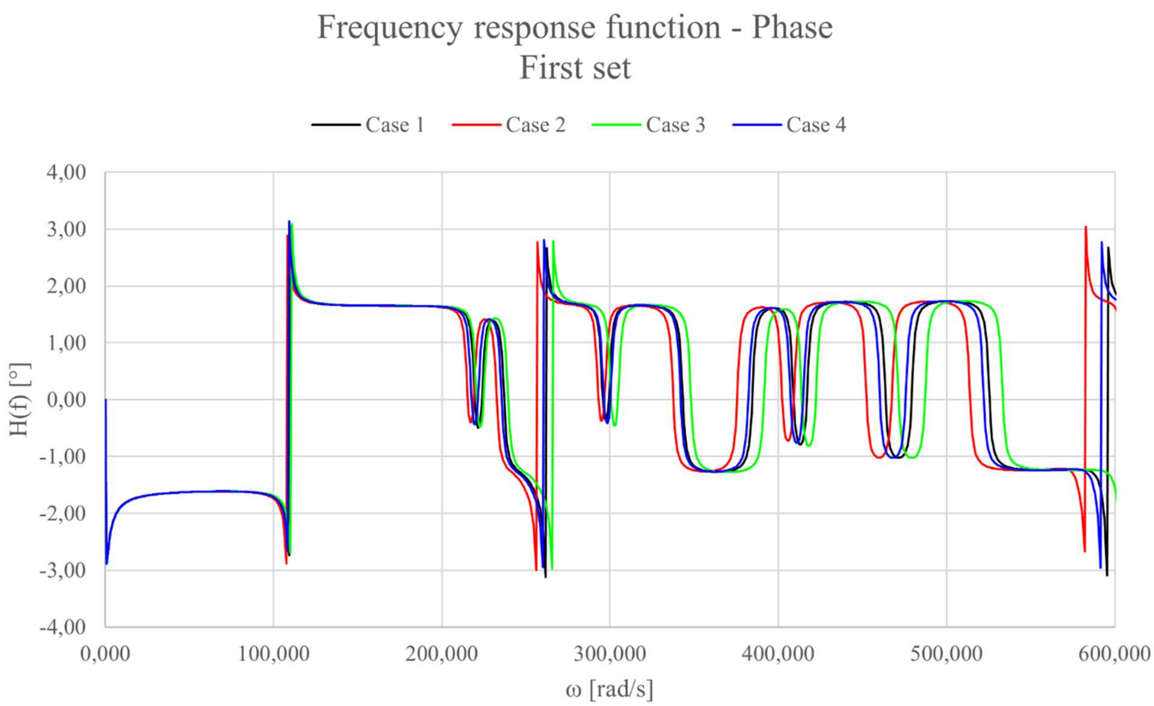

Figure 78 - Corrosion: phase of FRF (first set)

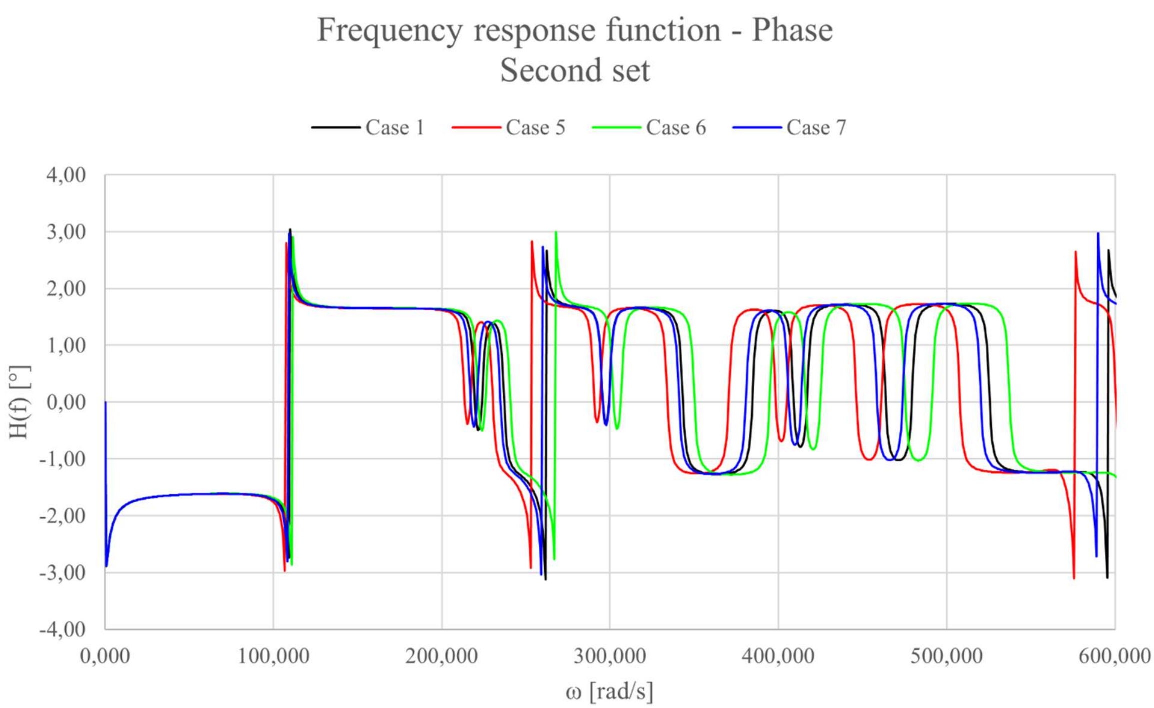

Figure 79 - Corrosion: phase of FRF (second set)

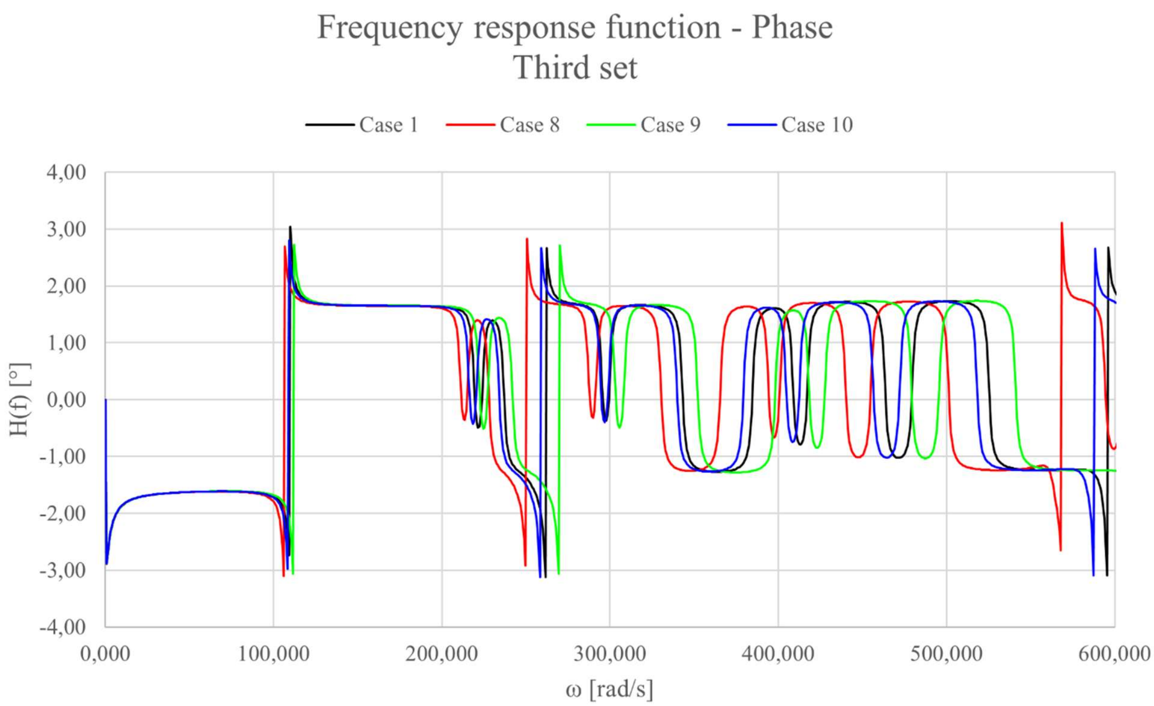

Figure 80 - Corrosion: phase of FRF (third set)

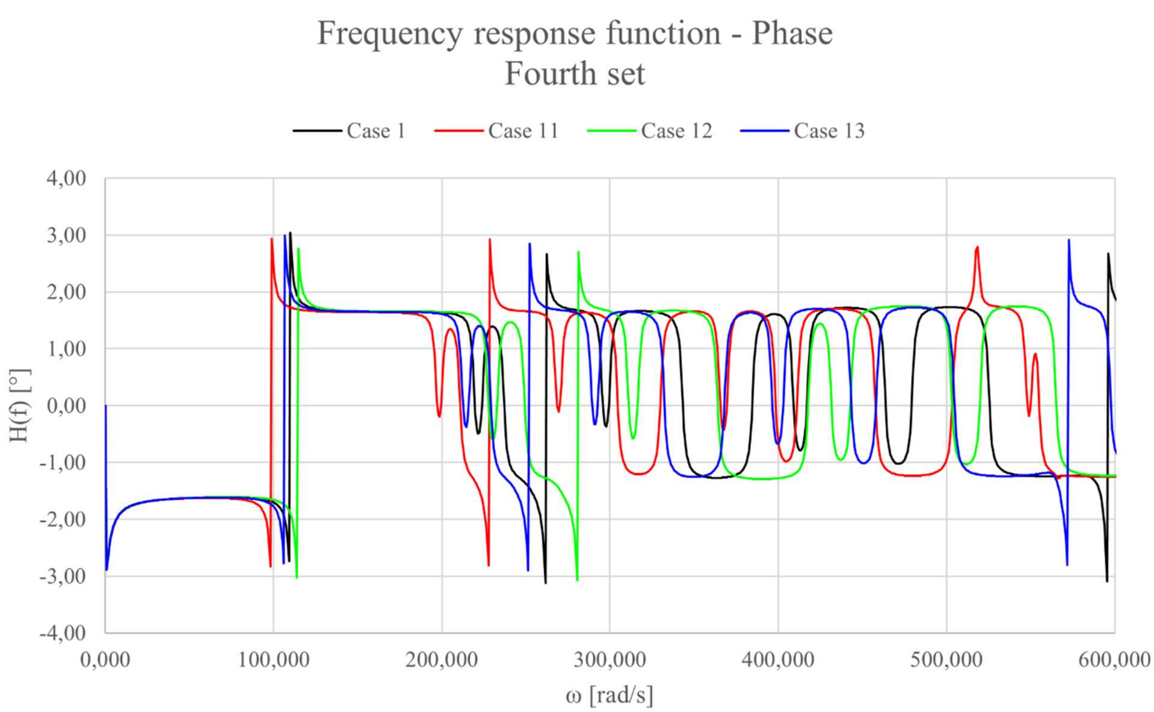

Figure 81 - Corrosion: phase of FRF (fourth set)

Table 15 - Corrosion: fundamental frequencies

Nr. case	f_1 [Hz]	f_2 [Hz]	f_3 [Hz]	f_4 [Hz]	f_5 [Hz]
1	17,4730	34,8007	37,6914	41,6516	46,8811
2	17,1872	34,1060	36,9873	40,8020	46,4582
3	17,6102	34,9592	38,0686	42,3118	47,6663
4	17,3717	34,4765	37,4497	41,4386	46,9794
5	17,0430	33,8129	36,6341	40,3163	46,0566
6	17,6912	35,1283	38,2825	42,6109	-
7	17,3295	34,3981	37,3446	41,2957	46,8661
8	16,8865	33,5113	36,2596	39,8145	45,6377
9	17,7705	35,2832	38,4869	42,9205	-
10	17,2911	34,3080	37,2401	41,1490	46,7504
11	15,7011	31,1814	33,5407	36,3276	42,4764
12	18,1548	36,0944	39,6418	44,6811	-
13	16,9627	33,6656	36,4479	40,0698	45,8495

5.2.4 Results

Once all the analyses have been carried out, the following results for each damage situation can be pointed out:

1. Loss of pre-strain due to relaxation

   The first damage case analysed gave very interesting results for the different types of plots which have been investigated:

   - Structure response in the time domain

     A general tendency can be individuated for each set: while in the case of relaxation of the lateral cables the response tends to decrease from a numerical point of view, reaching high negative values (i.e., the structure is moving in the opposite direction), in the case of relaxation of the cables composing the hexagon module, it tends to increase numerically. If both of them are subjected to relaxation, the response of the structure tends to slightly increase in the opposite direction. In the case of relaxation of some selected cables, the response does not change significantly, therefore a relaxation of only few cables do not affect the global health of the structure.

   - Structure response in the frequency domain

     In the frequency domain, the response of the structure tends to reach higher values when the cables are subjected to relaxation without a specific tendency. The only noticeable opposition of tendency is given by the imaginary part of the response in the case of relaxation of selected cables, where at the first natural frequency, a difference in the graph is noticeable.

   - Frequency response function

     More than the magnitude of the frequency response function, which is not subjected to important differences, it is worth it to underline the shift of the frequency response function at the natural frequencies of the structure: this result validates the damage identification based on the natural frequencies variation. In particular, at the first natural frequency, the shift is not very large, but it becomes more and more noticeable increasing the natural frequencies. For what concerns the phase of the frequency response function, the same tendency can be noticed in all the cases, except for the 4^{th} natural frequency, where a change of phase is evident.

2. Loss of pre-strain due to temperature gradients

In general, there are no huge differences between the healthy situation and the damage situations. The loss of pre-strain due to temperature gradients is a uniform loss of pre-strain (as stated previously). Therefore, it is very similar to the one due to relaxation, when all the cables are relaxed, and a similar reasoning can be made, considering that the biggest changes in the response have been identified in the case in which either the lateral cables or the cables composing the hexagon module are relaxed and not in the case in which both the elements are relaxed. It's again worth it to highlight the change of phase of the frequency response function at the 4^{th} natural frequency.

3. Corrosion of the steel elements

In the third damage situation, very huge changes can be individuated:

- Structure response in the time domain

  An interesting result has been obtained from the analysis of the response in the frequency domain: a higher response can be individuated when either the compression bars or the tension cables are subjected to corrosion, but a simultaneous reduction of their cross section gives a response with a lower magnitude than the previous two cases.

- Structure response in the frequency domain

  In the case of the response of the frequency domain, a higher peak is always reached by the corrosion cases than by the healthy situation, and when increasing the rate of corrosion extremely (fourth set), it is possible to notice a shift of the response.

- Frequency response function

  A shift of the frequency response function is noticeable in all the four sets of cases, but, as in the previous cases, at the 1^{st} natural frequency the shift is smaller. Increasing the rate of corrosion, the shift become larger and larger, even for the 1st natural frequency. It is worth it to underline that, if in the case of corrosion of the compression bars and of all the elements, the shift is in the left direction (i.e., a decrease in the natural frequencies of the structure as expected), in the case of corrosion of the tension cables, the shift is the right direction (i.e., an increase in the natural frequencies of the structure).

Since the effects due to temperature gradients are small compared to the other situations, a comparison of the variation of the natural frequencies has been done in the corrosion and in the relaxation case. The worst situation has been considered in both cases, corresponding to the case 10 of relaxation and to the case 8 of corrosion (considering that the case 11represents an extreme case with a very high improbability to occur).

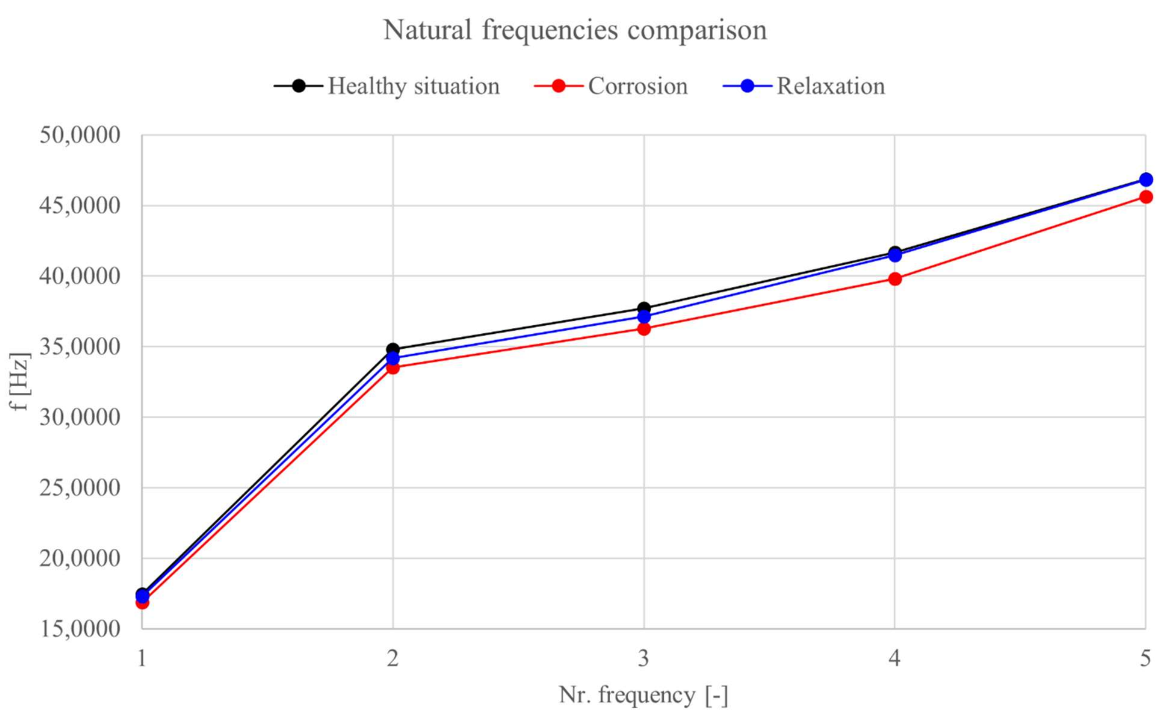

Figure 82 - Natural frequencies comparison between different damage cases

5.3 Damage identification

After individuating the tendencies of the structure responses and of the frequency response functions in the three different cases of damage, it was possible to identify the damage through the natural frequencies and to design the sensors' system.

The first assumption made is that the number of degrees of freedom of the response correspond directly to the number of sensors, considering uniaxial sensors for every degree of freedom of the structure.

Then, from the shift of the natural frequencies with respect to the healthy situation for the different types of damage previously described and for a different number of sensors, it was possible to identify the number of sensors able to detect all the damage cases in the structure.

For each case of damage, only the first three natural frequencies were reported; in the case of corrosion, the cases 11, 12 and 13 were not considered because they represent extreme cases with a very low probability to occur.

The methodology is further detailed in the sub-chapter 5.3.1, then the results for the different cases of damage will be showed, reporting the natural frequencies values for the different number of sensors and the graphs comparing the natural frequencies with respect to the different cases and number of sensors.

In the end, a comparison between the different results will be done and the final number of sensors to be placed in the structure will be reported.

5.3.1 Methodology

The damage identification methodology applied to the case study relies on the shift between the natural frequencies of the structure.

As previously stated, the number of sensors is directly related to the number of degrees of freedom of the response; therefore, changing the number of degrees of freedom of the response, the response itself will change and the natural frequencies will be different.

The structure has 132 degrees of freedom; the number of degrees of freedom of the response considered are listed in the table below.

Table 16 - Number of sensors

N_{dofs}	$N_{sensors}$
8	8
16	16
32	32
64	64
96	96
128	128

For each number of degrees of freedom, the frequency response function was calculated, and the natural frequencies were extracted as the frequencies corresponding to the peaks of the frequency response function.

Referring to the definition of damage indicator reported in the sub-chapter 5.1, it was then possible to determine if the specific frequency represents a good damage indicator or not.

For the sake of this analysis, the shift between the natural frequencies for different numbers of sensors was considered.

If the shift between the natural frequency detected in two different cases is high, an increasing number of sensors could detect more damage within the structure and probably a higher number of sensors is needed.

If the shift is very small, the number of sensors does not affect the detection of damage, then a minimum number of sensors corresponding to the case with the lowest number of the response's degrees of freedom can be considered.

In general, a shift of 10^{-2} Hz can be considered low.

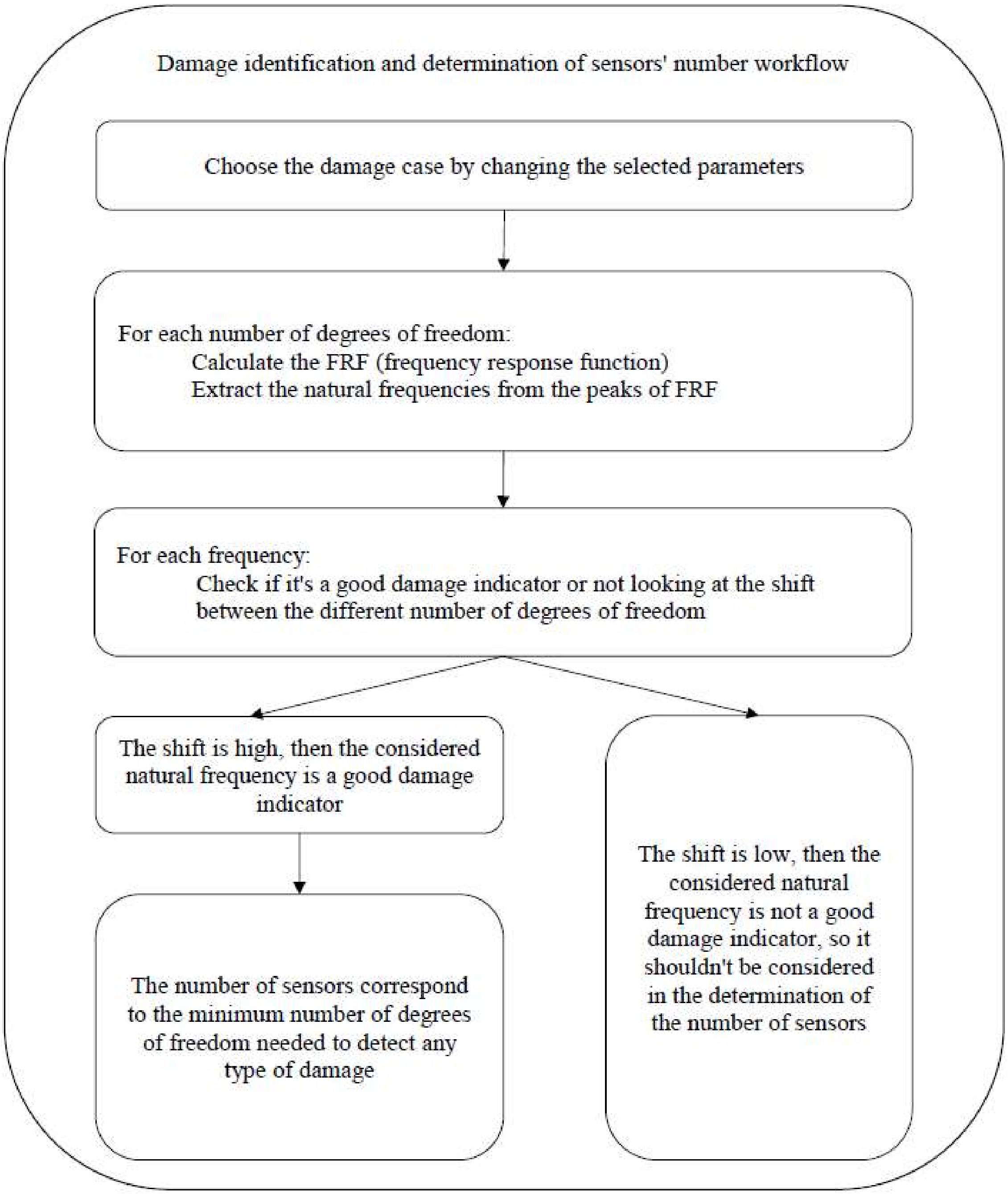

Figure 83 - Damage identification workflow

5.3.2 Loss of pre-strain due to relaxation

Table 17 - Relaxation: natural frequencies with respect to the nr. of dofs

Case 1

$\varepsilon_{lat} = 2{,}5*10^{-4}$
$\varepsilon_{hex} = 2{,}5*10^{-4}$

N_{dof}	f_1 [Hz]	f_2 [Hz]	f_3 [Hz]
8	17,4370	34,6609	37,6702
16	17,4419	34,7127	37,7404
32	17,4730	34,8007	37,6914
64	17,4390	34,6988	37,7312
96	17,4421	-	37,6299
128	17,4430	34,7053	37,6563

Case 2

$\varepsilon_{lat} = 2{,}5*10^{-4}$
$\varepsilon_{hex} = 1*10^{-4}$

N_{dof}	f_1 [Hz]	f_2 [Hz]	f_3 [Hz]
8	17,4055	34,5377	37,5066
16	17,4096	34,5812	37,5884
32	17,4138	34,5046	37,4700
64	17,4068	34,5686	37,5806
96	17,4100	-	37,4783
128	17,4111	34,5666	37,4880

Case 3

$\varepsilon_{lat} = 1*10^{-4}$
$\varepsilon_{hex} = 2{,}5*10^{-4}$

N_{dof}	f_1 [Hz]	f_2 [Hz]	f_3 [Hz]
8	17,3946	34,5263	37,5329
16	17,4000	34,5665	37,5539
32	17,4082	34,5041	37,5076
64	17,3977	34,5674	37,5581
96	17,4038	-	37,5641
128	17,4039	34,6062	37,5189

Case 4

$\varepsilon_{lat} = 1*10^{-4}$
$\varepsilon_{hex} = 1*10^{-4}$

N_{dof}	f_1 [Hz]	f_2 [Hz]	f_3 [Hz]
8	17,3555	34,4008	37,3636
16	17,3601	34,4340	37,3826
32	17,3687	34,3749	37,3349
64	17,3579	34,4361	37,3929
96	17,3643	-	37,4219
128	17,3646	34,4657	37,3475

Case 5

$\varepsilon_{lat} = 2{,}5*10^{-4}$
$\varepsilon_{hex} = 1*10^{-5}$

N_{dof}	f_1 [Hz]	f_2 [Hz]	f_3 [Hz]
8	17,3839	34,4590	37,4127
16	17,3877	34,5023	37,4897
32	17,3922	34,4230	37,3706
64	17,3848	34,4883	37,4831
96	17,3882	-	37,3975
128	17,3896	34,4800	37,3934

Case 6

$\varepsilon_{lat} = 1*10^{-5}$
$\varepsilon_{hex} = 2{,}5*10^{-4}$

N_{dof}	f_1 [Hz]	f_2 [Hz]	f_3 [Hz]
8	17,3636	34,4402	37,4479
16	17,3697	34,4776	37,4444
32	17,3817	34,4209	37,4266
64	17,3677	34,4884	37,4547
96	17,3765	-	37,5088
128	17,3760	34,5526	37,4352

Case 7			
$\varepsilon_{lat} = 1*10^{-5}$			
$\varepsilon_{hex} = 1*10^{-5}$			
N_{dof}	f_1 [Hz]	f_2 [Hz]	f_3 [Hz]
8	17,3098	34,2404	37,1836
16	17,3133	34,2673	37,1689
32	17,3228	34,2096	37,1567
64	17,3121	34,2787	37,1870
96	17,3191	-	37,2790
128	17,3189	34,3224	37,1682

Case 8			
$\varepsilon_{lat} = 2{,}5*10^{-4}$			
$\varepsilon_{hex} = 1*10^{-6}$			
N_{dof}	f_1 [Hz]	f_2 [Hz]	f_3 [Hz]
8	17,3815	34,4519	37,4029
16	17,3853	34,4929	37,4819
32	17,3898	34,4163	37,3585
64	17,3824	34,4797	37,4755
96	17,3858	-	37,3882
128	17,3872	34,4711	37,3821

Case 9			
$\varepsilon_{lat} = 1*10^{-6}$			
$\varepsilon_{hex} = 2{,}5*10^{-4}$			
N_{dof}	f_1 [Hz]	f_2 [Hz]	f_3 [Hz]
8	17,3605	34,4330	37,4406
16	17,3665	34,4682	37,4351
32	17,3787	34,4144	37,4193
64	17,3646	34,4793	37,4459
96	17,3735	-	37,5004
128	17,3729	34,5471	37,4279

Case 10			
$\varepsilon_{lat} = 1*10^{-6}$			
$\varepsilon_{hex} = 1*10^{-6}$			
N_{dof}	f_1 [Hz]	f_2 [Hz]	f_3 [Hz]
8	17,3055	34,2209	37,1667
16	17,3090	34,2494	37,1483
32	17,3186	34,1937	37,1383
64	17,3078	34,2625	37,1683
96	17,3150	-	37,2581
128	17,3147	34,3094	37,1506

Case 11			
$\varepsilon = 2{,}5*10\text{-}4$			
$\varepsilon_{sel} = 1*10\text{-}8$			
N_{dof}	f_1 [Hz]	f_2 [Hz]	f_3 [Hz]
8	17,4370	34,6609	37,6702
16	17,4419	34,7127	37,7404
32	17,4460	34,6319	37,6424
64	17,4390	34,6988	37,7312
96	17,4421	-	37,6299
128	17,4430	34,7053	37,6563

Case 12			
$\varepsilon = 1*10\text{-}4$			
$\varepsilon_{sel} = 1*10\text{-}8$			
N_{dof}	f_1 [Hz]	f_2 [Hz]	f_3 [Hz]
8	17,3555	34,4008	37,3636
16	17,3601	34,4340	37,3826
32	17,3687	34,3749	37,3349
64	17,3579	34,4361	37,3929
96	17,3643	-	37,4219
128	17,3646	34,4657	37,3475

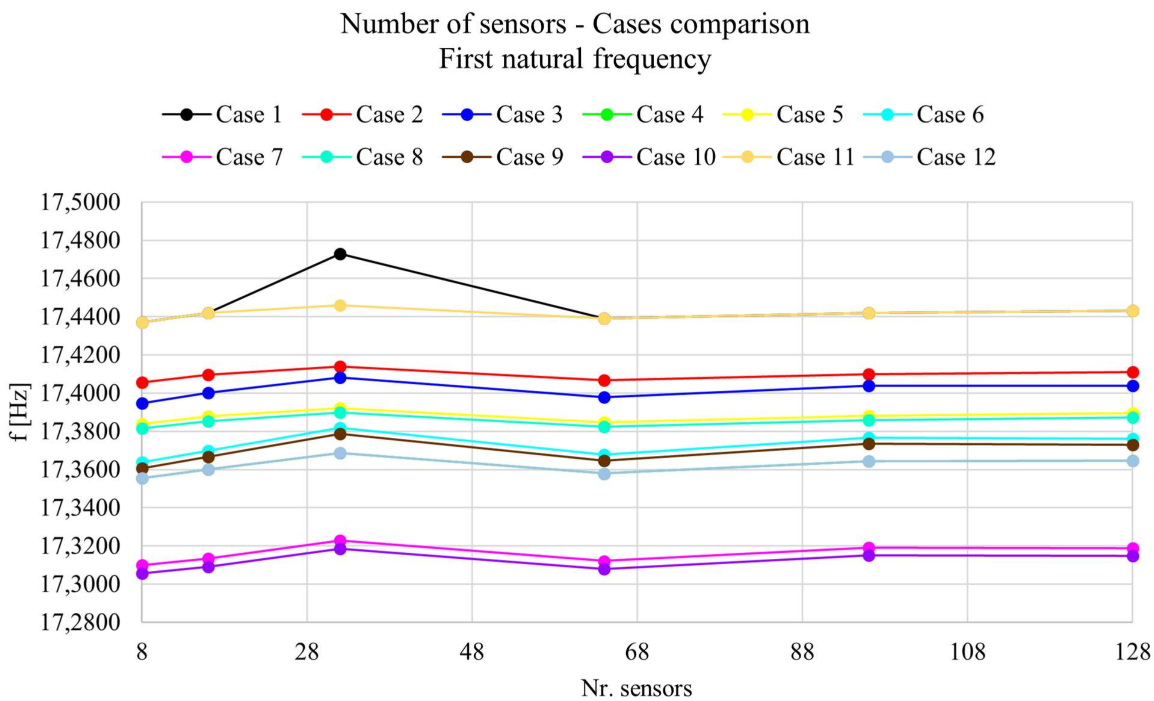

Figure 84 - Relaxation: f [Hz] vs. nr. sensors (first natural frequency)

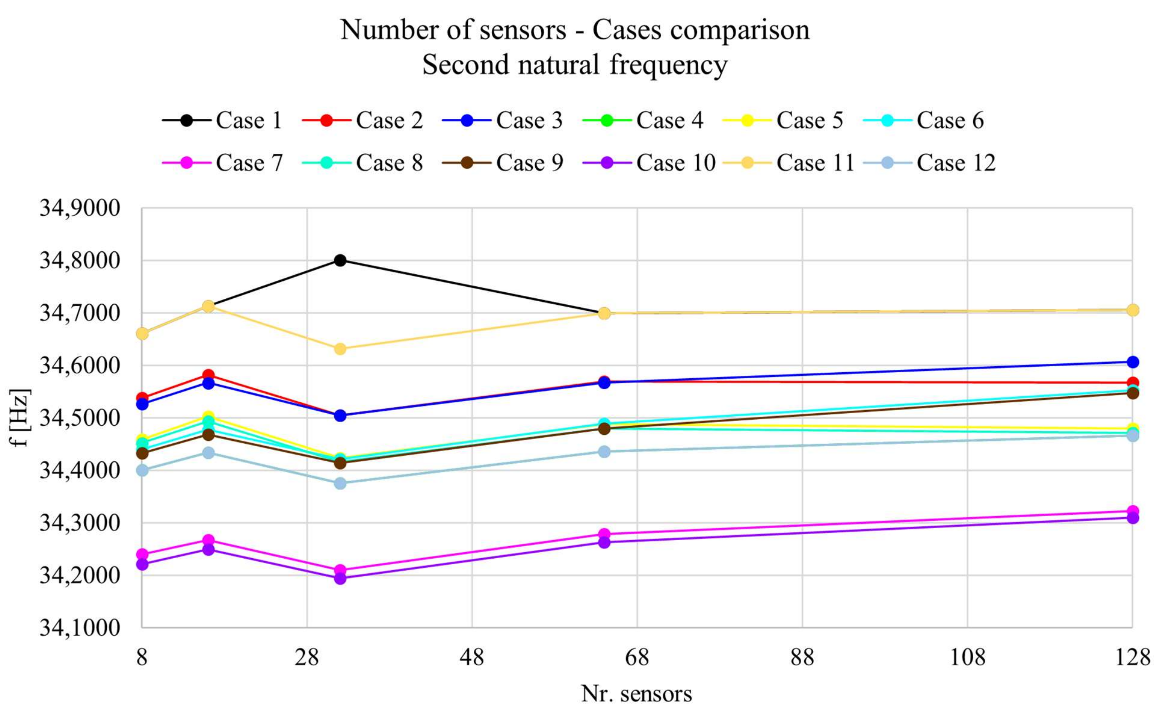

Figure 85 - Relaxation: f [Hz] vs. nr. sensors (second natural frequency)

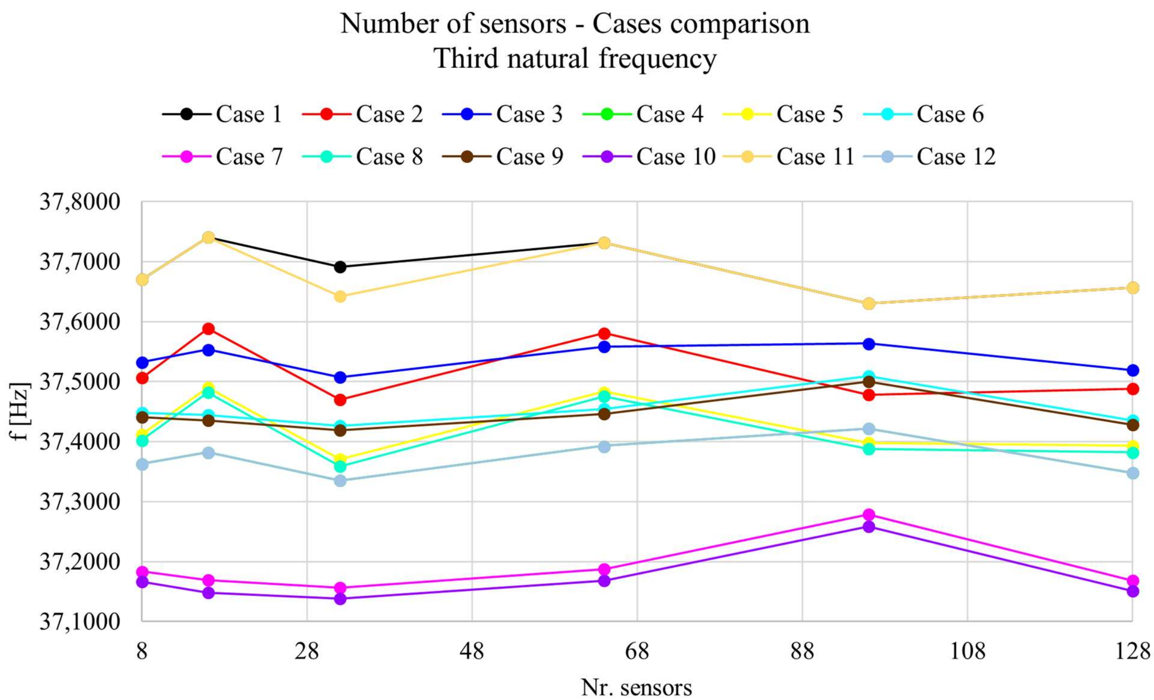

Figure 86 - Relaxation: f [Hz] vs. nr. sensors (third natural frequency)

5.3.3 Loss of pre-strain due to temperature gradients

Table 18 - Temperature effects: natural frequencies with respect to the nr. of dofs

Case 1			
$\varepsilon_{lat} = 2{,}5*10^{-4}$ $\varepsilon_{hex} = 2{,}5*10^{-4}$			
N_{dof}	f_1 [Hz]	f_2 [Hz]	f_3 [Hz]
8	17,4370	34,6609	37,6702
16	17,4419	34,7127	37,7404
32	17,4730	34,8007	37,6914
64	17,4390	34,6988	37,7312
96	17,4421	-	37,6299
128	17,4430	34,7053	37,6563

Case 2			
$\varepsilon_{lat} = 1*10^{-4}$ $\varepsilon_{hex} = 1*10^{-4}$			
N_{dof}	f_1 [Hz]	f_2 [Hz]	f_3 [Hz]
8	17,3555	34,4008	37,3636
16	17,3601	34,4340	37,3826
32	17,3687	34,3749	37,3349
64	17,3579	34,4361	37,3929
96	17,3643	-	37,4219
128	17,3646	34,4657	37,3475

Case 3			
$\varepsilon_{lat} = 5*10^{-5}$ $\varepsilon_{hex} = 5*10^{-5}$			
N_{dof}	f_1 [Hz]	f_2 [Hz]	f_3 [Hz]
8	17,3292	34,3085	37,2661
16	17,3330	34,3372	37,2642
32	17,3419	34,2843	37,2341
64	17,3314	34,3449	37,2801
96	17,3380	-	37,3404
128	17,3380	34,3888	37,2481

Case 4			
$\varepsilon_{lat} = 1*10^{-5}$ $\varepsilon_{hex} = 1*10^{-5}$			
N_{dof}	f_1 [Hz]	f_2 [Hz]	f_3 [Hz]
8	17,3098	34,2404	37,1836
16	17,3133	34,2673	37,1689
32	17,3228	34,2096	37,1567
64	17,3121	34,2787	37,1870
96	17,3191	-	37,2790
128	17,3189	34,3224	37,1682

Case 5			
$\varepsilon_{lat} = 5*10^{-6}$ $\varepsilon_{hex} = 5*10^{-6}$			
N_{dof}	f_1 [Hz]	f_2 [Hz]	f_3 [Hz]
8	17,3075	34,2292	37,1743
16	17,3109	34,2577	37,1577
32	17,3205	34,2005	37,1467
64	17,3097	34,2699	37,1767
96	17,3168	-	37,2680
128	17,3166	34,3152	37,1586

Case 6			
$\varepsilon_{lat} = 1*10^{-6}$ $\varepsilon_{hex} = 1*10^{-6}$			
N_{dof}	f_1 [Hz]	f_2 [Hz]	f_3 [Hz]
8	17,3055	34,2209	37,1667
16	17,3090	34,2494	37,1483
32	17,3186	34,1937	37,1383
64	17,3078	34,2625	37,1683
96	17,3150	-	37,2581
128	17,3147	34,3094	37,1506

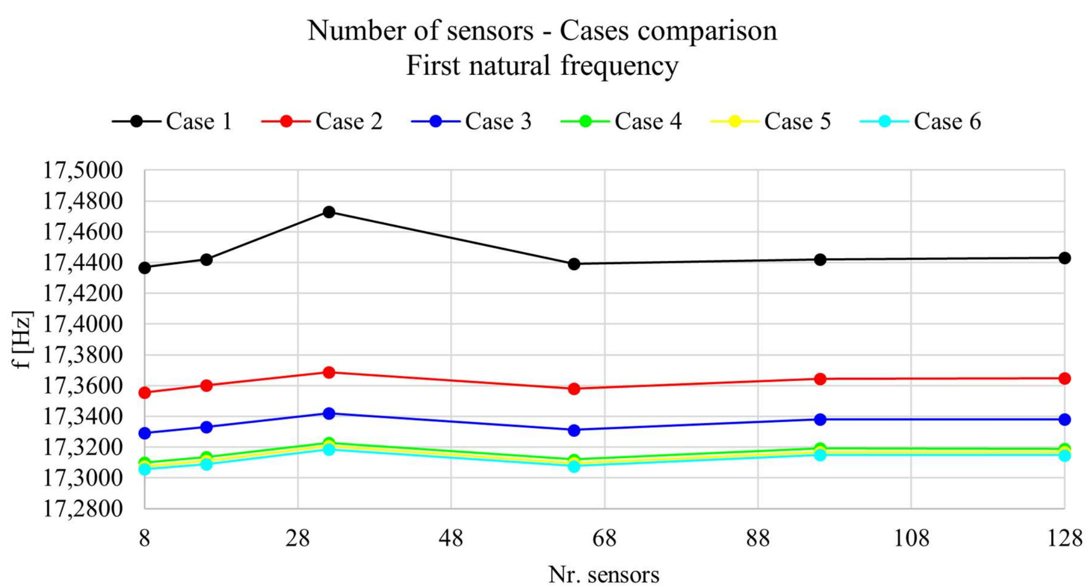

Figure 87 - Temperature effects: f [Hz] vs. nr. sensors (first natural frequency)

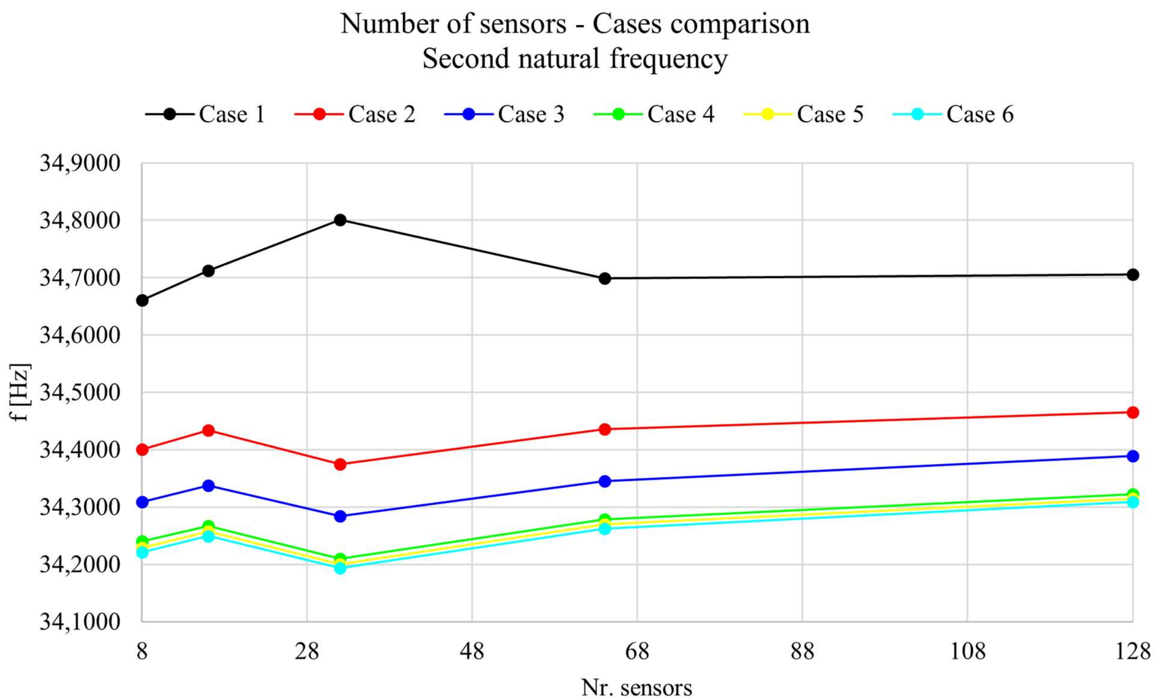

Figure 88 - Temperature effects: f [Hz] vs. nr. sensors (second natural frequency)

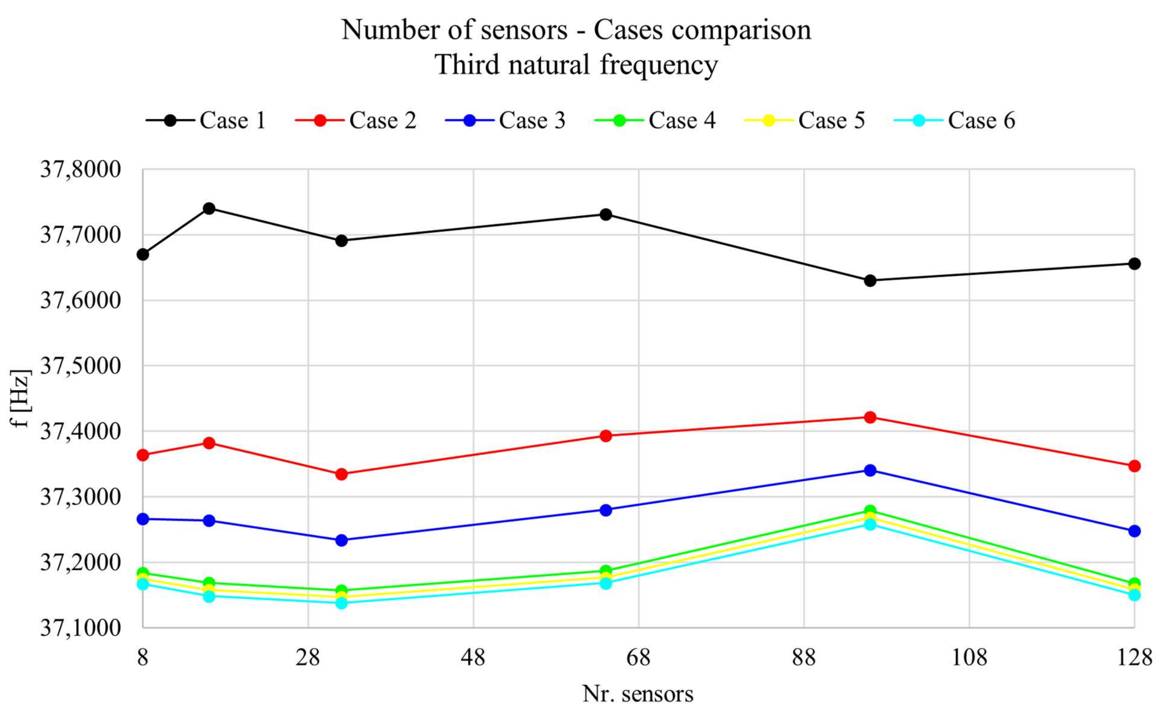

Figure 89 - Temperature effects: f [Hz] vs. nr. sensors (third natural frequency)

5.3.4 Corrosion of the steel elements

Table 19 – Corrosion: natural frequencies with respect to the nr. of dofs

Case 1			
A_{bars} = 30,00 cm^2 A_{cables} = 15,00 cm^2			
N_{dof}	f_1 [Hz]	f_2 [Hz]	f_3 [Hz]
8	17,4370	34,6609	37,6702
16	17,4419	34,7127	37,7404
32	17,4730	34,8007	37,6914
64	17,4390	34,6988	37,7312
96	17,4421	-	37,6299
128	17,4430	34,7053	37,6563

Case 2			
A_{bars} = 30,00 cm^2 A_{cables} = 13,66 cm^2			
N_{dof}	f_1 [Hz]	f_2 [Hz]	f_3 [Hz]
8	17,1781	34,1429	37,0198
16	17,1832	34,1997	37,1003
32	17,1872	34,1060	36,9873
64	17,1802	34,1839	37,0900
96	17,1832	-	36,9613
128	17,1842	34,1900	37,0036

Case 3			
A_{bars} = 28,09 cm^2 A_{cables} = 15,00 cm^2			
N_{dof}	f_1 [Hz]	f_2 [Hz]	f_3 [Hz]
8	17,6001	34,9941	38,0944
16	17,6054	35,0478	38,1740
32	17,6102	34,9592	38,0686
64	17,6023	35,0350	38,1639
96	17,6058	-	38,0646
128	17,6068	35,0419	38,0810

Case 4			
A_{bars} = 28,09 cm^2 A_{cables} = 13,66 cm^2			
N_{dof}	f_1 [Hz]	f_2 [Hz]	f_3 [Hz]
8	17,3610	34,5132	37,4767
16	17,3668	34,5673	37,5634
32	17,3717	34,4765	37,4497
64	17,3633	34,5530	37,5523
96	17,3669	-	37,4353
128	17,3681	34,5593	37,4629

Case 5			
A_{bars} = 30,00 cm^2 A_{cables} = 13,01 cm^2			
N_{dof}	f_1 [Hz]	f_2 [Hz]	f_3 [Hz]
8	17,0336	33,8474	36,6644
16	17,0390	33,9160	36,7444
32	17,0430	33,8129	36,6341
64	17,0358	33,8975	36,7338
96	17,0388	-	36,5974
128	17,0399	33,9039	36,6496

Case 6			
A_{bars} = 27,16 cm^2 A_{cables} = 15,00 cm^2			
N_{dof}	f_1 [Hz]	f_2 [Hz]	f_3 [Hz]
8	17,6821	35,1562	38,3082
16	17,6869	35,2036	38,3720
32	17,6912	35,1283	38,2825
64	17,6841	35,1919	38,3642
96	17,6872	-	38,2817
128	17,6882	35,1986	38,2951

Case 7			
A_{bars} = 27,16 cm^2 A_{cables} = 13,01 cm^2			
N_{dof}	f_1 [Hz]	f_2 [Hz]	f_3 [Hz]
8	17,3204	34,4271	37,3742
16	17,3254	34,4827	37,4577
32	17,3295	34,3981	37,3446
64	17,3224	34,4670	37,4476
96	17,3255	-	37,3274
128	17,3265	34,4736	37,3590

Case 8			
A_{bars} = 30,00 cm^2 A_{cables} = 12,38 cm^2			
N_{dof}	f_1 [Hz]	f_2 [Hz]	f_3 [Hz]
8	16,8756	33,5427	36,2905
16	16,8821	33,6055	36,3738
32	16,8865	33,5113	36,2596
64	16,8782	33,5862	36,3628
96	16,8817	-	36,2138
128	16,8830	33,5919	36,2755

Case 9			
A_{bars} = 26,24 cm^2 A_{cables} = 15,00 cm^2			
N_{dof}	f_1 [Hz]	f_2 [Hz]	f_3 [Hz]
8	17,7601	35,3098	38,5171
16	17,7655	35,3580	38,5836
32	17,7705	35,2832	38,4869
64	17,7624	35,3460	38,5763
96	17,7660	-	38,4896
128	17,7670	35,3533	38,5014

Case 10			
A_{bars} = 26,24 cm^2 A_{cables} = 12,38 cm^2			
N_{dof}	f_1 [Hz]	f_2 [Hz]	f_3 [Hz]
8	17,2817	34,3399	37,2720
16	17,2817	34,3399	37,2720
32	17,2911	34,3080	37,2401
64	17,2838	34,3872	37,3397
96	17,2870	-	37,2191
128	17,2880	34,3943	37,2563

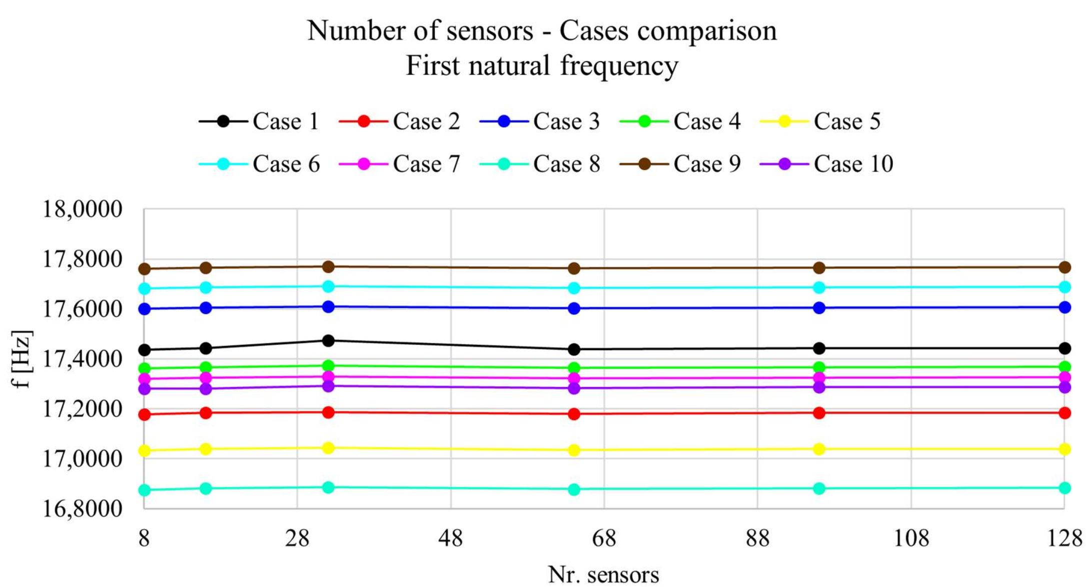

Figure 90 - Corrosion: f [Hz] vs. nr. sensors (first natural frequency)

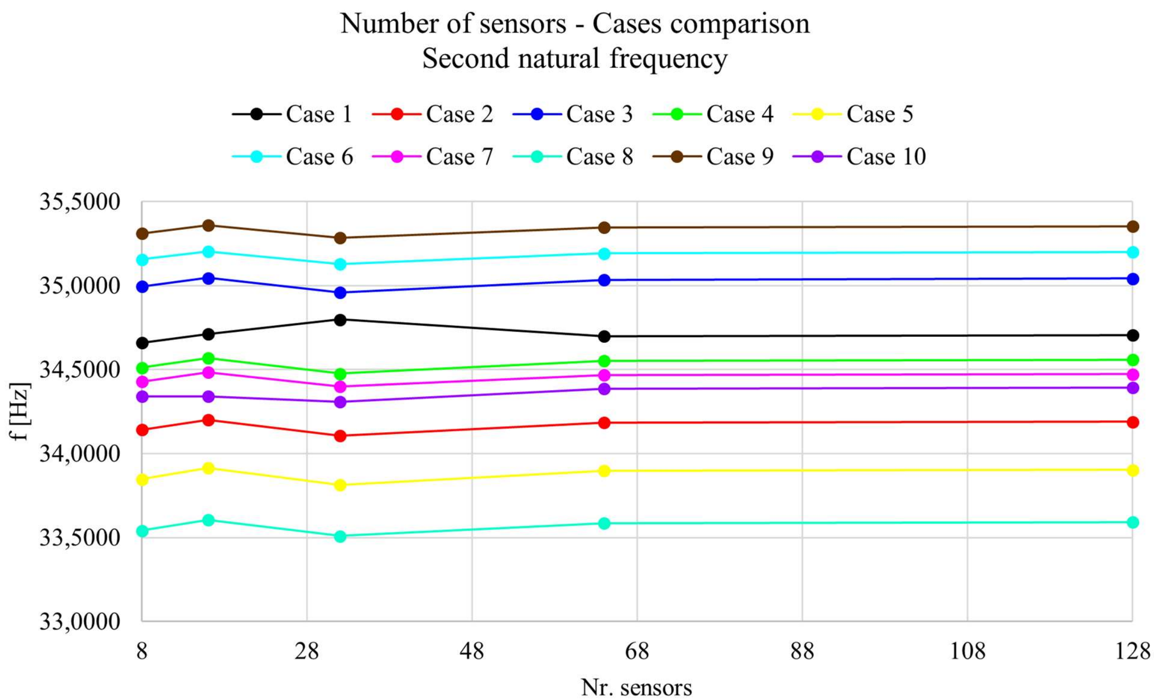

Figure 91 - Corrosion: f [Hz] vs. nr. sensors (second natural frequency)

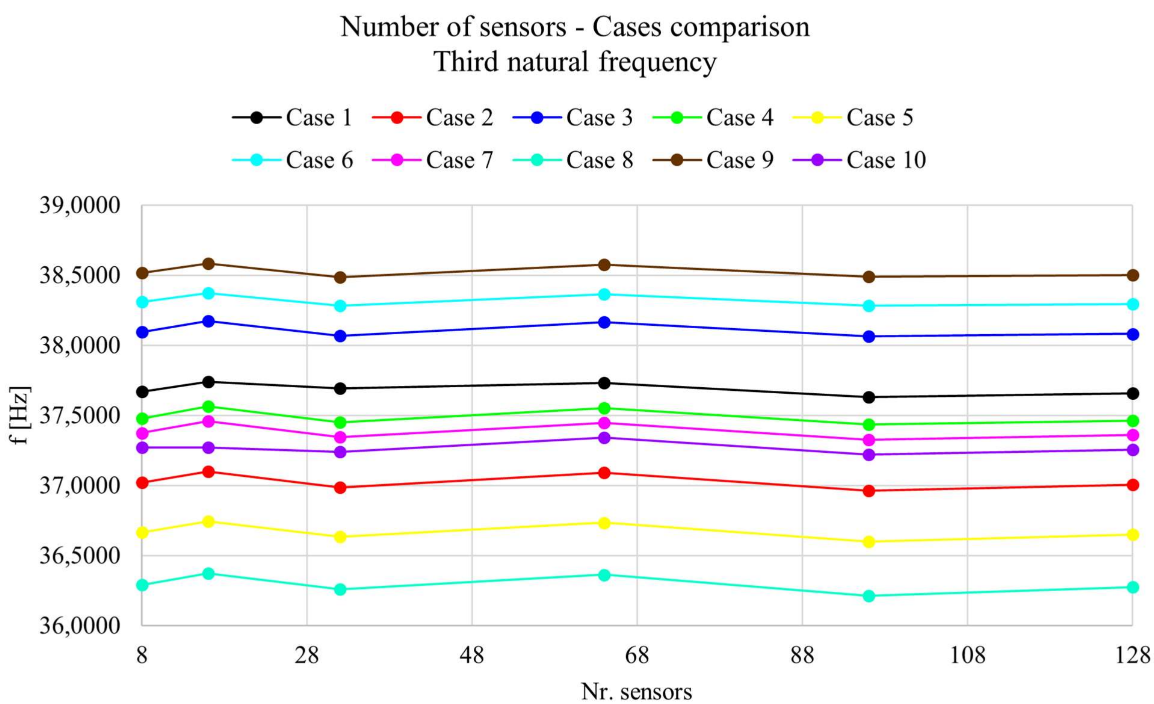

Figure 92 - Corrosion: f [Hz] vs. nr. sensors (third natural frequency)

5.3.5 Results

From the previous tables and graphs, the following results related to the first three natural frequencies can be summarized:

1. First natural frequency

   The graphs representing the first natural frequency show in all the three cases of damage that, when any type of damage occurs in the structure, there is a shift of the natural frequency (as previously noticed from the frequency response function graphs too). However, the increasing number of sensors does not change the natural frequency: this implies that the damage detected by 8 sensors will be the same damage detected by 128 sensors. The frequency shifts are listed in the table 20, considering the cases with the largest shift of frequency for every damage case.

   Table 20 - First natural frequency: shifts

Damage case	$\Delta f = f_1(N_{dofs} = 128) - f_1(N_{dofs} = 8)$
Relaxation (case 10)	0,0092 Hz
Temperature effects (case 6)	0,0092 Hz
Corrosion (case 8)	0,0073 Hz

   Consequently, it is possible to state that the first natural frequency does not represent a good indicator of the necessary number of sensors able to detect damage within the structure. It's then necessary to analyse other frequencies besides the first natural frequency. The number of sensors $N_{sensors}$ will be therefore 8 for each type of damage, as listed in the table below.

   Table 21 - Nr. of sensors (first natural frequency)

Type of damage	$N_{sensors}$
Relaxation	8
Temperature effects	8
Corrosion	8

2. Second natural frequency

For what concerns the second natural frequencies, in general, there is always a shift due to the presence of damage within the structure, and the frequencies' changes with respect to the number of sensors are clearer than in the first natural frequency's case. However, it is possible to distinguish the three cases of damage:

2.1 Loss of pre-strain due to relaxation

The shift is noticeable in particular in the case of 32 sensors: considering the healthy situation with 32 sensors, corresponding to the highest natural frequency, the natural frequency is equal to 34,8007 Hz; in the case 10, the natural frequency corresponding to 32 sensors is given by 34,4163 Hz. It is then possible to define again the case 10 as the worst case (i.e., the case with the largest shift of frequency). The differences of frequencies in the case 10 are given by:

Table 22 - Second natural frequency: shifts (relaxation)

Relaxation (case 10)	Δf
$f_2(N_{dofs} = 16) - f_2(N_{dofs} = 8)$	0,0284 Hz
$f_2(N_{dofs} = 32) - f_2(N_{dofs} = 16)$	-0,0556 Hz
$f_2(N_{dofs} = 64) - f_2(N_{dofs} = 32)$	0,0688 Hz
$f_2(N_{dofs} = 128) - f_2(N_{dofs} = 64)$	0,0468 Hz

It is immediately noticeable that the differences in the case of the second natural frequency are larger than in the case of the first natural frequency. The lowest natural frequency is given by the natural frequency corresponding to 32 sensors; then, it slowly increases again. The change from 32 to 64 sensors and then from 64 to 128 sensors is noticeable and it should be taken into account: the frequency varies, therefore the damage in more points of the structure could be possibly detected.

2.2 Loss of pre-strain due to temperature changes

A similar reasoning to the one made in the case of relaxation can be done, defining now the worst case as the case 6. The differences of frequencies in the case 6 are given by:

Table 23 - Second natural frequency: shifts (temperature effects)

Temperature effects (case 6)	Δf
$f_2(N_{dofs} = 16) - f_2(N_{dofs} = 8)$	0,0284 Hz
$f_2(N_{dofs} = 32) - f_2(N_{dofs} = 16)$	-0,0556 Hz
$f_2(N_{dofs} = 64) - f_2(N_{dofs} = 32)$	0,0688 Hz
$f_2(N_{dofs} = 128) - f_2(N_{dofs} = 64)$	0,0468 Hz

The lowest natural frequency is the one corresponding to 32 sensors; moreover, it is interesting to highlight that the worst case of relaxation and the worst case of temperature effects coincide. As the previous case of relaxation, increasing the number of sensors from 32 to 128 more damage points within the structure could be detected.

2.3 Corrosion of the steel elements

In the case of corrosion, the trend is the one already described in the analysis of the frequency response function: in the case of reduction of the cross-section area of compression bar, the natural frequencies increase, while in the case of reduction of the cross-section area of tension cables, the natural frequencies decrease. This is probably due to the fact that a change in the structure given by damage implies a change in the frequency response function (and then in the natural frequencies). However, a change in a cross-section area which is already small has almost certainly a bigger impact on the frequencies' changes. The highest natural frequency of the healthy situation is the one corresponding to 32 sensors, which is equal to 34,8007 Hz. The case with the largest shift of frequencies with respect to the healthy situation given by case 8 (reduction of 2 mm in tension cables). The third natural frequency of the case 8 with respect to a number of sensors equal to 32 is 33,5113 Hz. The worst case (i.e., the case with the largest shift in frequency from the healthy situation) is then defined as the case 8.

Table 24 - Second natural frequency: shifts (corrosion)

Corrosion (case 8)	Δf
$f_2(N_{dofs} = 16) - f_2(N_{dofs} = 8)$	0,0628 Hz
$f_2(N_{dofs} = 32) - f_2(N_{dofs} = 16)$	-0,0942 Hz
$f_2(N_{dofs} = 64) - f_2(N_{dofs} = 32)$	0,0749 Hz
$f_2(N_{dofs} = 128) - f_2(N_{dofs} = 64)$	0,0057 Hz

The lowest natural frequency then is the one corresponding to 32 sensors.

The common point to all the damage cases is that the second natural frequency of this order is not detectable considering 96 sensors. Then, a third case corresponding to the third natural frequency should be analysed. The number of sensors $N_{sensors}$ for each type of damage is reported in the table below.

Table 25 - Nr. of sensors (second natural frequency)

Type of damage	$N_{sensors}$
Relaxation	32
Temperature effects	32 - 64 - 128
Corrosion	32 - 64 - 128

3. Third natural frequency

Distinguishing the three different cases of damage, it is possible to obtain the following results:

3.1 Loss of pre-strain due to relaxation

The case presenting the largest shift with respect to the structure without any type of damage is again the case 10. The differences of frequencies in the case 10 are reported in the table listed below.

Table 26 - Third natural frequency: shifts (relaxation)

Relaxation (case 10)	Δf
$f_2(N_{dofs} = 16) - f_2(N_{dofs} = 8)$	-0,0184 Hz
$f_2(N_{dofs} = 32) - f_2(N_{dofs} = 16)$	-0,0100 Hz
$f_2(N_{dofs} = 64) - f_2(N_{dofs} = 32)$	0,0299 Hz
$f_2(N_{dofs} = 96) - f_2(N_{dofs} = 64)$	0,0899 Hz
$f_2(N_{dofs} = 128) - f_2(N_{dofs} = 96)$	-0,1076 Hz

The lowest third natural frequency in the worst case is given again by the frequency corresponding to 32 sensors, even though the biggest shift is given by the frequency corresponding to 96 sensors.

3.2 Loss of pre-strain due to temperature gradients

The case presenting the biggest shift with respect to the healthy situation is again case 6 (even if it's possible to notice that between case 4, 5 and 6 there is no huge difference). The differences of frequencies in case 6 are given by:

Table 27 - Third natural frequency: shifts (temperature effects)

Temperature effects (case 6)	Δf
$f_2(N_{dofs} = 16) - f_2(N_{dofs} = 8)$	-0,0184 Hz
$f_2(N_{dofs} = 32) - f_2(N_{dofs} = 16)$	-0,0100 Hz
$f_2(N_{dofs} = 64) - f_2(N_{dofs} = 32)$	0,0299 Hz
$f_2(N_{dofs} = 96) - f_2(N_{dofs} = 64)$	0,0899 Hz
$f_2(N_{dofs} = 128) - f_2(N_{dofs} = 96)$	-0,1076 Hz

The previous table shows that the lowest natural frequency can be found in correspondence of the 32 sensors case; moreover, the shift between the healthy situation and the case 6 in correspondence of 32 sensors and 64 sensors is the same. Once again, it is interesting to highlight that the worst case of relaxation and the worst case of temperature effects coincide.

3.3 Corrosion of the steel elements

The worst case is the case 8; the frequency shifts in case 8 are given by:

Table 28 - Third natural frequency: shifts (corrosion)

Corrosion (case 8)	Δf
$f_2(N_{dofs} = 16) - f_2(N_{dofs} = 8)$	0,0832 Hz
$f_2(N_{dofs} = 32) - f_2(N_{dofs} = 16)$	-0,1141 Hz
$f_2(N_{dofs} = 64) - f_2(N_{dofs} = 32)$	0,1031 Hz
$f_2(N_{dofs} = 96) - f_2(N_{dofs} = 64)$	-0,1490 Hz
$f_2(N_{dofs} = 128) - f_2(N_{dofs} = 96)$	0,0617 Hz

The two lowest natural frequencies in the case 8 are given by the frequencies corresponding to 32 sensors and 96 sensors. However, the difference between the frequency corresponding to 96 sensors and the frequency corresponding to 32 sensors is equal to -0,0210 Hz. Consequently, applying 96 sensors or 32 sensors is mostly the same.

Table 29 - Nr. of sensors (third natural frequency)

Type of damage	$N_{sensors}$
Relaxation	32 - 96
Temperature effects	32 - 64
Corrosion	32 - 96

5.4 Sensors' system design

Based on the reasonings made in the previous subchapter, it is therefore possible to determine the number of sensors able to completely detect the damage within the structure.

As summarized in the table listed below, the number of sensors can variate with respect to the considered mode, and the corresponding natural frequency, and the type of damage.

Table 30 - Nr. of sensors (summary)

Nr. mode	Type of damage	Nr. sensors
1	Loss of pre-strain due to relaxation	8
	Loss of pre-strain due to temperature gradients	8
	Corrosion of the steel elements	8
2	Loss of pre-strain due to relaxation	32
	Loss of pre-strain due to temperature gradients	32 - 64 - 128
	Corrosion of the steel elements	32 - 64 - 128
3	Loss of pre-strain due to relaxation	32 - 96
	Loss of pre-strain due to temperature gradients	32 - 64
	Corrosion of the steel elements	32 - 96

Then, the modulus of the maximum shift for each damage scenario and each frequency was considered, making a first attempt of definition of how good that frequency is as damage indicator.

Table 31 - Good indicators definition

Damage scenario	Nr. of mode	$\lvert\Delta f_{max}\rvert$ [Hz]	Good indicator
Relaxation of steel tension cables	1	0,0109	N
	2	0,0688	Y
	3	0,1076	Y
Effect of the temperature gradients on the elements of the structure	1	0,0109	N
	2	0,0688	Y
	3	0,1076	Y
Corrosion of the cross-section of the steel elements of the structure	1	0,0095	N
	2	0,0942	Y
	3	0,1490	Y

Moreover, the second natural frequency is not detected when N_{dofs} is equal to 96. Consequently, the second mode does not fully contain the needed information.

Table 32 - Reliable indicators definition

f_i	Type of damage indicator
f_1	Not reliable
f_2	Not reliable
f_3	Reliable

Eventually, it can be concluded that:

1. The first natural frequency cannot be taken into account because it does not represent a good indicator of the needed number of sensors.

2. The second natural frequency cannot be taken into account because it does not represent a reliable indicator of the needed number of sensors.

3. The third natural frequency should be taken into account to determine the number of sensors, considering that:

    a. In the case of loss of pre-strain due to relaxation, the biggest shift between the frequencies with respect to the number of sensors is in correspondence of the case with 96 sensors, but the lowest natural frequency is in correspondence of 32 sensors (representing then the biggest shift with respect to the healthy situation).

    b. In the case of loss of pre-strain due to temperature gradients, the lowest natural frequency is in correspondence of 32 sensors, but the shift between the healthy situation and the worst case in correspondence of 32 and 64 sensors is the same.

    c. In the case of corrosion of the steel elements, the lowest natural frequencies are represented by the ones corresponding to 32 and 96 sensors.

It can be then stated that 32 sensors is the minimum number of sensors at which the damage is noticeable.

An approximate positioning of the sensors within the structure can be also designed, considering that the worst cases of damage are all related to the damage in the tension cables.

In particular:

- In the case of loss of pre-strain due to relaxation, the worst case is related to a loss of pre-strain both in the tension cables composing the hexagon module and the lateral tension cables.

- In the case of corrosion of the steel elements, the worst case is related to a reduction of cross-section of the tension cables.

Therefore, 32 sensors uniformly distributed in the tension cables should be located to have a good detection of damage within the structure, avoiding any type of collapse.

6 Conclusions and possible future developments

During the development of this thesis, tensegrity systems have been widely analysed, in particular with respect to their application in civil engineering field. If on one hand tensegrity represents innovation, on the other hand it also represents a huge challenge, due to the peculiarity of its constructive system.

All the work contained in this thesis can be now summarised, in order to highlight the most important results which have been achieved. The first step has been to understand the tensegrity principle: tensegrity structures are still a relatively new type of structures, which have been defined in several different ways, and a very few examples of tensegrity principle applied to civil engineering has been really built, even though a lot of proposals have been made.

Since real examples of tensegrity structures are not very common within the civil engineering field, the consequent choice was to completely design by the beginning the structure. Due to the freedom in the choice of the structure, a modular tensegrity bridge was chosen.

The choice of the structure to design was justified by two main reasons:

1. Some research studies on tensegrity bridges have been already made. This allows to have a guideline on the design of the bridge, in order to have the best design possible, and therefore to be able to carry out a precise work.
2. The considered tensegrity bridge is modular: to have a structure which is adaptable to different types of situations, and which can be re-sized differently with respect to the project's needs was the fundamental point of the design. As stated in the second chapter, the structure has been designed as it has to be built in Vienna, but possibly it could be built in other places, with a different number of modules and a different length of the elements.

The structure was designed using the open-source finite element software SlangTNG, integrating with Matlab the codes related to the form-finding of the structure.

Once that the structure has been designed and completely verified, taking into account also all the different aspects related to tensegrity structures, the main task of the dissertation has been developed.

Structural health monitoring represents a widely developed field in civil engineering; however, since tensegrity structures are not widely employed, there are almost no examples of structural health monitoring applied to tensegrities.

A method to determine the number of sensors necessary to detect the damage within a tensegrity structure was then proposed: according to the well-known vibration-based structural health monitoring methods, the dynamics of the structure was studied and then the frequency response function was exploited to understand how the response of the structure varies with respect to the different cases of damage.

The choice of the case of damages was mainly justified by the willing of being as realistic as possible: corrosion, relaxation (in the case of pre-strained elements) and temperature effects for sure represent very common cases of damage, which can be detected in mostly all the structures.

The main point of the damage detection in this type of structures is given by the fundamental frequencies: the traditional techniques involving the structure's modal parameters are mainly based on the variation of the natural frequencies of the structures. Hence, introducing any kind of damage within the structure (which has been done changing the parameters within the finite element software), the fundamental frequencies change.

Uniaxial sensors are directly related to the degrees of freedom of the structure's response. Therefore, changing this parameter in the finite element software, the result is a change in the response of the structure in the time domain and in the frequency domain.

Consequently, for every case of damage and for every case of number of sensors, the frequency response function changes, implying a change in the detected natural frequencies of the structures (i.e., the frequencies corresponding to the peaks of the frequency response function).

In order to determine the number of sensors and approximately the location of the sensors within the structure, the natural frequencies' shifts between the different cases have been analysed, determining whether the considered natural frequency represents a good and reliable damage indicator or not.

In the final part of the dissertation, considering that the most affected part of the structure by the damage is represented by the tension cables, the result was therefore given by:

Sensors' system	
Nr. of sensors	32
Location of sensors	Uniformly distributed on the tension cables

As far as this thesis is concerned, it is possible to suggest some possible future developments. For example, the location of the sensors was approximately provided, considering the most affected part of the structure when any kind of damage is present within the structure.

Some optimization algorithms could be then employed in order to obtain a more precise localization of damage, for example based on the change of variation of the frequency response function, as proposed by Raich and Liszkai:

$$t = \sum_{i=1}^{n_e} \left(\int_{\omega_0}^{\omega_1} \left| \frac{\partial H(\omega)}{\partial x_i} \right| \right)^2$$

where x_i represents the damage vector, $H(\omega)$ represents the frequency response function and t represents the variation in the frequency response function.

Another aspect could be evaluating the same structure but with different dimensions of the module, or, even better, with a different type of module: a pentagon module instead of a hexagon module could be employed in order to understand if the same results are obtained or they change drastically. At the same way, other types of damage could be considered: for example, more drastic type of damage, such as the cutting of a tendon of the structure.

Varying the boundary conditions of the problem presented in this dissertation could lead to very interesting and important results, in order to understand better tensegrity structures, for which the research field is still largely open and in continuous development.

7 References

Ali, Nizar Bel Hadj, et al. "Design optimization and dynamic analysis of a tensegrity-based footbridge." *Engineering Structures* 32.11 (2010): 3650-3659.

Alvandi, A., and C. Cremona. "Assessment of vibration-based damage identification techniques." *Journal of sound and vibration* 292.1-2 (2006): 179-202.

Ashwear, Nasseradeen, and Anders Eriksson. "Influence of temperature on the vibration properties of tensegrity structures." *International Journal of Mechanical Sciences* 99 (2015): 237-250.

Ashwear, Nasseradeen, and Anders Eriksson. "Vibration health monitoring for tensegrity structures." *Mechanical Systems and Signal Processing* 85 (2017): 625-637.

Aswal, Neha, and Subhamoy Sen. "Design and Health Monitoring of Tensegrity Structures: An Overview." *Reliability, Safety and Hazard Assessment for Risk-Based Technologies* (2020): 523-533.

Bhalla, S., R. Panigrahi, and A. Gupta. "Damage assessment of tensegrity structures using piezo transducers." Meccanica 48.6 (2013): 1465-1478.

Bossens, F., R. A. De Callafon, and R. E. Skelton. "Modal Analysis of a Tensegrity Structure–an experimental study." *Dep. Mech. Aerosp. Eng. Dyn. Syst. Control Group, Univ. California, San Diego, USA* (2007).

Brehm, Maik, Volkmar Zabel, and Christian Bucher. "Optimal reference sensor positions using output-only vibration test data." *Mechanical systems and signal processing* 41.1-2 (2013): 196-225.

Buckminster, Fuller Richard. "Tensile-integrity structures." U.S. Patent No. 3,063,521. 13 Nov. 1962.

Chopra, Anil K. *Dynamics of structures*. Pearson Education India, 2007.

Comité Européen de Normalisation. "Eurocode 3: Design of steel structures–part 1-1: General rules and rules for buildings." Brussels, Belgium. CEN (2005).

De Boeck, J. *Tensegrity bridges: Concept design of pedestrian bridges using tensegrity as load carrying system.* Diss. Delft University of Technology, 2013.

Deraemaeker, Arnaud, et al. "Vibration-based structural health monitoring using output-only measurements under changing environment." *Mechanical systems and signal processing* 22.1 (2008): 34-56.

Doebling, Scott W., et al. "Damage identification and health monitoring of structural and mechanical systems from changes in their vibration characteristics: a literature review." (1996).

Du, Y. G., L. A. Clark, and A. H. C. Chan. "Residual capacity of corroded reinforcing bars." *Magazine of Concrete Research* 57.3 (2005): 135-147.

Emmerich, David Georges. "Emmerich on self-tensioning structures." *International Journal of Space Structures* 11.1-2 (1996): 29-36.

Faroughi, Shirko, and Jaehong Lee. "Analysis of tensegrity structures subject to dynamic loading using a Newmark approach." Journal of Building Engineering 2 (2015): 1-8.

Gan, Buntara Sthenly. *Computational Modeling of Tensegrity Structures*. Springer International Publishing, 2020.

Gao, Shun, Xian Xu, and Yaozhi Luo. "Re-study on tensegrity footbridges based on ring modules." *Advances in Structural Engineering* 23.5 (2020): 898-910.

Gilewski, Wojciech, Joanna Kłosowska, and Paulina Obara. "Applications of tensegrity structures in civil engineering." *Procedia Engineering* 111 (2015): 242-248.

Hanaor, A. "Geometrically rigid double-layer tensegrity grids." Int. J. Space Structs. 9 (1994): 227-238.

Harichandran, Aparna, and I. Yamini Sreevalli. "Form-finding of tensegrity structures based on force density method." *Indian Journal of Science and Technology* 9.24 (2016): 1-6.

Huston, D. *Structural sensing, health monitoring, and performance evaluation*. CRC press, 2010.

Jáuregui, Valentín Gómez. *Tensegrity structures and their application to architecture*. Vol. 2. Ed. Universidad de Cantabria, 2020.

Jones, Robert Millard. Buckling of bars, plates, and shells. Bull Ridge Corporation, 2006.

Kebiche, K., M. N. Kazi-Aoual, and R. Motro. "Geometrical non-linear analysis of tensegrity systems." *Engineering structures* 21.9 (1999): 864-876.

[Online] Kenneth Snelson website: http://kennethsnelson.net/faq/

Lee, Seunghye, and Jaehong Lee. "A novel method for topology design of tensegrity structures." *Composite Structures* 152 (2016): 11-19.

Miura, K., and S. Pellegrino. "Structural concepts. 1999."

Motro, Rene. *Tensegrity: structural systems for the future*. Elsevier, 2003.

Motro, R., S. Najari, and P. Jouanna. "Static and dynamic analysis of tensegrity systems." *Shell and Spatial Structures: Computational Aspects*. Springer, Berlin, Heidelberg, 1987. 270-279.

Moussa, B., N. Ben Kahla, and J. C. Pons. "Evolution of natural frequencies in tensegrity systems: a case study." *International Journal of Space Structures* 16.1 (2001): 57-73.

Pellegrino, Sergio. "Structural computations with the singular value decomposition of the equilibrium matrix." International Journal of Solids and Structures 30.21 (1993): 3025-3035.

Pellegrino, Sergio, and Christopher Reuben Calladine. "Matrix analysis of statically and kinematically indeterminate frameworks." International Journal of Solids and Structures 22.4 (1986): 409-428.

Pugh, Anthony. *An introduction to tensegrity*. University of California Press, 2020.

Raich, Anne M., and Tamas R. Liszkai. "Multi-objective optimization of sensor and excitation layouts for frequency response function-based structural damage identification." Computer-Aided Civil and Infrastructure Engineering 27.2 (2012): 95-117.

Rhode-Barbarigos, Landolf, et al. "Designing tensegrity modules for pedestrian bridges." *Engineering Structures* 32.4 (2010): 1158-1167.

Rhode-Barbarigos, Landolf, et al. "Design aspects of a deployable tensegrity-hollow-rope footbridge." *International Journal of Space Structures* 27.2-3 (2012): 81-95.

Rytter, A. "Vibration based inspection of civil engineering structures Ph. D." Aalborg University, Aalborg, Denmark (1993).

Salawu, O. S. "Detection of structural damage through changes in frequency: a review." *Engineering structures* 19.9 (1997): 718-723.

Skelton, Robert E., and Mauricio C. De Oliveira. *Tensegrity systems*. Vol. 1. New York: Springer, 2009.

Skelton, Robert E., et al. "An introduction to the mechanics of tensegrity structures." *Proceedings of the 40th IEEE conference on decision and control (Cat. No. 01CH37228)*. Vol. 5. IEEE, 2001.

Vassart, Nicolas, and René Motro. "Multiparametered formfinding method: application to tensegrity systems." *International journal of space structures* 14.2 (1999): 147-154.

Veenendaal, Diederik, and Philippe Block. "An overview and comparison of structural form finding methods for general networks." *International Journal of Solids and Structures* 49.26 (2012): 3741-3753.

Xu, Xian, Yafeng Wang, and Yaozhi Luo. "General approach for topology-finding of tensegrity structures." *Journal of Structural Engineering* 142.10 (2016): 04016061.

Zhang, J., et al. "Optimal sensor placement for modal identification of repetitive structures." *Proceedings of ISMA*. Vol. 27. 2016.

Zhang, Li-Yuan, et al. "Stiffness matrix based form-finding method of tensegrity structures." *Engineering structures* 58 (2014): 36-48.

8 Acknowledgments

First of all, I would like to thank the professor Christian Bucher for introducing me to the world of tensegrity structures and for the fundamental support for the completion of this thesis given during my year at the Technical University of Vienna and the professor Rosario Ceravolo for accepting of supervising my thesis at the Politecnico di Torino.

I decided to dedicate the result of these past months' work to my father: you have always been my greatest source of inspiration. Before deciding which degree to undertake, you told me that everything we do should be always done with passion and determination: even if sometimes it's difficult and it seems easier to give up, if we feel it's the right choice and if it makes up happy, we should always persist. Even when I thought I couldn't make it, I repeated this sentence to myself. And that's why I feel that if today I'm here, it's mostly thanks to you: I hope you can be proud of the person I am today, wherever you are.

Mum, you are my other rock: thanks for supporting me unconditionally. No matter what could ever happen, I know that every time I need you, you will always be there on my side. Even during difficult moments, what really comforts me is knowing that I will always have someone to laugh or to cry with when I come back home. Thanks also to Sergio, for always listening to me when I needed it in the last 13 years. Without you I wouldn't have ever reached this huge milestone.

It is said that we cannot choose our family, but I couldn't have picked a better one: to all the people who have always been part of it and to the ones who joined it later, you're my strength. In particular, thanks to my grandfather Vittorio: you have always been my biggest fan.

Elisabetta, you're not my blood sister, but it is as if you were: you have always represented a constant of my life and I'm sure you will always do. You are one of the few people who really knows me, and you always supported me to be the best version of myself. Without you these years wouldn't have been the same.

Caterina, we became friends as soon as you moved in my apartment in Vienna: you're the proof that strong bonds don't require a lot of time. You taught me to be less strict with myself: thanks to you I lived some of the most amazing moments of the last year.

Virginia and Pietro, thanks because you have always been there when I needed you the most.

I would like to thank also all the people who shared this journey, or a part of it with me, in particular my hometown friends, the colleagues from my bachelor and the colleagues from my master.

Appendix A

Topology of the structure

Connectivity of compression bars

Element	Node	Node
C1	1	17
C2	2	18
C3	3	13
C4	4	14
C5	5	15
C6	6	17
C7	10	17
C8	11	18
C9	12	13
C10	7	14
C11	8	15
C12	9	16
C13	5	12
C14	6	7
C15	1	8
C16	2	9
C17	3	10
C18	4	11
C19	7	30
C20	8	31
C21	9	26
C22	10	27
C23	11	28
C24	12	29
C25	23	30
C26	24	31
C27	25	26
C28	20	27
C29	21	28
C30	22	29
C31	11	25
C32	12	20

C33	7	21
C34	8	22
C35	9	23
C36	10	24
C37	20	43
C38	21	44
C39	22	39
C40	23	40
C41	24	41
C42	25	42
C43	36	43
C44	37	44
C45	38	39
C46	33	40
C47	34	41
C48	35	42
C49	24	38
C50	25	33
C51	20	34
C52	21	35
C53	22	36
C54	23	37
C55	33	56
C56	34	57
C57	35	52
C58	36	53
C59	37	54
C60	38	55
C61	49	56
C62	50	57
C63	51	52
C64	46	53
C65	47	54
C66	48	55
C67	37	51
C68	38	46
C69	33	47
C70	34	48
C71	35	49
C72	36	50

Connectivity of tension cables

Element	Node	Node
T1	1	2
T2	2	3
T3	3	4
T4	4	5
T5	5	6
T6	6	1
T7	7	8
T8	8	9
T9	9	10
T10	10	11
T11	11	12
T12	12	7
T13	1	13
T14	2	13
T15	7	13
T16	8	13
T17	2	14
T18	3	14
T19	8	14
T20	9	14
T21	3	15
T22	4	15
T23	9	15
T24	10	15
T25	4	16
T26	5	16
T27	10	16
T28	11	16
T29	5	17
T30	6	17
T31	11	17
T32	12	17
T33	6	18
T34	1	18
T35	12	18
T36	7	18

T37	20	21
T38	21	22
T39	22	23
T40	23	24
T41	24	25
T42	25	20
T43	7	26
T44	8	26
T45	20	26
T46	21	26
T47	8	27
T48	9	27
T49	21	27
T50	22	27
T51	9	28
T52	10	28
T53	22	28
T54	23	28
T55	10	29
T56	11	29
T57	23	29
T58	24	29
T59	11	30
T60	12	30
T61	24	30
T62	25	30
T63	12	31
T64	7	31
T65	25	31
T66	20	31
T67	33	34
T68	34	35
T69	35	36
T70	36	37
T71	37	38
T72	38	33
T73	20	39
T74	21	39
T75	33	39
T76	34	39

T77	21	40
T78	22	40
T79	34	40
T80	35	40
T81	22	41
T82	23	41
T83	35	41
T84	36	41
T85	23	42
T86	24	42
T87	36	42
T88	37	42
T89	24	43
T90	25	43
T91	37	43
T92	38	43
T93	25	44
T94	20	44
T95	38	44
T96	33	44
T97	46	47
T98	47	48
T99	48	49
T100	49	50
T101	50	51
T102	51	46
T103	33	52
T104	34	52
T105	46	52
T106	47	52
T107	34	53
T108	35	53
T109	47	53
T110	48	53
T111	35	54
T112	36	54
T113	48	54
T114	49	54
T115	36	55
T116	37	55

T117	49	55
T118	50	55
T119	37	56
T120	38	56
T121	50	56
T122	51	56
T123	38	57
T124	33	57
T125	51	57
T126	46	57

Appendix B

Form-finding Matlab code

```
clc
clear all
close all

% Import nodes coordinates
% coord(1) = nr. of coordinate
% coord(2) = x coordinate
% coord(3) = z coordinate
% coord(4) = y coordinate

nodes = [1, 0, 0, 0;
    2, 2, 0, 0;
    3, 3, 0, 1.73;
    4, 2, 0, 3.46;
    5, 0, 0, 3.46;
    6, -1, 0, 1.73;
    7, 0, 2.5, 0;
    8, 2, 2.5, 0;
    9, 3, 2.5, 1.73;
    10, 2, 2.5, 3.46;
    11, 0, 2.5, 3.46;
    12, -1, 2.5, 1.73;
    13, 1, 1.25, -0.228147;
    14, 2.697581, 1.25, 0.751952;
    15, 2.697581, 1.25, 2.71215;
    16, 1, 1.25, 3.685262;
    17, -0.697581, 1.25, 2.71215;
    18, -0.697581, 1.25, 0.751952;
    19, 1, 1.25, 1.73;
    20, 0, 5, 0;
    21, 2, 5, 0;
    22, 3, 5, 1.73;
    23, 2, 5, 3.46;
    24, 0, 5, 3.46;
    25, -1, 5, 1.73;
    26, 1, 3.75, -0.228147;
    27, 2.697581, 3.75, 0.751952;
    28, 2.697581, 3.75, 2.71215;
    29, 1, 3.75, 3.685262;
    30, -0.697581, 3.75, 2.71215;
    31, -0.697581, 3.75, 0.751952;
```

```
    32, 1, 3.75, 1.73;
    33, 0, 7.5, 0;
    34, 2, 7.5, 0;
    35, 3, 7.5, 1.73;
    36, 2, 7.5, 3.46;
    37, 0, 7.5, 3.46;
    38, -1, 7.5, 1.73;
    39, 1, 6.25, -0.228147;
    40, 2.697581, 6.25, 0.751952;
    41, 2.697581, 6.25, 2.71215;
    42, 1, 6.25, 3.685262;
    43, -0.697581, 6.25, 2.71215;
    44, -0.697581, 6.25, 0.751952;
    45, 1, 6.25, 1.73;
    46, 0, 10, 0;
    47, 2, 10, 0;
    48, 3, 10, 1.73;
    49, 2, 10, 3.46;
    50, 0, 10, 3.46;
    51, -1, 10, 1.73;
    52, 1, 8.75, -0.228147;
    53, 2.697581, 8.75, 0.751952;
    54, 2.697581, 8.75, 2.71215;
    55, 1, 8.75, 3.685262;
    56, -0.697581, 8.75, 2.71215;
    57, -0.697581, 8.75, 0.751952;
    58, 1, 8.75, 1.73];

% Import bars coordinates
% bars(1) = number of bar
% bars(2) = first node of the bar
% bars(3) = second node of the bar

bars = [1, 1, 17;
    2, 2, 18;
    3, 3, 13;
    4, 4, 14;
    5, 5, 15;
    6, 6, 16;
    7, 10, 17;
    8, 11, 18;
    9, 12, 13;
    10, 7, 14;
    11, 8, 15;
    12, 9, 16;
    13, 5, 12;
    14, 6, 7;
```

```
15, 1, 8;
16, 2, 9;
17, 3, 10;
18, 4, 11;
19, 7, 30;
20, 8, 31;
21, 9, 26;
22, 10, 27;
23, 11, 28;
24, 12, 29;
25, 23, 30;
26, 24, 31;
27, 25, 26;
28, 20, 27;
29, 21, 28;
30, 22, 29;
31, 11, 25;
32, 12, 20;
33, 7, 21;
34, 8, 22;
35, 9, 23;
36, 10, 24;
37, 20, 43;
38, 21, 44;
39, 22, 39;
40, 23, 40;
41, 24, 41;
42, 25, 42;
43, 36, 43;
44, 37, 44;
45, 38, 39;
46, 33, 40;
47, 34, 41;
48, 35, 42;
49, 24, 38;
50, 25, 33;
51, 20, 34;
52, 21, 35;
53, 22, 36;
54, 23, 37;
55, 20, 56;
56, 21, 57;
57, 22, 52;
58, 23, 53;
59, 24, 54;
60, 25, 55;
61, 49, 56;
```

```
    62, 50, 57;
    63, 51, 52;
    64, 46, 53;
    65, 47, 54;
    66, 48, 55;
    67, 37, 51;
    68, 38, 46;
    69, 33, 47;
    70, 34, 48;
    71, 35, 49;
    72, 36, 50];

% Import cables coordinates
% cables(1) = number of cable
% cables(2) = first node of the cable
% cables(3) = second node of the cable

cables = [73, 1, 2;
    74, 2, 3;
    75, 3, 4;
    76, 4, 5;
    77, 5, 6;
    78, 6, 1;
    79, 7, 8;
    80, 8, 9;
    81, 9, 10;
    82, 10, 11;
    83, 11, 12;
    84, 12, 7;
    85, 1, 13;
    86, 2, 13;
    87, 7, 13;
    88, 8, 13;
    89, 2, 14;
    90, 3, 14;
    91, 8, 14;
    92, 9, 14;
    93, 3, 15;
    94, 4, 15;
    95, 9, 15;
    96, 10, 15;
    97, 4, 16;
    98, 5, 16;
    99, 10, 16;
    100, 11, 16;
    101, 5, 17;
    102, 6, 17;
```

```
103, 11, 17;
104, 12, 17;
105, 6, 18;
106, 1, 18;
107, 12, 18;
108, 7, 18;
109, 20, 21;
110, 21, 22;
111, 22, 23;
112, 23, 24;
113, 24, 25;
114, 25, 20;
115, 7, 26;
116, 8, 26;
117, 20, 26;
118, 21, 26;
119, 8, 27;
120, 9, 27;
121, 21, 27;
122, 22, 27;
123, 9, 28;
124, 10, 28;
125, 22, 28;
126, 23, 28;
127, 10, 29;
128, 11, 29;
129, 23, 29;
130, 24, 29;
131, 11, 30;
132, 12, 30;
133, 24, 30;
134, 25, 30;
135, 12, 31;
136, 7, 31;
137, 25, 31;
138, 20, 31;
139, 33, 34;
140, 34, 35;
141, 35, 36;
142, 36, 37;
143, 37, 38;
144, 38, 33;
145, 20, 39;
146, 21, 39;
147, 33, 39;
148, 34, 39;
149, 21, 40;
```

```
150, 22, 40;
151, 34, 40;
152, 35, 40;
153, 22, 41;
154, 23, 41;
155, 35, 41;
156, 36, 41;
157, 23, 42;
158, 24, 42;
159, 36, 42;
160, 37, 42;
161, 24, 43;
162, 25, 43;
163, 37, 43;
164, 38, 43;
165, 25, 44;
166, 20, 44;
167, 38, 44;
168, 33, 44;
169, 46, 47;
170, 47, 48;
171, 48, 49;
172, 49, 50;
173, 50, 51;
174, 51, 46;
175, 33, 52;
176, 34, 52;
177, 46, 52;
178, 47, 52;
179, 34, 53;
180, 35, 53;
181, 47, 53;
182, 48, 53;
183, 35, 54;
184, 36, 54;
185, 48, 54;
186, 49, 54;
187, 36, 55;
188, 37, 55;
189, 49, 55;
190, 50, 55;
191, 37, 56;
192, 38, 56;
193, 50, 56;
194, 51, 56;
195, 38, 57;
196, 33, 57;
```

```
    197, 51, 57;
    198, 46, 57];

elements = [bars ; cables];

% Build connectivity matrix
% i = index for the number of bars
% j = index for the number of nodes

N = length(elements);
M = length(nodes);

for i = 1:N
   for j = 1:M
       if j == elements(i,2)
           C(i,j) = +1;
       elseif j == elements(i,3)
           C(i,j) = -1;
       else
           C(i,j) = 0;
       end
   end
end

% Build the equilibrium matrix [A] = [C]'*diag([C][x,y,z])

for i = 1:M
    x_coord(i) = nodes(i,2);
    y_coord(i) = nodes(i,4);
    z_coord(i) = nodes(i,3);
end

x_coord = x_coord';
y_coord = y_coord';
z_coord = z_coord';

x_diag = C*x_coord;
y_diag = C*y_coord;
z_diag = C*z_coord;

CX = diag(x_diag);
CY = diag(y_diag);
CZ = diag(z_diag);

lm = size(C,1);

for i = 1:lm
    L(i) = sqrt(x_diag(i)+y_diag(i)+z_diag(i)); % Lengths
```

```
end

A = [C'*CX ; C'*CY ; C'*CZ];

% First rank condition
% Rank of A, static and kinematic indeterminacy

m = size(A,1);
n = size(A,2);
r = rank(A);
s = n - r;
k = m - r;

if r < N
    fprintf('First rank condition is satisfied \n')
else
    fprintf('First rank condition is not satisfied \n')
end

% SVD of [A]

[U,V,W] = svd(A);
Uk = [U(1:m,r+1:m)];
Wk = W';
W(1:n,1:r) = [Wk(1:r,1:n)]';

% Calculate tension coefficients
% Form-finding without any external action
% Tension coefficients are so-called prestress coefficients

stress = load('stress0.txt'); %N

for i = 1:198
    if i <= 72
        tension(i) = stress(i)*0.003;
    else
        tension(i) = stress(i)*0.0015;
    end
end

q = tension./L;

% Obtain the force density matrix [D] = [C]'[Q][C]
% [Q] is the diagonal square matrix containing the force-
density
% coefficients that are not fixed

Q = diag(q);
```

```
D = C'*Q*C;
%%
% Build the infinitesimal and inextensional matrix
% The matrix [U] results from the SVD of the equilibrium
matrix [A]

dim = 3;
I = eye(dim);
K = kron(I,D);
Uk = [U(1:m,r+1:m)];
L = Uk'*K*Uk;

useigL = real(eig(L));
eigL = sort(useigL);

% Check if there is one or more positive nonzero values in
the eigenvalues

for i = 1:length(eigL)
    if eigL(i) < (M-dim)
        fprintf('There is one or more positive non zero
values \n')
        break;
    end
end

% Second rank condition

rd = rank(D);

if rd < (M-dim)
    fprintf('Second rank condition is satisfied \n')
else
    fprintf('Second rank condition is not satisfied \n')
end
```

Appendix C

Structural verifications

Verification 1a: compression bars

Element	Node	Node	σ_N [N/m^2]	Compression
C1	1	17	-6,35E+05	VERIFIED
C2	2	18	-9,02E+06	VERIFIED
C3	3	13	-1,57E+07	VERIFIED
C4	4	14	-9,04E+06	VERIFIED
C5	5	15	-1,03E+07	VERIFIED
C6	6	17	-6,30E+06	VERIFIED
C7	10	17	-1,08E+07	VERIFIED
C8	11	18	-1,03E+07	VERIFIED
C9	12	13	-1,05E+07	VERIFIED
C10	7	14	-5,06E+06	VERIFIED
C11	8	15	-2,96E+06	VERIFIED
C12	9	16	-7,35E+06	VERIFIED
C13	5	12	-2,01E+07	VERIFIED
C14	6	7	-2,33E+07	VERIFIED
C15	1	8	0,00E+00	VERIFIED
C16	2	9	-9,14E+06	VERIFIED
C17	3	10	-2,18E+07	VERIFIED
C18	4	11	-2,79E+07	VERIFIED
C19	7	30	-8,30E+06	VERIFIED
C20	8	31	-3,52E+06	VERIFIED
C21	9	26	-1,45E+07	VERIFIED
C22	10	27	-1,25E+07	VERIFIED
C23	11	28	-6,43E+06	VERIFIED
C24	12	29	-5,21E+06	VERIFIED
C25	23	30	-7,63E+06	VERIFIED
C26	24	31	-1,36E+07	VERIFIED
C27	25	26	-1,15E+07	VERIFIED
C28	20	27	-3,77E+06	VERIFIED
C29	21	28	-9,79E+06	VERIFIED
C30	22	29	-6,67E+06	VERIFIED
C31	11	25	-2,10E+07	VERIFIED
C32	12	20	-2,11E+07	VERIFIED
C33	7	21	0,00E+00	VERIFIED

C34	8	22	-1,53E+07	VERIFIED
C35	9	23	-1,94E+07	VERIFIED
C36	10	24	-2,00E+07	VERIFIED
C37	20	43	-9,79E+06	VERIFIED
C38	21	44	-3,77E+06	VERIFIED
C39	22	39	-1,15E+07	VERIFIED
C40	23	40	-1,36E+07	VERIFIED
C41	24	41	-7,63E+06	VERIFIED
C42	25	42	-6,67E+06	VERIFIED
C43	36	43	-6,43E+06	VERIFIED
C44	37	44	-1,25E+07	VERIFIED
C45	38	39	-1,45E+07	VERIFIED
C46	33	40	-3,52E+06	VERIFIED
C47	34	41	-8,30E+06	VERIFIED
C48	35	42	-5,21E+06	VERIFIED
C49	24	38	-1,94E+07	VERIFIED
C50	25	33	-1,53E+07	VERIFIED
C51	20	34	0,00E+00	VERIFIED
C52	21	35	-2,11E+07	VERIFIED
C53	22	36	-2,10E+07	VERIFIED
C54	23	37	-2,00E+07	VERIFIED
C55	33	56	-2,96E+06	VERIFIED
C56	34	57	-5,06E+06	VERIFIED
C57	35	52	-1,05E+07	VERIFIED
C58	36	53	-1,03E+07	VERIFIED
C59	37	54	-1,08E+07	VERIFIED
C60	38	55	-7,35E+06	VERIFIED
C61	49	56	-1,03E+07	VERIFIED
C62	50	57	-9,04E+06	VERIFIED
C63	51	52	-1,57E+07	VERIFIED
C64	46	53	-9,02E+06	VERIFIED
C65	47	54	-6,35E+05	VERIFIED
C66	48	55	-6,30E+06	VERIFIED
C67	37	51	-2,18E+07	VERIFIED
C68	38	46	-9,14E+06	VERIFIED
C69	33	47	0,00E+00	VERIFIED
C70	34	48	-2,33E+07	VERIFIED
C71	35	49	-2,01E+07	VERIFIED
C72	36	50	-2,79E+07	VERIFIED

Verification 1a: tension cables

Element	Node	Node	σ_N [N/m^2]	Tension
T1	1	2	5,25E+07	VERIFIED
T2	2	3	3,02E+07	VERIFIED
T3	3	4	1,54E+07	VERIFIED
T4	4	5	1,84E+07	VERIFIED
T5	5	6	1,43E+07	VERIFIED
T6	6	1	1,12E+07	VERIFIED
T7	7	8	5,25E+07	VERIFIED
T8	8	9	6,56E+06	VERIFIED
T9	9	10	3,11E+07	VERIFIED
T10	10	11	3,39E+07	VERIFIED
T11	11	12	2,35E+07	VERIFIED
T12	12	7	1,36E+07	VERIFIED
T13	1	13	5,25E+07	VERIFIED
T14	2	13	8,87E+06	VERIFIED
T15	7	13	2,40E+07	VERIFIED
T16	8	13	3,12E+07	VERIFIED
T17	2	14	2,40E+07	VERIFIED
T18	3	14	8,87E+06	VERIFIED
T19	8	14	5,25E+07	VERIFIED
T20	9	14	1,36E+07	VERIFIED
T21	3	15	2,35E+07	VERIFIED
T22	4	15	3,39E+07	VERIFIED
T23	9	15	3,11E+07	VERIFIED
T24	10	15	6,56E+06	VERIFIED
T25	4	16	5,25E+07	VERIFIED
T26	5	16	1,12E+07	VERIFIED
T27	10	16	1,43E+07	VERIFIED
T28	11	16	1,84E+07	VERIFIED
T29	5	17	1,54E+07	VERIFIED
T30	6	17	3,02E+07	VERIFIED
T31	11	17	5,80E+07	VERIFIED
T32	12	17	6,35E+07	VERIFIED
T33	6	18	5,53E+07	VERIFIED
T34	1	18	6,08E+07	VERIFIED
T35	12	18	4,92E+07	VERIFIED
T36	7	18	1,69E+07	VERIFIED
T37	20	21	1,06E+07	VERIFIED

T38	21	22	5,13E+07	VERIFIED
T39	22	23	4,37E+07	VERIFIED
T40	23	24	1,97E+07	VERIFIED
T41	24	25	8,02E+06	VERIFIED
T42	25	20	4,76E+07	VERIFIED
T43	7	26	4,63E+07	VERIFIED
T44	8	26	1,57E+07	VERIFIED
T45	20	26	1,73E+07	VERIFIED
T46	21	26	4,57E+07	VERIFIED
T47	8	27	3,57E+07	VERIFIED
T48	9	27	1,04E+07	VERIFIED
T49	21	27	2,66E+07	VERIFIED
T50	22	27	3,03E+07	VERIFIED
T51	9	28	4,33E+07	VERIFIED
T52	10	28	4,36E+07	VERIFIED
T53	22	28	4,56E+07	VERIFIED
T54	23	28	4,27E+07	VERIFIED
T55	10	29	5,80E+07	VERIFIED
T56	11	29	6,11E+07	VERIFIED
T57	23	29	5,64E+07	VERIFIED
T58	24	29	5,95E+07	VERIFIED
T59	11	30	4,01E+07	VERIFIED
T60	12	30	3,82E+07	VERIFIED
T61	24	30	2,44E+07	VERIFIED
T62	25	30	4,47E+07	VERIFIED
T63	12	31	4,95E+07	VERIFIED
T64	7	31	2,17E+07	VERIFIED
T65	25	31	2,69E+07	VERIFIED
T66	20	31	4,78E+07	VERIFIED
T67	33	34	4,14E+07	VERIFIED
T68	34	35	1,23E+07	VERIFIED
T69	35	36	1,46E+07	VERIFIED
T70	36	37	4,06E+07	VERIFIED
T71	37	38	4,19E+07	VERIFIED
T72	38	33	3,01E+07	VERIFIED
T73	20	39	2,92E+07	VERIFIED
T74	21	39	4,22E+07	VERIFIED
T75	33	39	4,21E+07	VERIFIED
T76	34	39	3,02E+07	VERIFIED
T77	21	40	4,61E+07	VERIFIED
T78	22	40	3,68E+07	VERIFIED

T79	34	40	5,95E+07	VERIFIED
T80	35	40	5,64E+07	VERIFIED
T81	22	41	6,11E+07	VERIFIED
T82	23	41	5,80E+07	VERIFIED
T83	35	41	3,68E+07	VERIFIED
T84	36	41	4,61E+07	VERIFIED
T85	23	42	3,02E+07	VERIFIED
T86	24	42	4,21E+07	VERIFIED
T87	36	42	4,22E+07	VERIFIED
T88	37	42	2,92E+07	VERIFIED
T89	24	43	3,01E+07	VERIFIED
T90	25	43	4,19E+07	VERIFIED
T91	37	43	4,06E+07	VERIFIED
T92	38	43	1,46E+07	VERIFIED
T93	25	44	1,23E+07	VERIFIED
T94	20	44	4,14E+07	VERIFIED
T95	38	44	4,78E+07	VERIFIED
T96	33	44	2,69E+07	VERIFIED
T97	46	47	2,17E+07	VERIFIED
T98	47	48	4,95E+07	VERIFIED
T99	48	49	4,47E+07	VERIFIED
T100	49	50	2,44E+07	VERIFIED
T101	50	51	3,82E+07	VERIFIED
T102	51	46	4,01E+07	VERIFIED
T103	33	52	6,08E+07	VERIFIED
T104	34	52	5,53E+07	VERIFIED
T105	46	52	6,35E+07	VERIFIED
T106	47	52	5,80E+07	VERIFIED
T107	34	53	4,27E+07	VERIFIED
T108	35	53	4,56E+07	VERIFIED
T109	47	53	4,36E+07	VERIFIED
T110	48	53	4,33E+07	VERIFIED
T111	35	54	3,03E+07	VERIFIED
T112	36	54	2,66E+07	VERIFIED
T113	48	54	1,04E+07	VERIFIED
T114	49	54	3,57E+07	VERIFIED
T115	36	55	4,57E+07	VERIFIED
T116	37	55	1,73E+07	VERIFIED
T117	49	55	1,57E+07	VERIFIED
T118	50	55	4,63E+07	VERIFIED
T119	37	56	4,76E+07	VERIFIED

T120	38	56	8,02E+06	VERIFIED
T121	50	56	1,97E+07	VERIFIED
T122	51	56	4,37E+07	VERIFIED
T123	38	57	5,13E+07	VERIFIED
T124	33	57	1,06E+07	VERIFIED
T125	51	57	1,69E+07	VERIFIED
T126	46	57	4,92E+07	VERIFIED

Verification 1b: compression bars

Element	Node	Node	σ_N [N/m^2]	Compression
C1	1	17	-1,27E+06	VERIFIED
C2	2	18	-7,82E+06	VERIFIED
C3	3	13	-2,08E+07	VERIFIED
C4	4	14	-1,04E+07	VERIFIED
C5	5	15	-1,00E+07	VERIFIED
C6	6	17	-6,64E+06	VERIFIED
C7	10	17	-1,03E+07	VERIFIED
C8	11	18	-1,20E+07	VERIFIED
C9	12	13	-1,54E+07	VERIFIED
C10	7	14	-4,28E+06	VERIFIED
C11	8	15	-3,06E+06	VERIFIED
C12	9	16	-6,84E+06	VERIFIED
C13	5	12	-1,97E+07	VERIFIED
C14	6	7	-2,39E+07	VERIFIED
C15	1	8	0,00E+00	VERIFIED
C16	2	9	-8,87E+06	VERIFIED
C17	3	10	-2,11E+07	VERIFIED
C18	4	11	-2,71E+07	VERIFIED
C19	7	30	-8,56E+06	VERIFIED
C20	8	31	-2,67E+06	VERIFIED
C21	9	26	-1,96E+07	VERIFIED
C22	10	27	-1,40E+07	VERIFIED
C23	11	28	-6,21E+06	VERIFIED
C24	12	29	-5,05E+06	VERIFIED
C25	23	30	-7,50E+06	VERIFIED
C26	24	31	-1,51E+07	VERIFIED
C27	25	26	-1,64E+07	VERIFIED
C28	20	27	-3,06E+06	VERIFIED
C29	21	28	-1,00E+07	VERIFIED

C30	22	29	-6,45E+06	VERIFIED
C31	11	25	-2,02E+07	VERIFIED
C32	12	20	-2,07E+07	VERIFIED
C33	7	21	0,00E+00	VERIFIED
C34	8	22	-1,48E+07	VERIFIED
C35	9	23	-1,87E+07	VERIFIED
C36	10	24	-1,92E+07	VERIFIED
C37	20	43	-1,00E+07	VERIFIED
C38	21	44	-3,06E+06	VERIFIED
C39	22	39	-1,64E+07	VERIFIED
C40	23	40	-1,51E+07	VERIFIED
C41	24	41	-7,50E+06	VERIFIED
C42	25	42	-6,45E+06	VERIFIED
C43	36	43	-6,21E+06	VERIFIED
C44	37	44	-1,40E+07	VERIFIED
C45	38	39	-1,96E+07	VERIFIED
C46	33	40	-2,67E+06	VERIFIED
C47	34	41	-8,56E+06	VERIFIED
C48	35	42	-5,05E+06	VERIFIED
C49	24	38	-1,87E+07	VERIFIED
C50	25	33	-1,48E+07	VERIFIED
C51	20	34	0,00E+00	VERIFIED
C52	21	35	-2,07E+07	VERIFIED
C53	22	36	-2,02E+07	VERIFIED
C54	23	37	-1,92E+07	VERIFIED
C55	33	56	-3,06E+06	VERIFIED
C56	34	57	-4,28E+06	VERIFIED
C57	35	52	-1,54E+07	VERIFIED
C58	36	53	-1,20E+07	VERIFIED
C59	37	54	-1,03E+07	VERIFIED
C60	38	55	-6,84E+06	VERIFIED
C61	49	56	-1,00E+07	VERIFIED
C62	50	57	-1,04E+07	VERIFIED
C63	51	52	-2,08E+07	VERIFIED
C64	46	53	-7,82E+06	VERIFIED
C65	47	54	-1,27E+06	VERIFIED
C66	48	55	-6,64E+06	VERIFIED
C67	37	51	-2,11E+07	VERIFIED
C68	38	46	-8,87E+06	VERIFIED
C69	33	47	0,00E+00	VERIFIED
C70	34	48	-2,39E+07	VERIFIED

C71	35	49	-1,97E+07	VERIFIED
C72	36	50	-2,71E+07	VERIFIED

Verification 1b: tension cables

Element	Node	Node	σ_N [N/m^2]	Tension
T1	1	2	5,25E+07	VERIFIED
T2	2	3	3,81E+07	VERIFIED
T3	3	4	1,84E+07	VERIFIED
T4	4	5	1,80E+07	VERIFIED
T5	5	6	1,39E+07	VERIFIED
T6	6	1	1,26E+07	VERIFIED
T7	7	8	5,25E+07	VERIFIED
T8	8	9	1,30E+07	VERIFIED
T9	9	10	3,31E+07	VERIFIED
T10	10	11	3,38E+07	VERIFIED
T11	11	12	2,59E+07	VERIFIED
T12	12	7	1,98E+07	VERIFIED
T13	1	13	5,25E+07	VERIFIED
T14	2	13	1,52E+07	VERIFIED
T15	7	13	2,59E+07	VERIFIED
T16	8	13	3,17E+07	VERIFIED
T17	2	14	2,59E+07	VERIFIED
T18	3	14	1,52E+07	VERIFIED
T19	8	14	5,25E+07	VERIFIED
T20	9	14	1,98E+07	VERIFIED
T21	3	15	2,59E+07	VERIFIED
T22	4	15	3,38E+07	VERIFIED
T23	9	15	3,31E+07	VERIFIED
T24	10	15	1,30E+07	VERIFIED
T25	4	16	5,25E+07	VERIFIED
T26	5	16	1,26E+07	VERIFIED
T27	10	16	1,39E+07	VERIFIED
T28	11	16	1,80E+07	VERIFIED
T29	5	17	1,84E+07	VERIFIED
T30	6	17	3,81E+07	VERIFIED
T31	11	17	5,31E+07	VERIFIED
T32	12	17	5,89E+07	VERIFIED
T33	6	18	5,02E+07	VERIFIED
T34	1	18	5,60E+07	VERIFIED

T35	12	18	4,85E+07	VERIFIED
T36	7	18	2,14E+07	VERIFIED
T37	20	21	1,17E+07	VERIFIED
T38	21	22	5,18E+07	VERIFIED
T39	22	23	4,32E+07	VERIFIED
T40	23	24	1,93E+07	VERIFIED
T41	24	25	8,21E+06	VERIFIED
T42	25	20	4,69E+07	VERIFIED
T43	7	26	4,64E+07	VERIFIED
T44	8	26	1,53E+07	VERIFIED
T45	20	26	1,56E+07	VERIFIED
T46	21	26	4,63E+07	VERIFIED
T47	8	27	3,50E+07	VERIFIED
T48	9	27	1,23E+07	VERIFIED
T49	21	27	2,67E+07	VERIFIED
T50	22	27	3,02E+07	VERIFIED
T51	9	28	4,30E+07	VERIFIED
T52	10	28	4,49E+07	VERIFIED
T53	22	28	5,16E+07	VERIFIED
T54	23	28	4,07E+07	VERIFIED
T55	10	29	5,33E+07	VERIFIED
T56	11	29	5,66E+07	VERIFIED
T57	23	29	5,16E+07	VERIFIED
T58	24	29	5,49E+07	VERIFIED
T59	11	30	3,91E+07	VERIFIED
T60	12	30	4,40E+07	VERIFIED
T61	24	30	2,67E+07	VERIFIED
T62	25	30	4,49E+07	VERIFIED
T63	12	31	4,94E+07	VERIFIED
T64	7	31	2,17E+07	VERIFIED
T65	25	31	2,75E+07	VERIFIED
T66	20	31	4,75E+07	VERIFIED
T67	33	34	4,09E+07	VERIFIED
T68	34	35	1,10E+07	VERIFIED
T69	35	36	1,32E+07	VERIFIED
T70	36	37	4,02E+07	VERIFIED
T71	37	38	4,18E+07	VERIFIED
T72	38	33	3,10E+07	VERIFIED
T73	20	39	2,95E+07	VERIFIED
T74	21	39	4,23E+07	VERIFIED
T75	33	39	4,21E+07	VERIFIED

T76	34	39	3,20E+07	VERIFIED
T77	21	40	5,17E+07	VERIFIED
T78	22	40	3,55E+07	VERIFIED
T79	34	40	5,49E+07	VERIFIED
T80	35	40	5,16E+07	VERIFIED
T81	22	41	5,66E+07	VERIFIED
T82	23	41	5,33E+07	VERIFIED
T83	35	41	3,55E+07	VERIFIED
T84	36	41	5,17E+07	VERIFIED
T85	23	42	3,20E+07	VERIFIED
T86	24	42	4,21E+07	VERIFIED
T87	36	42	4,23E+07	VERIFIED
T88	37	42	2,95E+07	VERIFIED
T89	24	43	3,10E+07	VERIFIED
T90	25	43	4,18E+07	VERIFIED
T91	37	43	4,02E+07	VERIFIED
T92	38	43	1,32E+07	VERIFIED
T93	25	44	1,10E+07	VERIFIED
T94	20	44	4,09E+07	VERIFIED
T95	38	44	4,75E+07	VERIFIED
T96	33	44	2,75E+07	VERIFIED
T97	46	47	2,17E+07	VERIFIED
T98	47	48	4,94E+07	VERIFIED
T99	48	49	4,49E+07	VERIFIED
T100	49	50	2,67E+07	VERIFIED
T101	50	51	4,40E+07	VERIFIED
T102	51	46	3,91E+07	VERIFIED
T103	33	52	5,60E+07	VERIFIED
T104	34	52	5,02E+07	VERIFIED
T105	46	52	5,89E+07	VERIFIED
T106	47	52	5,31E+07	VERIFIED
T107	34	53	4,07E+07	VERIFIED
T108	35	53	5,16E+07	VERIFIED
T109	47	53	4,49E+07	VERIFIED
T110	48	53	4,30E+07	VERIFIED
T111	35	54	3,02E+07	VERIFIED
T112	36	54	2,67E+07	VERIFIED
T113	48	54	1,23E+07	VERIFIED
T114	49	54	3,50E+07	VERIFIED
T115	36	55	4,63E+07	VERIFIED
T116	37	55	1,56E+07	VERIFIED

T117	49	55	1,53E+07	VERIFIED
T118	50	55	4,64E+07	VERIFIED
T119	37	56	4,69E+07	VERIFIED
T120	38	56	8,21E+06	VERIFIED
T121	50	56	1,93E+07	VERIFIED
T122	51	56	4,32E+07	VERIFIED
T123	38	57	5,18E+07	VERIFIED
T124	33	57	1,17E+07	VERIFIED
T125	51	57	2,14E+07	VERIFIED
T126	46	57	4,85E+07	VERIFIED

Verification 2a

Node	d_x [m]	d_y [m]	d_z [m]	$\|d_x\| << l_e$	$\|d_y\| << l_e$	$\|d_z\| << l_e$
1	0,00E+00	0,00E+00	0,00E+00	VERIFIED	VERIFIED	VERIFIED
2	0,00E+00	0,00E+00	0,00E+00	VERIFIED	VERIFIED	VERIFIED
3	-9,53E-05	5,54E-04	-1,27E-04	VERIFIED	VERIFIED	VERIFIED
4	4,75E-04	7,83E-04	-1,01E-04	VERIFIED	VERIFIED	VERIFIED
5	7,16E-04	8,43E-04	3,65E-04	VERIFIED	VERIFIED	VERIFIED
6	1,24E-03	1,05E-04	3,77E-04	VERIFIED	VERIFIED	VERIFIED
7	0,00E+00	0,00E+00	0,00E+00	VERIFIED	VERIFIED	VERIFIED
8	0,00E+00	0,00E+00	0,00E+00	VERIFIED	VERIFIED	VERIFIED
9	-1,39E-04	1,27E-04	-2,95E-04	VERIFIED	VERIFIED	VERIFIED
10	2,85E-04	4,57E-04	-2,24E-04	VERIFIED	VERIFIED	VERIFIED
11	4,17E-04	3,32E-04	-3,72E-04	VERIFIED	VERIFIED	VERIFIED
12	3,67E-04	8,57E-05	-1,06E-04	VERIFIED	VERIFIED	VERIFIED
13	-2,53E-05	1,01E-05	-2,79E-04	VERIFIED	VERIFIED	VERIFIED
14	1,10E-04	1,43E-04	-3,80E-04	VERIFIED	VERIFIED	VERIFIED
15	6,44E-04	5,33E-04	4,36E-05	VERIFIED	VERIFIED	VERIFIED
16	5,44E-04	6,62E-04	6,21E-04	VERIFIED	VERIFIED	VERIFIED
17	4,33E-04	3,17E-04	-4,23E-05	VERIFIED	VERIFIED	VERIFIED
18	1,09E-04	3,33E-06	-1,48E-05	VERIFIED	VERIFIED	VERIFIED
19	0,00E+00	0,00E+00	0,00E+00	VERIFIED	VERIFIED	VERIFIED
20	0,00E+00	0,00E+00	0,00E+00	VERIFIED	VERIFIED	VERIFIED
21	0,00E+00	0,00E+00	0,00E+00	VERIFIED	VERIFIED	VERIFIED
22	-1,29E-04	2,52E-05	-2,81E-04	VERIFIED	VERIFIED	VERIFIED
23	-7,53E-05	1,38E-06	-4,83E-04	VERIFIED	VERIFIED	VERIFIED
24	7,53E-05	-1,38E-06	-4,83E-04	VERIFIED	VERIFIED	VERIFIED
25	1,29E-04	-2,52E-05	-2,81E-04	VERIFIED	VERIFIED	VERIFIED
26	-1,46E-05	5,86E-06	-2,53E-04	VERIFIED	VERIFIED	VERIFIED

27	6,72E-05	5,83E-05	-3,11E-04	VERIFIED	VERIFIED	VERIFIED
28	4,75E-04	1,56E-04	-1,70E-04	VERIFIED	VERIFIED	VERIFIED
29	1,22E-04	2,07E-04	-2,14E-05	VERIFIED	VERIFIED	VERIFIED
30	-1,07E-04	8,34E-05	-1,68E-04	VERIFIED	VERIFIED	VERIFIED
31	-4,47E-05	-2,45E-05	-2,76E-04	VERIFIED	VERIFIED	VERIFIED
32	0,00E+00	0,00E+00	0,00E+00	VERIFIED	VERIFIED	VERIFIED
33	0,00E+00	0,00E+00	0,00E+00	VERIFIED	VERIFIED	VERIFIED
34	0,00E+00	0,00E+00	0,00E+00	VERIFIED	VERIFIED	VERIFIED
35	-3,67E-04	-8,57E-05	-1,06E-04	VERIFIED	VERIFIED	VERIFIED
36	-4,17E-04	-3,32E-04	-3,72E-04	VERIFIED	VERIFIED	VERIFIED
37	-2,85E-04	-4,57E-04	-2,24E-04	VERIFIED	VERIFIED	VERIFIED
38	1,39E-04	-1,27E-04	-2,95E-04	VERIFIED	VERIFIED	VERIFIED
39	1,46E-05	-5,86E-06	-2,53E-04	VERIFIED	VERIFIED	VERIFIED
40	4,47E-05	2,45E-05	-2,76E-04	VERIFIED	VERIFIED	VERIFIED
41	1,07E-04	-8,34E-05	-1,68E-04	VERIFIED	VERIFIED	VERIFIED
42	-1,22E-04	-2,07E-04	-2,14E-05	VERIFIED	VERIFIED	VERIFIED
43	-4,75E-04	-1,56E-04	-1,70E-04	VERIFIED	VERIFIED	VERIFIED
44	-6,72E-05	-5,83E-05	-3,11E-04	VERIFIED	VERIFIED	VERIFIED
45	0,00E+00	0,00E+00	0,00E+00	VERIFIED	VERIFIED	VERIFIED
46	0,00E+00	0,00E+00	0,00E+00	VERIFIED	VERIFIED	VERIFIED
47	0,00E+00	0,00E+00	0,00E+00	VERIFIED	VERIFIED	VERIFIED
48	-1,24E-03	-1,05E-04	3,77E-04	VERIFIED	VERIFIED	VERIFIED
49	-7,16E-04	-8,43E-04	3,65E-04	VERIFIED	VERIFIED	VERIFIED
50	-4,75E-04	-7,83E-04	-1,01E-04	VERIFIED	VERIFIED	VERIFIED
51	9,53E-05	-5,54E-04	-1,27E-04	VERIFIED	VERIFIED	VERIFIED
52	2,53E-05	-1,01E-05	-2,79E-04	VERIFIED	VERIFIED	VERIFIED
53	-1,09E-04	-3,33E-06	-1,48E-05	VERIFIED	VERIFIED	VERIFIED
54	-4,33E-04	-3,17E-04	-4,23E-05	VERIFIED	VERIFIED	VERIFIED
55	-5,44E-04	-6,62E-04	6,21E-04	VERIFIED	VERIFIED	VERIFIED
56	-6,44E-04	-5,33E-04	4,36E-05	VERIFIED	VERIFIED	VERIFIED
57	-1,10E-04	-1,43E-04	-3,80E-04	VERIFIED	VERIFIED	VERIFIED
58	0,00E+00	0,00E+00	0,00E+00	VERIFIED	VERIFIED	VERIFIED

Verification 2b

Node	d_x [m]	d_y [m]	d_z [m]	$\|d_x\| << l_e$	$\|d_y\| << l_e$	$\|d_z\| << l_e$
1	0,00E+00	0,00E+00	0,00E+00	VERIFIED	VERIFIED	VERIFIED
2	0,00E+00	0,00E+00	0,00E+00	VERIFIED	VERIFIED	VERIFIED
3	-6,25E-06	5,48E-04	-1,14E-04	VERIFIED	VERIFIED	VERIFIED
4	4,04E-04	7,50E-04	-1,55E-04	VERIFIED	VERIFIED	VERIFIED

5	6,48E-04	8,59E-04	3,23E-04	VERIFIED	VERIFIED	VERIFIED
6	1,16E-03	1,21E-04	3,43E-04	VERIFIED	VERIFIED	VERIFIED
7	0,00E+00	0,00E+00	0,00E+00	VERIFIED	VERIFIED	VERIFIED
8	0,00E+00	0,00E+00	0,00E+00	VERIFIED	VERIFIED	VERIFIED
9	-7,58E-05	9,46E-05	-2,79E-04	VERIFIED	VERIFIED	VERIFIED
10	2,53E-04	4,39E-04	-2,47E-04	VERIFIED	VERIFIED	VERIFIED
11	3,85E-04	3,43E-04	-4,04E-04	VERIFIED	VERIFIED	VERIFIED
12	2,62E-04	1,16E-04	-1,16E-04	VERIFIED	VERIFIED	VERIFIED
13	-2,67E-05	1,07E-05	-8,23E-05	VERIFIED	VERIFIED	VERIFIED
14	1,18E-04	1,36E-04	-3,85E-04	VERIFIED	VERIFIED	VERIFIED
15	6,09E-04	5,07E-04	3,97E-05	VERIFIED	VERIFIED	VERIFIED
16	5,04E-04	6,56E-04	5,57E-04	VERIFIED	VERIFIED	VERIFIED
17	3,78E-04	3,41E-04	-7,54E-05	VERIFIED	VERIFIED	VERIFIED
18	9,50E-05	1,54E-05	-3,08E-05	VERIFIED	VERIFIED	VERIFIED
19	0,00E+00	0,00E+00	0,00E+00	VERIFIED	VERIFIED	VERIFIED
20	0,00E+00	0,00E+00	0,00E+00	VERIFIED	VERIFIED	VERIFIED
21	0,00E+00	0,00E+00	0,00E+00	VERIFIED	VERIFIED	VERIFIED
22	-4,83E-05	-3,60E-06	-2,76E-04	VERIFIED	VERIFIED	VERIFIED
23	-7,35E-05	-1,70E-05	-5,08E-04	VERIFIED	VERIFIED	VERIFIED
24	7,35E-05	1,70E-05	-5,08E-04	VERIFIED	VERIFIED	VERIFIED
25	4,83E-05	3,60E-06	-2,76E-04	VERIFIED	VERIFIED	VERIFIED
26	-1,54E-05	6,17E-06	-6,44E-05	VERIFIED	VERIFIED	VERIFIED
27	6,86E-05	4,62E-05	-3,05E-04	VERIFIED	VERIFIED	VERIFIED
28	4,69E-04	1,29E-04	-1,84E-04	VERIFIED	VERIFIED	VERIFIED
29	1,03E-04	2,06E-04	-9,70E-05	VERIFIED	VERIFIED	VERIFIED
30	-1,28E-04	1,07E-04	-1,87E-04	VERIFIED	VERIFIED	VERIFIED
31	-5,06E-05	-1,29E-05	-2,78E-04	VERIFIED	VERIFIED	VERIFIED
32	0,00E+00	0,00E+00	0,00E+00	VERIFIED	VERIFIED	VERIFIED
33	0,00E+00	0,00E+00	0,00E+00	VERIFIED	VERIFIED	VERIFIED
34	0,00E+00	0,00E+00	0,00E+00	VERIFIED	VERIFIED	VERIFIED
35	-2,62E-04	-1,16E-04	-1,16E-04	VERIFIED	VERIFIED	VERIFIED
36	-3,85E-04	-3,43E-04	-4,04E-04	VERIFIED	VERIFIED	VERIFIED
37	-2,53E-04	-4,39E-04	-2,47E-04	VERIFIED	VERIFIED	VERIFIED
38	7,58E-05	-9,46E-05	-2,79E-04	VERIFIED	VERIFIED	VERIFIED
39	1,54E-05	-6,17E-06	-6,44E-05	VERIFIED	VERIFIED	VERIFIED
40	5,06E-05	1,29E-05	-2,78E-04	VERIFIED	VERIFIED	VERIFIED
41	1,28E-04	-1,07E-04	-1,87E-04	VERIFIED	VERIFIED	VERIFIED
42	-1,03E-04	-2,06E-04	-9,70E-05	VERIFIED	VERIFIED	VERIFIED
43	-4,69E-04	-1,29E-04	-1,84E-04	VERIFIED	VERIFIED	VERIFIED
44	-6,86E-05	-4,62E-05	-3,05E-04	VERIFIED	VERIFIED	VERIFIED
45	0,00E+00	0,00E+00	0,00E+00	VERIFIED	VERIFIED	VERIFIED

46	0,00E+00	0,00E+00	0,00E+00	VERIFIED	VERIFIED	VERIFIED
47	0,00E+00	0,00E+00	0,00E+00	VERIFIED	VERIFIED	VERIFIED
48	-1,16E-03	-1,21E-04	3,43E-04	VERIFIED	VERIFIED	VERIFIED
49	-6,48E-04	-8,59E-04	3,23E-04	VERIFIED	VERIFIED	VERIFIED
50	-4,04E-04	-7,50E-04	-1,55E-04	VERIFIED	VERIFIED	VERIFIED
51	6,25E-06	-5,48E-04	-1,14E-04	VERIFIED	VERIFIED	VERIFIED
52	2,67E-05	-1,07E-05	-8,23E-05	VERIFIED	VERIFIED	VERIFIED
53	-9,50E-05	-1,54E-05	-3,08E-05	VERIFIED	VERIFIED	VERIFIED
54	-3,78E-04	-3,41E-04	-7,54E-05	VERIFIED	VERIFIED	VERIFIED
55	-5,04E-04	-6,56E-04	5,57E-04	VERIFIED	VERIFIED	VERIFIED
56	-6,09E-04	-5,07E-04	3,97E-05	VERIFIED	VERIFIED	VERIFIED
57	-1,18E-04	-1,36E-04	-3,85E-04	VERIFIED	VERIFIED	VERIFIED
58	0,00E+00	0,00E+00	0,00E+00	VERIFIED	VERIFIED	VERIFIED

Verification 3a

Element	Node	Node	$N_{c,Rd}$ [N]	N_{Ed} [N]	$N_{c,Rd} > N_{Ed}$
C1	1	17	785714,29	3821,00	VERIFIED
C2	2	18	785714,29	23453,00	VERIFIED
C3	3	13	785714,29	62503,00	VERIFIED
C4	4	14	785714,29	31214,00	VERIFIED
C5	5	15	785714,29	30013,00	VERIFIED
C6	6	17	785714,29	19910,00	VERIFIED
C7	10	17	785714,29	30892,00	VERIFIED
C8	11	18	785714,29	36133,00	VERIFIED
C9	12	13	785714,29	46066,00	VERIFIED
C10	7	14	785714,29	12837,00	VERIFIED
C11	8	15	785714,29	9166,90	VERIFIED
C12	9	16	785714,29	20529,00	VERIFIED
C13	5	12	785714,29	59020,00	VERIFIED
C14	6	7	785714,29	71750,00	VERIFIED
C15	1	8	785714,29	0,00	VERIFIED
C16	2	9	785714,29	26624,00	VERIFIED
C17	3	10	785714,29	63197,00	VERIFIED
C18	4	11	785714,29	81294,00	VERIFIED
C19	7	30	785714,29	25676,00	VERIFIED
C20	8	31	785714,29	7999,30	VERIFIED
C21	9	26	785714,29	58737,00	VERIFIED
C22	10	27	785714,29	41936,00	VERIFIED

C23	11	28	785714,29	18640,00	VERIFIED
C24	12	29	785714,29	15139,00	VERIFIED
C25	23	30	785714,29	22488,00	VERIFIED
C26	24	31	785714,29	45242,00	VERIFIED
C27	25	26	785714,29	49247,00	VERIFIED
C28	20	27	785714,29	9176,80	VERIFIED
C29	21	28	785714,29	30024,00	VERIFIED
C30	22	29	785714,29	19352,00	VERIFIED
C31	11	25	785714,29	60549,00	VERIFIED
C32	12	20	785714,29	62154,00	VERIFIED
C33	7	21	785714,29	0,00	VERIFIED
C34	8	22	785714,29	44331,00	VERIFIED
C35	9	23	785714,29	56199,00	VERIFIED
C36	10	24	785714,29	57560,00	VERIFIED
C37	20	43	785714,29	30024,00	VERIFIED
C38	21	44	785714,29	9176,80	VERIFIED
C39	22	39	785714,29	49247,00	VERIFIED
C40	23	40	785714,29	45242,00	VERIFIED
C41	24	41	785714,29	22488,00	VERIFIED
C42	25	42	785714,29	19352,00	VERIFIED
C43	36	43	785714,29	18640,00	VERIFIED
C44	37	44	785714,29	41936,00	VERIFIED
C45	38	39	785714,29	58737,00	VERIFIED
C46	33	40	785714,29	7999,30	VERIFIED
C47	34	41	785714,29	25676,00	VERIFIED
C48	35	42	785714,29	15139,00	VERIFIED
C49	24	38	785714,29	56199,00	VERIFIED
C50	25	33	785714,29	44331,00	VERIFIED
C51	20	34	785714,29	0,00	VERIFIED
C52	21	35	785714,29	62154,00	VERIFIED
C53	22	36	785714,29	60549,00	VERIFIED
C54	23	37	785714,29	57560,00	VERIFIED
C55	33	56	785714,29	9166,90	VERIFIED
C56	34	57	785714,29	12837,00	VERIFIED
C57	35	52	785714,29	46066,00	VERIFIED
C58	36	53	785714,29	36133,00	VERIFIED
C59	37	54	785714,29	30892,00	VERIFIED
C60	38	55	785714,29	20529,00	VERIFIED
C61	49	56	785714,29	30013,00	VERIFIED
C62	50	57	785714,29	31214,00	VERIFIED
C63	51	52	785714,29	62503,00	VERIFIED

C64	46	53	785714,29	23453,00	VERIFIED
C65	47	54	785714,29	3821,00	VERIFIED
C66	48	55	785714,29	19910,00	VERIFIED
C67	37	51	785714,29	63197,00	VERIFIED
C68	38	46	785714,29	26624,00	VERIFIED
C69	33	47	785714,29	0,00	VERIFIED
C70	34	48	785714,29	71750,00	VERIFIED
C71	35	49	785714,29	59020,00	VERIFIED
C72	36	50	785714,29	81294,00	VERIFIED

Verification 3b

Element	Node	Node	$N_{t,Rd}$ [N]	N_{Ed} [N]	$N_{t,Rd} > N_{Ed}$
T1	1	2	392857,14	78750,00	VERIFIED
T2	2	3	392857,14	57184,00	VERIFIED
T3	3	4	392857,14	27573,00	VERIFIED
T4	4	5	392857,14	26957,00	VERIFIED
T5	5	6	392857,14	20899,00	VERIFIED
T6	6	1	392857,14	18849,00	VERIFIED
T7	7	8	392857,14	78750,00	VERIFIED
T8	8	9	392857,14	19497,00	VERIFIED
T9	9	10	392857,14	49610,00	VERIFIED
T10	10	11	392857,14	50688,00	VERIFIED
T11	11	12	392857,14	38855,00	VERIFIED
T12	12	7	392857,14	29746,00	VERIFIED
T13	1	13	392857,14	79628,00	VERIFIED
T14	2	13	392857,14	88298,00	VERIFIED
T15	7	13	392857,14	75293,00	VERIFIED
T16	8	13	392857,14	83963,00	VERIFIED
T17	2	14	392857,14	72766,00	VERIFIED
T18	3	14	392857,14	32098,00	VERIFIED
T19	8	14	392857,14	17492,00	VERIFIED
T20	9	14	392857,14	77629,00	VERIFIED
T21	3	15	392857,14	64754,00	VERIFIED
T22	4	15	392857,14	28977,00	VERIFIED
T23	9	15	392857,14	12309,00	VERIFIED
T24	10	15	392857,14	70336,00	VERIFIED
T25	4	16	392857,14	69564,00	VERIFIED
T26	5	16	392857,14	22879,00	VERIFIED
T27	10	16	392857,14	23369,00	VERIFIED

T28	11	16	392857,14	69401,00	VERIFIED
T29	5	17	392857,14	52519,00	VERIFIED
T30	6	17	392857,14	18457,00	VERIFIED
T31	11	17	392857,14	40006,00	VERIFIED
T32	12	17	392857,14	45284,00	VERIFIED
T33	6	18	392857,14	64516,00	VERIFIED
T34	1	18	392857,14	67374,00	VERIFIED
T35	12	18	392857,14	77469,00	VERIFIED
T36	7	18	392857,14	61120,00	VERIFIED
T37	20	21	392857,14	78750,00	VERIFIED
T38	21	22	392857,14	22846,00	VERIFIED
T39	22	23	392857,14	38797,00	VERIFIED
T40	23	24	392857,14	47592,00	VERIFIED
T41	24	25	392857,14	38797,00	VERIFIED
T42	25	20	392857,14	22846,00	VERIFIED
T43	7	26	392857,14	79882,00	VERIFIED
T44	8	26	392857,14	84888,00	VERIFIED
T45	20	26	392857,14	77379,00	VERIFIED
T46	21	26	392857,14	82385,00	VERIFIED
T47	8	27	392857,14	58718,00	VERIFIED
T48	9	27	392857,14	65966,00	VERIFIED
T49	21	27	392857,14	39990,00	VERIFIED
T50	22	27	392857,14	67395,00	VERIFIED
T51	9	28	392857,14	74059,00	VERIFIED
T52	10	28	392857,14	32518,00	VERIFIED
T53	22	28	392857,14	41317,00	VERIFIED
T54	23	28	392857,14	71188,00	VERIFIED
T55	10	29	392857,14	61351,00	VERIFIED
T56	11	29	392857,14	16524,00	VERIFIED
T57	23	29	392857,14	19859,00	VERIFIED
T58	24	29	392857,14	60239,00	VERIFIED
T59	11	30	392857,14	62693,00	VERIFIED
T60	12	30	392857,14	46544,00	VERIFIED
T61	24	30	392857,14	44207,00	VERIFIED
T62	25	30	392857,14	63388,00	VERIFIED
T63	12	31	392857,14	63080,00	VERIFIED
T64	7	31	392857,14	47963,00	VERIFIED
T65	25	31	392857,14	77483,00	VERIFIED
T66	20	31	392857,14	53214,00	VERIFIED
T67	33	34	392857,14	78750,00	VERIFIED
T68	34	35	392857,14	29746,00	VERIFIED

T69	35	36	392857,14	38855,00	VERIFIED
T70	36	37	392857,14	50688,00	VERIFIED
T71	37	38	392857,14	49610,00	VERIFIED
T72	38	33	392857,14	19497,00	VERIFIED
T73	20	39	392857,14	82385,00	VERIFIED
T74	21	39	392857,14	77379,00	VERIFIED
T75	33	39	392857,14	84888,00	VERIFIED
T76	34	39	392857,14	79882,00	VERIFIED
T77	21	40	392857,14	53214,00	VERIFIED
T78	22	40	392857,14	77483,00	VERIFIED
T79	34	40	392857,14	47963,00	VERIFIED
T80	35	40	392857,14	63080,00	VERIFIED
T81	22	41	392857,14	63388,00	VERIFIED
T82	23	41	392857,14	44207,00	VERIFIED
T83	35	41	392857,14	46544,00	VERIFIED
T84	36	41	392857,14	62693,00	VERIFIED
T85	23	42	392857,14	60239,00	VERIFIED
T86	24	42	392857,14	19859,00	VERIFIED
T87	36	42	392857,14	16524,00	VERIFIED
T88	37	42	392857,14	61351,00	VERIFIED
T89	24	43	392857,14	71188,00	VERIFIED
T90	25	43	392857,14	41317,00	VERIFIED
T91	37	43	392857,14	32518,00	VERIFIED
T92	38	43	392857,14	74059,00	VERIFIED
T93	25	44	392857,14	67395,00	VERIFIED
T94	20	44	392857,14	39990,00	VERIFIED
T95	38	44	392857,14	65966,00	VERIFIED
T96	33	44	392857,14	58718,00	VERIFIED
T97	46	47	392857,14	78750,00	VERIFIED
T98	47	48	392857,14	18849,00	VERIFIED
T99	48	49	392857,14	20899,00	VERIFIED
T100	49	50	392857,14	26957,00	VERIFIED
T101	50	51	392857,14	27573,00	VERIFIED
T102	51	46	392857,14	57184,00	VERIFIED
T103	33	52	392857,14	83963,00	VERIFIED
T104	34	52	392857,14	75293,00	VERIFIED
T105	46	52	392857,14	88298,00	VERIFIED
T106	47	52	392857,14	79628,00	VERIFIED
T107	34	53	392857,14	61120,00	VERIFIED
T108	35	53	392857,14	77469,00	VERIFIED
T109	47	53	392857,14	67374,00	VERIFIED

T110	48	53	392857,14	64516,00	VERIFIED
T111	35	54	392857,14	45284,00	VERIFIED
T112	36	54	392857,14	40006,00	VERIFIED
T113	48	54	392857,14	18457,00	VERIFIED
T114	49	54	392857,14	52519,00	VERIFIED
T115	36	55	392857,14	69401,00	VERIFIED
T116	37	55	392857,14	23369,00	VERIFIED
T117	49	55	392857,14	22879,00	VERIFIED
T118	50	55	392857,14	69564,00	VERIFIED
T119	37	56	392857,14	70336,00	VERIFIED
T120	38	56	392857,14	12309,00	VERIFIED
T121	50	56	392857,14	28977,00	VERIFIED
T122	51	56	392857,14	64754,00	VERIFIED
T123	38	57	392857,14	77629,00	VERIFIED
T124	33	57	392857,14	17492,00	VERIFIED
T125	51	57	392857,14	32098,00	VERIFIED
T126	46	57	392857,14	72766,00	VERIFIED

Verification 4

Element	Length [mm]	Effective length [mm]	N_{cr} [N]	λ [-]	φ [-]	χ [-]	$N_{b,Rd}$ [N]	N_{Ed} [N]	$N_{b,Rd} > N_{Ed}$
C1	3066,7	3066,7	157834	2,29	3,72	0,15	112604	3821	VERIFIED
C2	3066,7	3066,7	157834	2,29	3,72	0,15	112604	23453	VERIFIED
C3	3066,7	3066,7	157834	2,29	3,72	0,15	112604	62503	VERIFIED
C4	3066,7	3066,7	157834	2,29	3,72	0,15	112604	31214	VERIFIED
C5	3066,7	3066,7	157834	2,29	3,72	0,15	112604	30013	VERIFIED
C6	3066,7	3066,7	157834	2,29	3,72	0,15	112604	19910	VERIFIED
C7	3066,7	3066,7	157834	2,29	3,72	0,15	112604	30892	VERIFIED
C8	3066,7	3066,7	157834	2,29	3,72	0,15	112604	36133	VERIFIED
C9	3066,7	3066,7	157834	2,29	3,72	0,15	112604	46066	VERIFIED
C10	3066,7	3066,7	157834	2,29	3,72	0,15	112604	12837	VERIFIED
C11	3066,7	3066,7	157834	2,29	3,72	0,15	112604	9167	VERIFIED
C12	3066,7	3066,7	157834	2,29	3,72	0,15	112604	20529	VERIFIED
C13	3201,6	3201,6	144820	2,39	3,98	0,14	104607	59020	VERIFIED
C14	3201,6	3201,6	144820	2,39	3,98	0,14	104607	71750	VERIFIED
C15	3201,6	3201,6	144820	2,39	3,98	0,14	104607	0	VERIFIED
C16	3201,6	3201,6	144820	2,39	3,98	0,14	104607	26624	VERIFIED
C17	3201,6	3201,6	144820	2,39	3,98	0,14	104607	63197	VERIFIED
C18	3201,6	3201,6	144820	2,39	3,98	0,14	104607	81294	VERIFIED

C19	3066,7	3066,7	157834	2,29	3,72	0,15	112604	25676	VERIFIED
C20	3066,7	3066,7	157834	2,29	3,72	0,15	112604	7999	VERIFIED
C21	3066,7	3066,7	157834	2,29	3,72	0,15	112604	58737	VERIFIED
C22	3066,7	3066,7	157834	2,29	3,72	0,15	112604	41936	VERIFIED
C23	3066,7	3066,7	157834	2,29	3,72	0,15	112604	18640	VERIFIED
C24	3066,7	3066,7	157834	2,29	3,72	0,15	112604	15139	VERIFIED
C25	3066,7	3066,7	157834	2,29	3,72	0,15	112604	22488	VERIFIED
C26	3066,7	3066,7	157834	2,29	3,72	0,15	112604	45242	VERIFIED
C27	3066,7	3066,7	157834	2,29	3,72	0,15	112604	49247	VERIFIED
C28	3066,7	3066,7	157834	2,29	3,72	0,15	112604	9177	VERIFIED
C29	3066,7	3066,7	157834	2,29	3,72	0,15	112604	30024	VERIFIED
C30	3066,7	3066,7	157834	2,29	3,72	0,15	112604	19352	VERIFIED
C31	3201,6	3201,6	144820	2,39	3,98	0,14	104607	60549	VERIFIED
C32	3201,6	3201,6	144820	2,39	3,98	0,14	104607	62154	VERIFIED
C33	3201,6	3201,6	144820	2,39	3,98	0,14	104607	0	VERIFIED
C34	3201,6	3201,6	144820	2,39	3,98	0,14	104607	44331	VERIFIED
C35	3201,6	3201,6	144820	2,39	3,98	0,14	104607	56199	VERIFIED
C36	3201,6	3201,6	144820	2,39	3,98	0,14	104607	57560	VERIFIED
C37	3066,7	3066,7	157834	2,29	3,72	0,15	112604	30024	VERIFIED
C38	3066,7	3066,7	157834	2,29	3,72	0,15	112604	9177	VERIFIED
C39	3066,7	3066,7	157834	2,29	3,72	0,15	112604	49247	VERIFIED
C40	3066,7	3066,7	157834	2,29	3,72	0,15	112604	45242	VERIFIED
C41	3066,7	3066,7	157834	2,29	3,72	0,15	112604	22488	VERIFIED
C42	3066,7	3066,7	157834	2,29	3,72	0,15	112604	19352	VERIFIED
C43	3066,7	3066,7	157834	2,29	3,72	0,15	112604	18640	VERIFIED
C44	3066,7	3066,7	157834	2,29	3,72	0,15	112604	41936	VERIFIED
C45	3066,7	3066,7	157834	2,29	3,72	0,15	112604	58737	VERIFIED
C46	3066,7	3066,7	157834	2,29	3,72	0,15	112604	7999	VERIFIED
C47	3066,7	3066,7	157834	2,29	3,72	0,15	112604	25676	VERIFIED
C48	3066,7	3066,7	157834	2,29	3,72	0,15	112604	15139	VERIFIED
C49	3201,6	3201,6	144820	2,39	3,98	0,14	104607	56199	VERIFIED
C50	3201,6	3201,6	144820	2,39	3,98	0,14	104607	44331	VERIFIED
C51	3201,6	3201,6	144820	2,39	3,98	0,14	104607	0	VERIFIED
C52	3201,6	3201,6	144820	2,39	3,98	0,14	104607	62154	VERIFIED
C53	3201,6	3201,6	144820	2,39	3,98	0,14	104607	60549	VERIFIED
C54	3201,6	3201,6	144820	2,39	3,98	0,14	104607	57560	VERIFIED
C55	3066,7	3066,7	157834	2,29	3,72	0,15	112604	9167	VERIFIED
C56	3066,7	3066,7	157834	2,29	3,72	0,15	112604	12837	VERIFIED
C57	3066,7	3066,7	157834	2,29	3,72	0,15	112604	46066	VERIFIED
C58	3066,7	3066,7	157834	2,29	3,72	0,15	112604	36133	VERIFIED
C59	3066,7	3066,7	157834	2,29	3,72	0,15	112604	30892	VERIFIED

C60	3066,7	3066,7	157834	2,29	3,72	0,15	112604	20529	VERIFIED
C61	3066,7	3066,7	157834	2,29	3,72	0,15	112604	30013	VERIFIED
C62	3066,7	3066,7	157834	2,29	3,72	0,15	112604	31214	VERIFIED
C63	3066,7	3066,7	157834	2,29	3,72	0,15	112604	62503	VERIFIED
C64	3066,7	3066,7	157834	2,29	3,72	0,15	112604	23453	VERIFIED
C65	3066,7	3066,7	157834	2,29	3,72	0,15	112604	3821	VERIFIED
C66	3066,7	3066,7	157834	2,29	3,72	0,15	112604	19910	VERIFIED
C67	3201,6	3201,6	144820	2,39	3,98	0,14	104607	63197	VERIFIED
C68	3201,6	3201,6	144820	2,39	3,98	0,14	104607	26624	VERIFIED
C69	3201,6	3201,6	144820	2,39	3,98	0,14	104607	0	VERIFIED
C70	3201,6	3201,6	144820	2,39	3,98	0,14	104607	71750	VERIFIED
C71	3201,6	3201,6	144820	2,39	3,98	0,14	104607	59020	VERIFIED
C72	3201,6	3201,6	144820	2,39	3,98	0,14	104607	81294	VERIFIED